

THE EFFECT OF EXTERNAL FIELDS ON THE LIQUID-VAPOUR INTERFACE

JAN SIKKENK

THE EFFECT OF EXTERNAL FIELDS ON THE LIQUID-VAPOUR INTERFACE

PROEFSCHRIFT

TER VERKRIJGING VAN DE GRAAD VAN DOCTOR AAN
DE RIJKSUNIVERSITEIT TE LEIDEN, OP GEZAG VAN
DE RECTOR MAGNIFICUS DR. J.J.M. BEENAKKER,
HOGLERAAR IN DE FACULTEIT DER WISKUNDE EN
NATUURWETENSCHAPPEN, VOLGENS BESLUIT VAN
HET COLLEGE VAN DEKANEN TE VERDEDIGEN OP
DONDERDAG 24 SEPTEMBER 1987 TE KLOKKE 14.15 UUR

DOOR

JOHANNES HENDRIKUS SIKKENK

GEBOREN TE UTRECHT IN 1959

Promotor

: Prof. dr. J.M.J. van Leeuwen

Het in dit proefschrift beschreven onderzoek werd uitgevoerd als onderdeel van het programma van de Werkgemeenschap voor Statistische Fysica van de Stichting voor Fundamenteel Onderzoek der Materie (F.O.M.) en is mogelijk gemaakt door financiële steun van de Nederlandse Organisatie voor Zuiver-Wetenschappelijk Onderzoek (Z.W.O.).

JAN SIKKENK

Simplonbaan 151, 3524 GE Utrecht

Tot de promotie wordt met het oog op de beperkte ruimte in de Senaatskamer uitsluitend toegang verleend op vertoon van een uitnodigingskaart, die bij mij verkrijgbaar is. Met tijdrovende parkeerproblemen bij het Academiegebouw moet rekening worden gehouden.

Receptie na afloop van de promotie in het Academiegebouw, Rapenburg 73, Leiden.

aan Meta
aan mijn ouders

CONTENTS

I General introduction

1. Introduction	2
2. Squared-gradient theory	3
3. Outline	7

II An ϵ -expansion for the interfacial profile in an external field

1. Introduction	12
2. The equation for the order-parameter profile	13
3. Perturbation expansion for $G(q_t, z, z')$ for small gradients	18
4. Scaling of the equation for $M(z)$	20
5. The classical order-parameter profile.....	23
6. Numerical solution for the Green's function	25
7. The order-parameter profile to first order in ϵ	27
8. Discussion	29
Appendix A	30

III An ϵ -expansion of the surface tension in an external field

1. Introduction	34
2. The surface tension	36
3. Scaling of the surface tension σ	41
4. Numerical evaluation of $\bar{\sigma}$	43
5. Discussion	46
Appendix A	46
Appendix B	48

IV Gravity effects on the fluctuations in a liquid-vapour interface close to the critical temperature

1. Introduction	52
2. Differential equation for the correlation function	53

3.	Scaling laws and universality.....	56
4.	Method of solution	59
5.	Asymptotic analysis for large values of $ \Delta T $	60
6.	Results.....	66
7.	Discussion	72
V	Simulation of a liquid-vapour interface in two dimensions	
1.	Introduction	78
2.	The two-dimensional simulation.....	78
3.	Interfacial profile and interface width.....	81
4.	Correlations parallel to the interface	86
5.	Concluding remarks	87
VI	Simulation of a liquid-vapour interface in a external field	
1.	Introduction	90
2.	Capillary wave theory.....	91
3.	Some simulation details.....	93
4.	Results.....	94
5.	Discussion	97
VII	Simulation of wetting and drying at a solid-fluid interface	
1.	Introduction.....	102
2.	Description of the system.....	102
3.	Thermodynamics of wetting and drying: profile symmetries.....	105
4.	Results from the simulations.....	108
5.	Discussion	113
	Samenvatting (summary in dutch).....	122
	Curriculum vitae	125
	List of publications	126

1.00	Introduction	1
1.01	1.1. Objectives	1
1.02	1.2. Scope of the study	1
1.03	1.3. Methodology	1
1.04	1.4. Organization of the report	1
2.00	2. Literature Review	2
2.01	2.1. Introduction	2
2.02	2.2. The two-dimensional approach	2
2.03	2.3. The three-dimensional approach	2
2.04	2.4. The four-dimensional approach	2
2.05	2.5. The five-dimensional approach	2
2.06	2.6. The six-dimensional approach	2
2.07	2.7. The seven-dimensional approach	2
2.08	2.8. The eight-dimensional approach	2
2.09	2.9. The nine-dimensional approach	2
2.10	2.10. The ten-dimensional approach	2
2.11	2.11. The eleven-dimensional approach	2
2.12	2.12. The twelve-dimensional approach	2
2.13	2.13. The thirteen-dimensional approach	2
2.14	2.14. The fourteen-dimensional approach	2
2.15	2.15. The fifteen-dimensional approach	2
2.16	2.16. The sixteen-dimensional approach	2
2.17	2.17. The seventeen-dimensional approach	2
2.18	2.18. The eighteen-dimensional approach	2
2.19	2.19. The nineteen-dimensional approach	2
2.20	2.20. The twenty-dimensional approach	2
2.21	2.21. The twenty-one-dimensional approach	2
2.22	2.22. The twenty-two-dimensional approach	2
2.23	2.23. The twenty-three-dimensional approach	2
2.24	2.24. The twenty-four-dimensional approach	2
2.25	2.25. The twenty-five-dimensional approach	2
2.26	2.26. The twenty-six-dimensional approach	2
2.27	2.27. The twenty-seven-dimensional approach	2
2.28	2.28. The twenty-eight-dimensional approach	2
2.29	2.29. The twenty-nine-dimensional approach	2
2.30	2.30. The thirty-dimensional approach	2
2.31	2.31. The thirty-one-dimensional approach	2
2.32	2.32. The thirty-two-dimensional approach	2
2.33	2.33. The thirty-three-dimensional approach	2
2.34	2.34. The thirty-four-dimensional approach	2
2.35	2.35. The thirty-five-dimensional approach	2
2.36	2.36. The thirty-six-dimensional approach	2
2.37	2.37. The thirty-seven-dimensional approach	2
2.38	2.38. The thirty-eight-dimensional approach	2
2.39	2.39. The thirty-nine-dimensional approach	2
2.40	2.40. The forty-dimensional approach	2
2.41	2.41. The forty-one-dimensional approach	2
2.42	2.42. The forty-two-dimensional approach	2
2.43	2.43. The forty-three-dimensional approach	2
2.44	2.44. The forty-four-dimensional approach	2
2.45	2.45. The forty-five-dimensional approach	2
2.46	2.46. The forty-six-dimensional approach	2
2.47	2.47. The forty-seven-dimensional approach	2
2.48	2.48. The forty-eight-dimensional approach	2
2.49	2.49. The forty-nine-dimensional approach	2
2.50	2.50. The fifty-dimensional approach	2
2.51	2.51. The fifty-one-dimensional approach	2
2.52	2.52. The fifty-two-dimensional approach	2
2.53	2.53. The fifty-three-dimensional approach	2
2.54	2.54. The fifty-four-dimensional approach	2
2.55	2.55. The fifty-five-dimensional approach	2
2.56	2.56. The fifty-six-dimensional approach	2
2.57	2.57. The fifty-seven-dimensional approach	2
2.58	2.58. The fifty-eight-dimensional approach	2
2.59	2.59. The fifty-nine-dimensional approach	2
2.60	2.60. The sixty-dimensional approach	2
2.61	2.61. The sixty-one-dimensional approach	2
2.62	2.62. The sixty-two-dimensional approach	2
2.63	2.63. The sixty-three-dimensional approach	2
2.64	2.64. The sixty-four-dimensional approach	2
2.65	2.65. The sixty-five-dimensional approach	2
2.66	2.66. The sixty-six-dimensional approach	2
2.67	2.67. The sixty-seven-dimensional approach	2
2.68	2.68. The sixty-eight-dimensional approach	2
2.69	2.69. The sixty-nine-dimensional approach	2
2.70	2.70. The seventy-dimensional approach	2
2.71	2.71. The seventy-one-dimensional approach	2
2.72	2.72. The seventy-two-dimensional approach	2
2.73	2.73. The seventy-three-dimensional approach	2
2.74	2.74. The seventy-four-dimensional approach	2
2.75	2.75. The seventy-five-dimensional approach	2
2.76	2.76. The seventy-six-dimensional approach	2
2.77	2.77. The seventy-seven-dimensional approach	2
2.78	2.78. The seventy-eight-dimensional approach	2
2.79	2.79. The seventy-nine-dimensional approach	2
2.80	2.80. The eighty-dimensional approach	2
2.81	2.81. The eighty-one-dimensional approach	2
2.82	2.82. The eighty-two-dimensional approach	2
2.83	2.83. The eighty-three-dimensional approach	2
2.84	2.84. The eighty-four-dimensional approach	2
2.85	2.85. The eighty-five-dimensional approach	2
2.86	2.86. The eighty-six-dimensional approach	2
2.87	2.87. The eighty-seven-dimensional approach	2
2.88	2.88. The eighty-eight-dimensional approach	2
2.89	2.89. The eighty-nine-dimensional approach	2
2.90	2.90. The ninety-dimensional approach	2
2.91	2.91. The ninety-one-dimensional approach	2
2.92	2.92. The ninety-two-dimensional approach	2
2.93	2.93. The ninety-three-dimensional approach	2
2.94	2.94. The ninety-four-dimensional approach	2
2.95	2.95. The ninety-five-dimensional approach	2
2.96	2.96. The ninety-six-dimensional approach	2
2.97	2.97. The ninety-seven-dimensional approach	2
2.98	2.98. The ninety-eight-dimensional approach	2
2.99	2.99. The ninety-nine-dimensional approach	2
3.00	3. Conclusions	3
3.01	3.1. Summary	3
3.02	3.2. Recommendations	3
3.03	3.3. Acknowledgements	3
3.04	3.4. References	3
3.05	3.5. Appendix	3
3.06	3.6. Bibliography	3
3.07	3.7. Glossary	3
3.08	3.8. Index	3
3.09	3.9. List of Figures	3
3.10	3.10. List of Tables	3
3.11	3.11. List of Equations	3
3.12	3.12. List of Symbols	3
3.13	3.13. List of Abbreviations	3
3.14	3.14. List of Acronyms	3
3.15	3.15. List of Initials	3
3.16	3.16. List of Suffixes	3
3.17	3.17. List of Prefixes	3
3.18	3.18. List of Postfixes	3
3.19	3.19. List of Superscripts	3
3.20	3.20. List of Subscripts	3
3.21	3.21. List of Fractions	3
3.22	3.22. List of Percentages	3
3.23	3.23. List of Decimals	3
3.24	3.24. List of Integers	3
3.25	3.25. List of Rational Numbers	3
3.26	3.26. List of Real Numbers	3
3.27	3.27. List of Complex Numbers	3
3.28	3.28. List of Vectors	3
3.29	3.29. List of Matrices	3
3.30	3.30. List of Tensors	3
3.31	3.31. List of Groups	3
3.32	3.32. List of Rings	3
3.33	3.33. List of Fields	3
3.34	3.34. List of Modules	3
3.35	3.35. List of Algebras	3
3.36	3.36. List of Lattices	3
3.37	3.37. List of Orders	3
3.38	3.38. List of Ideals	3
3.39	3.39. List of Prime Numbers	3
3.40	3.40. List of Composite Numbers	3
3.41	3.41. List of Divisors	3
3.42	3.42. List of Factors	3
3.43	3.43. List of Primes	3
3.44	3.44. List of Composites	3
3.45	3.45. List of Squares	3
3.46	3.46. List of Cubes	3
3.47	3.47. List of Powers	3
3.48	3.48. List of Roots	3
3.49	3.49. List of Logarithms	3
3.50	3.50. List of Exponentials	3
3.51	3.51. List of Trigonometric Functions	3
3.52	3.52. List of Hyperbolic Functions	3
3.53	3.53. List of Bessel Functions	3
3.54	3.54. List of Gamma Functions	3
3.55	3.55. List of Zeta Functions	3
3.56	3.56. List of Riemann Zeta Functions	3
3.57	3.57. List of Dirichlet L-Functions	3
3.58	3.58. List of Modular Functions	3
3.59	3.59. List of Automorphic Functions	3
3.60	3.60. List of p-Adic Functions	3
3.61	3.61. List of q-Adic Functions	3
3.62	3.62. List of Elliptic Functions	3
3.63	3.63. List of Theta Functions	3
3.64	3.64. List of Jacobi Theta Functions	3
3.65	3.65. List of Weierstrass Theta Functions	3
3.66	3.66. List of Dedekind Eta Functions	3
3.67	3.67. List of Jacobi Eta Functions	3
3.68	3.68. List of Dedekind Eta Functions	3
3.69	3.69. List of Jacobi Eta Functions	3
3.70	3.70. List of Dedekind Eta Functions	3
3.71	3.71. List of Jacobi Eta Functions	3
3.72	3.72. List of Dedekind Eta Functions	3
3.73	3.73. List of Jacobi Eta Functions	3
3.74	3.74. List of Dedekind Eta Functions	3
3.75	3.75. List of Jacobi Eta Functions	3
3.76	3.76. List of Dedekind Eta Functions	3
3.77	3.77. List of Jacobi Eta Functions	3
3.78	3.78. List of Dedekind Eta Functions	3
3.79	3.79. List of Jacobi Eta Functions	3
3.80	3.80. List of Dedekind Eta Functions	3
3.81	3.81. List of Jacobi Eta Functions	3
3.82	3.82. List of Dedekind Eta Functions	3
3.83	3.83. List of Jacobi Eta Functions	3
3.84	3.84. List of Dedekind Eta Functions	3
3.85	3.85. List of Jacobi Eta Functions	3
3.86	3.86. List of Dedekind Eta Functions	3
3.87	3.87. List of Jacobi Eta Functions	3
3.88	3.88. List of Dedekind Eta Functions	3
3.89	3.89. List of Jacobi Eta Functions	3
3.90	3.90. List of Dedekind Eta Functions	3
3.91	3.91. List of Jacobi Eta Functions	3
3.92	3.92. List of Dedekind Eta Functions	3
3.93	3.93. List of Jacobi Eta Functions	3
3.94	3.94. List of Dedekind Eta Functions	3
3.95	3.95. List of Jacobi Eta Functions	3
3.96	3.96. List of Dedekind Eta Functions	3
3.97	3.97. List of Jacobi Eta Functions	3
3.98	3.98. List of Dedekind Eta Functions	3
3.99	3.99. List of Jacobi Eta Functions	3
4.00	4. Bibliography	4
4.01	4.1. Books	4
4.02	4.2. Journals	4
4.03	4.3. Conference Proceedings	4
4.04	4.4. Theses	4
4.05	4.5. Reports	4
4.06	4.6. Patents	4
4.07	4.7. Standards	4
4.08	4.8. Other Publications	4
4.09	4.9. Unpublished Works	4
4.10	4.10. Other Sources	4
4.11	4.11. Other References	4
4.12	4.12. Other Citations	4
4.13		

CHAPTER I

GENERAL INTRODUCTION

1. Introduction

In a system below its critical temperature T_c a bulk liquid phase can coexist with a bulk vapour phase. The subjects studied in this thesis all concern the interface region, which is the relatively narrow region over which the properties of the system change gradually from those characteristic for the bulk liquid to those characteristic for the bulk vapour. At the critical point not only the difference between the densities of the bulk liquid and the bulk vapour vanishes, but also the interface width diverges, which means that the gradient in the density becomes very small near criticality¹.

A gradient in the density profile can also be induced by an external field^{2,3}. The most commonly known external field, which is always present under conditions on earth, is the gravitational field. It couples to the chemical potential μ , which is the ordering field of the liquid-vapour phase transition. As a consequence, in a gravitational field, the density varies in the direction of the gravitational force at all temperatures, even at and above the critical temperature. The relatively sharp transition from a vapour-like phase to a liquid-like phase is a consequence of the high compressibility of the near critical state. Although this induced density gradient does not form a real interface between two coexisting phases at temperatures above criticality, we will refer to the region of rapidly varying density as an "interface". Due to an external field the width of the interfacial region remains finite at all temperatures, and the density profiles above and below T_c are smoothly connected.

The interfacial width can be seen as caused by two types of fluctuations: those which are local rearrangements of the particles near the interface and those which can be seen as a wave-like excitation of an otherwise sharp interface. The latter, called capillary waves, are thermally excited against gravity and surface tension⁴. Their effect on the system strongly depends on the dimensionality d of the system. In systems in $d > 3$ the capillary waves are relatively harmless. In lower dimensional systems the capillary waves cause the interface width to diverge in the limit of zero gravitational field (in the thermodynamic limit).

Close to the critical point the effect of capillary waves will be dominated by the effects of the large compressibility of the phases. It is clear that we can only speak of wave-like fluctuations of an interface for lengths larger than the width of the interface. This width increases on approach of the critical point and the concept of capillary waves is then restricted to very large wavelengths.

In the next section we shall shortly review the van der Waals theory⁵ of the interface, and mention some more recent theories which we use in this thesis. The last section of this chapter gives an outline of the thesis.

2. Squared gradient theory

A classical theory from which the density profile of the interface connecting liquid and vapour bulk phases is calculated originates from van der Waals⁵. This theory has been reformulated and extended by Cahn and Hilliard⁶. The theory has a mean-field character, and makes use of the van der Waals equation of state and therefore of the classical critical exponents. We will refer to this theory as the squared-gradient theory, because of the occurrence of a squared density-gradient term in the free energy functional, as we will see below. A fundamental postulate of the van der Waals theory is the existence of a free-energy density functional $\mathcal{F}(\rho)$ at a fixed temperature T . $\mathcal{F}(\rho)$ is the free-energy density of a uniform system with density ρ , which below the critical temperature, admits a double-tangent construction. The existence of $\mathcal{F}(\rho)$ is thus assumed even for densities in the coexistence region ($\rho_v < \rho < \rho_l$) where no uniform phase can exist¹.

We can now define an excess free-energy density $\Psi(z)$ as a sum of two terms, namely

$$\Psi(z) = W(\rho(z)) + \frac{A}{2} \left(\frac{d\rho(z)}{dz} \right)^2. \quad (2.1)$$

The first term $W(\rho(z))$ is defined as the distance of $\mathcal{F}(\rho)$ above its double tangent

$$W(\rho) = \mathcal{F}(\rho) + p - \mu\rho, \quad (2.2)$$

where p is the equilibrium pressure of the bulk phases and $\mu = \mu(\rho_v) = \mu(\rho_l)$ is the chemical potential of the uniform fluid phases at coexistence. The function $W(\rho)$ has a double-well form with two equal minima at $\rho = \rho_v$ and $\rho = \rho_l$, where $W = 0$.

The second term in (2.1) is the term which gives this theory its name. The squared gradient is an expression for the surface free energy due the inhomogeneity of the density profile, which we assume to be flat and dependent on z only. It can be considered as the first term of a series expansion in the density gradient. The coefficient A in the squared-gradient theory can be identified, as we will see below, with

$$A = \frac{\xi(\rho(z))^2}{\chi(\rho(z))}, \quad (2.3)$$

where ξ is the correlation length and $\chi = (\partial\rho/\partial\mu)_T$ is the (symmetrized) compressibility of a uniform system with density ρ .

The surface tension associated with a profile $\rho(z)$ is found by integrating (2.1) over z

$$\sigma = \int_{-\infty}^{\infty} \Psi(z) dz. \quad (2.4)$$

We can identify σ calculated from (2.4) with the excess Helmholtz free energy

$$\sigma = \int_{-\infty}^0 \left[\mathcal{F}(\rho) + \frac{A}{2} \left(\frac{d\rho}{dz} \right)^2 - \mathcal{F}(\rho_v) \right] dz + \int_0^{\infty} \left[\mathcal{F}(\rho) + \frac{A}{2} \left(\frac{d\rho}{dz} \right)^2 - \mathcal{F}(\rho_l) \right] dz, \quad (2.5)$$

provided we take the dividing surface ($z=0$) as the location of the Gibbs dividing surface, given through

$$\int_{-\infty}^0 [\rho(z) - \rho_v] dz + \int_0^{\infty} [\rho(z) - \rho_l] dz = 0. \quad (2.6)$$

Considering σ as a functional of $\rho(z)$ we get an equation for the profile $\rho(z)$ which minimizes σ under the constraint (2.6):

$$A \frac{d^2}{dz^2} \rho = \frac{dW(\rho)}{d\rho} = \mu(\rho(z)) - \mu, \quad (2.7)$$

with the thermodynamic potential $\mu(\rho) = \partial \mathcal{F} / \partial \rho$

Eq. (2.7) has a first integral (since $\rho(z) = \rho_l$ or ρ_v at $z = \pm \infty$)

$$\frac{A}{2} \left(\frac{d\rho}{dz} \right)^2 = W(\rho). \quad (2.8)$$

With (2.8) we get that the surface tension of the equilibrium profile is

$$\sigma = \int_{-\infty}^{\infty} A \left(\frac{d\rho}{dz} \right)^2 dz = \int_{-\infty}^{\infty} 2 W(\rho) dz = \int_{\rho_v}^{\rho_l} d\rho \left(2A W(\rho) \right)^{1/2}. \quad (2.9)$$

We note that in this theory the surface tension σ is the result of two equal contributions: the direct free energy associated with the gradient and the free energy which is a consequence of the fact that in the interface region $W(\rho)$ is not at its minimum as it is in the bulk phases. The last expression on the right-hand side of (2.11) is especially useful because it does not require the knowledge of $\rho(z)$ explicitly. When we use the van der Waals equation of state for the chemical potential close to the critical point (2.7) can be solved, yielding the classical van der Waals profile¹

$$\rho(z) = \frac{1}{2}(\rho_l + \rho_v) - \frac{1}{2}(\rho_l - \rho_v) \tanh(z/2\xi_{cxc}), \quad (2.10)$$

where ξ_{cxc} is the correlation length in the homogeneous bulk phases, which diverges near criticality as $\xi_{cxc} \sim |T_c - T|^{-\nu}$ ($\nu = 1/2$). Apart from a non-universal amplitude and scale the classical van der Waals profile has a universal, system independent, form. The width of the profile diverges near criticality as ξ_{cxc}

diverges, and the surface tension calculated from (2.8) vanishes as $\sigma \sim |T_c - T|^\mu$, where $\mu = 3/2$.

The van der Waals theory is closely related to the Ornstein-Zernike theory for the correlation functions⁷. Let $\rho(r, R)$ be the density of pairs of molecules at $r = (x, y, z)$ and $R = (X, Y, Z)$. We define a pair-correlation function $G(r, R)$ as⁸

$$G(r, R) = [\rho(r, R) - \rho(z)\rho(Z)]/m^2 \quad (2.11)$$

For distances $|r - R|$ large compared to the intermolecular distance, $\rho(r, R)$ will vary only slowly with r . Considering $G(r, R)$ as the local density at r which is perturbed by the existence of a particle at R , one obtains in analogy with (2.7)

$$A \nabla^2 \rho(r, R) = \mu(\rho(r, R)) - \mu. \quad (2.12)$$

Subtraction of (2.12) and (2.7) yields an equation for the pair-correlation function $G(r, R)$

$$m^2 A \nabla^2 G(r, R) = \mu(\rho(r, R)) - \mu(\rho(z)). \quad (2.13)$$

Since $G(r, R)$ is small in the region where (2.12) holds we expand the right-hand side of (2.13) in a Taylor series around $\rho(z)$ and linearize, so as to obtain

$$A \nabla G(r, R) = \frac{\partial \mu(\rho(z))}{\partial \rho(z)} G(r, R) = \frac{1}{\chi(\rho(z))} G(r, R). \quad (2.14)$$

Substituting (2.3) into (2.13) we get for the correlation function in an interface

$$\left[\nabla^2 - \xi^{-2}(\rho(z)) \right] G(r, R) = 0. \quad (2.15)$$

In a uniform system of density ρ , ξ is a constant and (2.15) reduces to the Ornstein-Zernike equation. The resulting correlation function

$$G_{OZ}(r - R) \propto \frac{e^{-|r - R|/\xi}}{|r - R|} \quad (2.16)$$

has the well-known Ornstein-Zernike form. This justifies the identification (2.3).

The van der Waals theory of interfacial phenomena has a number of shortcomings. In the first place the van der Waals theory is a mean-field theory (showing itself by the classical critical exponents), and as such it is not able to take into account correctly the role of the fluctuations in the neighbourhood of the critical point. In relation to this we stress the fact that the van der Waals theory is independent of the dimensionality of the system. In the second place the van der Waals theory completely neglects the capillary fluctuations of the interface and as a consequence it will never show a diverging interface width in zero external field.

A recent development in the van der Waals theories tries to remedy the strictly classical behaviour. Fisk and Widom⁷ incorporated the correct scaling forms for the chemical potential $\mu(p)$, the compressibility $\chi(p)$, and the correlation

length $\xi(\rho)$, into the theory, and allow for the use of the correct non-classical critical exponents. Furthermore, they provide a method to construct an analytical expression for $W(\rho)$ for densities inside the coexistence region. Their approach, however, is only a phenomenological improvement over the classical theory, and it does not provide a systematic way to deal with the critical phenomena. In the van der Waals theory A is strictly independent of ρ (and derivatives of ρ). In reality this certainly is not true, as we see from the behaviour of (2.3) near the critical point⁹. There A diverges as $[(T_c - T)/T_c]^{-\nu\eta}$ as function of temperature, and it will be a non-analytic function of the density as well. The exponent η measures the deviation of the correlation function from Ornstein-Zernike behaviour. It has in reality a value very close to zero, so digressions from the Ornstein-Zernike theory are small and the errors made by taking A constant are thought to be small. In the Fisk-Widom form of the van der Waals theory the coefficient A is still taken as constant. The Fisk-Widom theory also leads to universal density profiles, but it does not include the effects of capillary waves either.

Van Leeuwen and Sengers^{2,3,8,10} have calculated the effects of an external field on the interfacial profile, in the spirit of the theory of Fisk and Widom. They consider gravitational potentials of the form gz . This gravity field turns up in the equation for the density profile as a simple shift of the chemical potential μ , which is the ordering field of the liquid-vapour phase transition, thus giving instead of (2.7)

$$A \frac{d^2}{dz^2} \rho = \mu(\rho(z)) - \mu + gz. \quad (2.17)$$

In the equation (2.15) for the correlation function $G(r, R)$ the gravity is present only implicitly through the dependence of $\rho(z)$ on the gravitational field. The gravity not only affects the interface, but also the bulk phases itself, because of the fact that the compressibility is large in the neighbourhood of the critical point. For densities outside the coexistence region van Leeuwen and Sengers use an explicit phenomenological scaling form of the equation of state, whereas inside this region the Fisk-Widom theory is used to construct the function $W(\rho)$. As a result of gravity even at and above the critical point the interface width stays finite. Although this theory also lacks the possibility to include capillary wave effects adequately, the idea to consider an interface in an external field is attractive, because the capillary wave divergence can be controlled by means of an external field.

A theory which treats the influence of fluctuations around a mean-field theory in a systematic and consistent way is the renormalization-group approach¹¹. This theory starts from the Landau-Ginzburg-Wilson Hamiltonian density and calculates the effect of the fluctuations on the partition function and correlation functions. In the Hamiltonian density a function $W(\rho)$ occurs which is equivalent to the function $W(\rho)$ in eq. (2.2). As we are interested in (or confined to) the critical region the

choice for $W(\rho)$ is very simple, namely

$$W(\rho) = a\rho^2 + b\rho^4 + \dots, \quad (2.18)$$

which is equivalent to the so called ϕ^4 -theory. The mean-field approximation can be found in this theory by approximating the integrations in the partition function by the term which maximizes the integrand.

Ohta and Kawasaki¹² have carried out a renormalization calculation for the interface near four dimensions in the form of a systematic series expansion, known as the ϵ -expansion, where $\epsilon=4-d$. Although the convergence of the expansion is problematic one obtains results for $d=3$ by taking $\epsilon=1$. The calculation of Ohta and Kawasaki gives the influence of fluctuations around the optimal profile in the zero field case, as it is determined by an equation of the type (2.7), and they also obtain results for the surface tension^{12,13}, via a formula like (2.5). The first-order approximation for the critical exponent μ is

$$\mu = \frac{3}{2} - \frac{1}{4}\epsilon \quad (2.19)$$

which is surprisingly good in all dimensions (exact in $d=2$ and $d=4$, nearly exact in $d=3$, where $\mu \approx 1.26$). The divergences due to the capillary waves are in principle present in the renormalization theory. When considering a theory in the ϵ -expansion the effect of capillary waves is not important because of the expansion near $d=4$. When putting $\epsilon=1$ the capillary-wave divergences are not recovered in any order in ϵ . Jasnow and Rudnick¹⁴ have tried to connect the renormalization theory of the interface and the capillary wave theory. They however did not include compressibility effects and as a result they find a non-universal density profile which diverges at the critical point.

3. Outline

The subjects treated in this thesis belong to various aspects of interfacial phenomena. They all have one feature in common: The liquid-vapour interface in the problem is influenced by an external field. In our case this external field is either the gravitational field or a field caused by the presence of a substrate. The thesis can be roughly divided into two parts. In the first part (chapter II-IV) a theoretical analysis is given of the interface near criticality. In the second part we study the interface by means of molecular-dynamics simulation far from the critical point, to avoid distortion effects, due to the large compressibility, and to see most purely the effect of capillary fluctuations.

In chapter II we study the interface in the presence of an external gravity-like potential in an ϵ -expansion, which is based on the theory of Ohta and Kawasaki¹². This theory gives the smooth cross-over from the density profiles below the critical

temperature to the density profiles above T_c . The profiles are universal in the sense that microscopic details of the interaction do not matter, but they have in comparison with the zero field case one additional parameter, which describes the cross-over. In the zero-gravity limit the results of Ohta and Kawasaki are recovered.

In chapter III we use the ϵ -expansion to calculate to first order in ϵ the surface tension associated with the density profiles calculated in chapter II. When calculating the surface in an external field we do not want to attribute the effects of the distortion of the bulk phases to the surface tension. Moreover, the integrals in (2.5) do not even converge when a gravitational potential is present. The idea however to evaluate σ as the integral over the difference of the actual free energy of the interface and the free energy of a hypothetical system, which is formed by two bulk phases divided by a sharp surface like in (2.5), remains possible. What reference profile we should take to get a consistent definition of the surface tension is not directly clear. The ϵ -expansion is able to discriminate between possible candidates for the reference profile, because some choices give non-convergent theories. A good reference profile leads to a ϵ -expansion which in principle can be extended to arbitrary order in ϵ . In chapter III we define a reference profile as the profile formed by the densities we get when we consider for a certain z -position a uniform system in a constant external field of strength gz . Below T_c the reference profile has a jump in $z=0$. This jump decreases on approach of criticality and is zero at and above the critical point. The reference profile approaches the real profile only sufficiently far above T_c . As a result of this definition the surface tension does not vanish at the critical temperature but at a temperature slightly above T_c when its gradients in the density profile are negligible.

In chapter IV we calculate in a Fisk-Widom like approach the correlations along and perpendicular to the interface in the presence of an external field. These calculations form an extension of the theory of van Leeuwen and Sengers⁸ who have calculated the density profiles in a scaled squared-gradient theory above as well as below T_c . The theory is restricted to a region very close to the critical point. This region is so small that experiments are on the edge of feasibility. Nevertheless the distortion effect due to the large compressibility of the nearly critical phases is a real effect, which in practice prevents that the interface diverges at criticality. Below the critical temperature the transverse correlations are found to approach the capillary length for temperatures relatively far from criticality (but still in the critical region). This capillary length diverges in the limit of zero gravity, denoting the development of long-ranged correlations in absence of a gravitational field. The correlation length perpendicular to the interface has two maxima in the wings of the density profile and a local minimum in the center. The calculations are complemented with approximate expressions for the limiting behaviour of the correlation profiles.

In chapter V and VI we discuss molecular-dynamics simulations of interfaces in two dimensions (for a Lennard-Jones fluid) far away from the critical temperature. In chapter V, we consider the effects of the system-size on suppression of the capillary waves when no external field is present, and we measure the development of long-ranged correlations along the interface as first predicted by Wertheim¹⁴. In chapter VI we add a gravitational potential to the simulation system, and measure how the capillary waves on the interface are suppressed by the external field. The results of chapters V and VI essentially confirm the capillary wave picture.

The last chapter treats a subject which stands somewhat apart from the other subjects in this thesis. We study in chapter VII how the adsorption of a fluid on a substrate varies when changing the substrate-fluid interactions. Thermodynamically the stable state of the system changes, depending on the strength of the substrate-fluid interactions (or also on the temperature), from a state with a microscopically thin layer of adsorbed atoms to a state with a macroscopically thick layer. At the point where the character of the stable state changes, there is a phase transition, called the wetting transition. Theoretically this transition can be continuous or of first order for systems with short-ranged interactions. For small substrate-fluid interactions the wall prefers a vapour phase and we can have a phase transition analogous to the wetting transition, characterized by a microscopic vapour layer on the substrate which changes to a macroscopic layer at the drying transition. By means of molecular-dynamics simulations we determine for realistic short-range interactions the interfacial profiles between the various coexisting phases and the location of both phase transitions.

References

- 1) J.S. Rowlinson and B. Widom, *Molecular Theory of Capillarity* (Clarendon, Oxford, 1982).
- 2) J.M.J. van Leeuwen and J.V. Sengers, *Physica* **128A** (1984) 99.
- 3) J.V. Sengers and J.M.J. van Leeuwen, *Physica* **116A** (1982) 345.
- 4) F.P. Buff, R.A. Lovett and F.H. Stillinger, *Phys. Rev. Lett.* **15** (1965) 621.
- 5) J.D. van der Waals, *Z. Physik. Chem.* **13** (1894) 657.
- 6) J.W. Cahn and J.E. Hilliard, *J. Chem. Phys.* **42** (1958) 93.
- 7) S. Fisk and B. Widom, *J. Chem. Phys.* **50** (1969) 3219.
- 8) J.M.J. van Leeuwen and J.V. Sengers, *Physica* **138A** (1986) 1.

- 9) B. Widom in *Phase Transitions and Critical Phenomena*, vol. 2, C. Domb and M.S. Green, eds. (Academic Press, New York, 1972), p. 79.
- 10) J.M.J. van Leeuwen and J.V. Sengers, *Physica* **132A** (1985) 207.
- 11) D. Jasnow, *Rep. Progr. Phys.* **47** (1984) 1059.
- 12) T. Ohta and K. Kawasaki, *Progress of Theor. Phys.* **58** (1977) 467.
- 13) E. Brézin and S. Feng, *Phys. Rev. B* **29** (1984) 472.
- 14) D. Jasnow and J. Rudnick, *Phys. Rev. Lett.* **41** (1978) 698.
- 15) M.S. Wertheim, *J. Chem. Phys.* **65** (1976) 2377.

CHAPTER II

**AN ϵ - EXPANSION FOR THE INTERFACIAL PROFILE
IN AN EXTERNAL FIELD**

ABSTRACT

The interfacial profile for the order parameter is calculated for a system with a LGW-Hamiltonian extended with an external field coupling to the order parameter. The calculation is restricted to the vicinity of the critical point and is carried out to first order in the ϵ -expansion. The profile is found to be a universal function of the scaled distance and temperature, such that the potential parameter is absorbed in the scaling. The field localizes and distorts the profile and both effects are incorporated correctly to order ϵ .

1. Introduction

The formation of an interface between two coexisting phases is an outstanding problem of statistical physics. In particular the onset of the interface near criticality has been subject of many theoretical investigations¹. Some time ago Ohta and Kawasaki² constructed a theory for the interface on the basis of an ϵ -expansion for critical phenomena. Although such a theory does not lead to realistic interfacial profiles it is the first case, where a discussion could be based on a theory which acknowledges all the subtleties of the critical phenomena. In the same spirit they calculated the surface tension associated with the profile up to first order in $\epsilon=4-d$. This calculation has later been simplified by Brézin and Feng³.

A fundamental shortcoming of the ϵ -expansion for an interface is that it cannot be applied to three-dimensional systems ($\epsilon=1$). For $d \leq 3$ a new divergency occurs due to the capillary waves, which cause the interfacial width to diverge (although very weakly) in an infinite system⁴. This divergency is not a typical critical phenomenon, but appears all along the coexistence line between the two phases. In practice either finite size or an external field cuts off the capillary waves and keeps the interfacial width finite. Jasnow and Rudnick⁵ have discussed the role of a stabilizing field in the context of the renormalization theory for a $d=3$ system. They find that the interfacial profile is the result of a convolution of an intrinsic profile (as exists for $d>3$) and a Gaussian broadening, of which the width is controlled by the strength of the stabilizing field. The explicit dependence of the interface on the external field is seen by these authors as a lack of universality.

The external field, however not only localizes the interface, but also distorts it. Such effects are left out of the calculation of Jasnow and Rudnick. The distortion will become increasingly important when one approaches criticality (from below T_c) as the phases become more and more susceptible to a field. In fact even above T_c an "interface" will survive, which is completely induced by the field and is not a result of spontaneous symmetry breaking any more.

In this chapter we direct our attention to these distortion effects, by studying the ϵ -expansion of the profile in a weak external field. Van Leeuwen and Sengers^{6,7} have shown that these distortion effects are to be expected in a very narrow regime around criticality. In this regime the interface is already so broad that capillary waves have a minor influence. Further below T_c the bounding of the capillary waves amplitudes by the field becomes more important and in this sense our work is complementary to that of Jasnow and Rudnick.

In the theory no sharp distinction between distortion and localizing effects can be made. Approaching the problem from a higher dimension ($d=4$) all excitations with respect to the mean field profile are treated systematically including those, which are blamed for the divergence of the interfacial width in absence of the

field. In the strict ϵ -expansion the problem with localization of the interface as it exists for $d \leq 3$ does not appear. It is only visible when one would consider $d \leq 3$ in intermediate stages of the calculation.

We construct the ϵ -expansion of the interface in a field following closely the method outlined by Ohta and Kawasaki². The main difference is that integrals which can be done analytically in the field free case, now have to be done numerically. This requires also that we have to reformulate the subtraction techniques needed in the renormalization process.

Although our purpose is to study the interface in a fluid we will use in this chapter the language for magnetic systems. The advantage is the explicit up-down symmetry and the closer connection with the usual renormalization theories^{8,9,10}.

The organization of the remainder of the chapter is as follows. In section 2 we derive the differential equation for the order-parameter profile, and discuss the divergences occurring in the theory. These divergences are removed by a proper choice of the renormalization constants of the homogeneous theory. Then the theory is free of divergences for $d < 4$. When $\epsilon = 4 - d$ approaches zero relatively harmless divergences in ϵ appear which can be shown to cancel on the basis of the large transverse momentum behaviour of the Green's function.

In order to facilitate the numerical integration of the Green's functions we develop in section 4 a perturbation expansion valid for small gradients, through which we can evaluate the asymptotic contributions to the integrals analytically. In section 4 we introduce scaled parameters such that the equation for the order-parameter profile is brought into its universal form. In section 5 we calculate the mean field profile in a gravitational field. In section 6 we outline the method for solving the Green's function and present the results of the calculations. The results for the renormalized order-parameter profile are given in section 7 and the paper closes with a discussion of the results.

2. The equation for the order-parameter profile

The calculation of the equation for the magnetization density profile of an interface in an external field $H(r)$ is a problem similar to the calculation of the equation of state in a homogeneous system. Following Ohta and Kawasaki² we derive this equation in the two-phase region from the Landau-Ginzburg-Wilson (LGW) Hamiltonian for the renormalized local order parameter $S(r)$,

$$\mathcal{H}(S) = \int d^d r \left\{ \frac{1}{2} Z(u) (\nabla S(r))^2 + \frac{1}{2} (t Z_2(u) + \delta t) S(r)^2 + \frac{u}{4!} Z_4(u) S(r)^4 - H(r) S(r) \right\}, \quad (2.1)$$

where the renormalization constants $Z(u)$, $Z_2(u)$, $Z_4(u)$ and δt can be calculated by renormalizing the theory at zero momentum. t is a measure of the reduced temperature difference $(T - T_c)/T_c$ and u is the dimensionless renormalized coupling constant (the subscript c denotes the value at criticality).

In the field free system ($H(r)=0$) the expectation value of the local order parameter $S(r)$ vanishes at the critical temperature ($t=0$). When an external field is included, however, this field will induce a non-zero magnetization even above T_c . In this chapter we will take the external field $H(r)$ to be similar to the gravitational potential for fluids

$$H(z) = gz, \quad (2.2)$$

where the field is directed along the z -axis of the system. The mean magnetization density $M(z)$,

$$M(z) = \langle S(z) \rangle, \quad (2.3)$$

will be a function of z , corresponding to a magnetization along the direction in which the magnetic field $H(z)$ varies. For $T < T_c$ the profile $M(z)$ survives even when $g \rightarrow 0$ and we will then speak about $M(z)$ as an interface.

In principle we can evaluate the right-hand side of (2.3) by a Feynman graph expansion. It is however much more convenient to introduce first a field $\psi(r)$ which has zero expectation value by construction¹⁰⁻¹²,

$$\psi(r) = S(r) - M(r). \quad (2.4)$$

Expanding the Hamiltonian (2.1) in the new variables $\psi(r)$ we get

$$\mathcal{H}(\psi) = \sum_{n=0}^{\infty} \int d\mathbf{r}_1 \cdots d\mathbf{r}_n \frac{1}{n!} \mathcal{H}^{(n)}(\mathbf{r}_1, \dots, \mathbf{r}_n) \psi(\mathbf{r}_1) \dots \psi(\mathbf{r}_n), \quad (2.5)$$

where

$$\mathcal{H}^{(n)}(\mathbf{r}_1, \dots, \mathbf{r}_n) = \frac{\delta \mathcal{H}(S)}{\delta S(\mathbf{r}_1) \dots \delta S(\mathbf{r}_n)} \Big|_{\{S\}=\{M\}}. \quad (2.6)$$

Explicitly we have

$$\begin{aligned} \mathcal{H}^{(0)} = \int d\mathbf{r} \left\{ \frac{1}{2} Z(u) (\nabla M(\mathbf{r}))^2 + \frac{1}{2} (t Z_2(u) + \delta t) M(\mathbf{r})^2 \right. \\ \left. + \frac{u}{4!} M(\mathbf{r})^4 - gz M(\mathbf{r}) \right\}, \end{aligned} \quad (2.7)$$

$$\mathcal{H}^{(1)}(\mathbf{r}_1) = -Z(u) \nabla^2 M(\mathbf{r}_1) + (t Z_2(u) + \delta t) M(\mathbf{r}_1) + \frac{u}{6} Z_4(u) M(\mathbf{r}_1)^3 - gz, \quad (2.8)$$

$$\mathcal{H}^{(2)}(r_1, r_2) = \left[-Z(u)\nabla_1^2 + iZ_2(u) + \delta t + \frac{u}{2}Z_4(u)M(r_1)^2 \right] \delta(r_1 - r_2), \quad (2.9)$$

etc.

By expanding the left-hand side of

$$\langle \psi(r) \rangle = 0 \quad (2.10)$$

in Feynman graphs, we obtain an expansion of the equation of state, which is equivalent to the equation from which one calculates $M(z)$.

To first order in the loop-expansion only the graph in fig. 1 contributes, therefore

$$0 = -Z(u) \frac{d^2}{dz^2} M(z) + (iZ_2(u) + \delta t) M(z) - gz + \frac{u}{6} Z_4(u) M(z)^3 + \frac{u}{2} \frac{M(z)}{V_{d-1}} \text{Tr}\{[\mathcal{H}^{(2)}]^{-1} \delta(z - z')\}_{z=z'}, \quad (2.11)$$

where $V_{d-1} = \int d^{d-1}r_i$ and r_i are the directions perpendicular to the external field.

The renormalization constants are identical to those in the zero field case, which have been evaluated up to the one loop order as^{9,13}

$$Z(u) = 1 + \mathcal{O}(u^2), \quad (2.12a)$$

$$Z_2(u) = 1 + \frac{1}{2}uJ + \mathcal{O}(u^2), \quad (2.12b)$$

$$Z_4(u) = 1 + \frac{3}{2}uJ + \mathcal{O}(u^2), \quad (2.12c)$$

$$\delta t = -\frac{u}{2} \left(\frac{1}{2\pi} \right)^d \int d^d q \frac{1}{q^2}, \quad (2.12d)$$

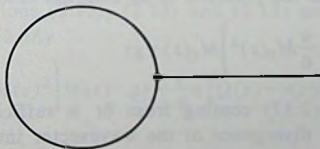


Fig. 1. The one-loop contribution.

where

$$J = \left(\frac{1}{2\pi} \right)^d \int dq \frac{1}{(q^2+1)^2} = \frac{S_{4-\epsilon}}{\epsilon} \left(1 - \frac{\epsilon}{2} + O(\epsilon^2) \right), \quad (2.13)$$

with

$$S_d = \frac{2\pi^{d/2}}{\Gamma(d/2)} \frac{1}{(2\pi)^d}. \quad (2.14)$$

The value of the coupling constant u is chosen to be the fixed point value u^* ¹⁰

$$u^* S_{4-\epsilon} = \frac{2}{3}\epsilon + O(\epsilon^2). \quad (2.15)$$

Substitution of eqs. (2.12) into (2.11) gives as result the following equation, correct up to order u^2 , from which the profile $M(z)$ can be calculated,

$$\begin{aligned} \frac{d^2 M(z)}{dz^2} = & \left(t + \frac{u}{6} M(z)^2 \right) M(z) - gz + \frac{u}{2} J \left(t + \frac{u}{2} M(z)^2 \right) M(z) \\ & + \frac{u}{2} \left[S_{d-1} \int_0^\infty dq_t q_t^{d-2} \Delta G(q_t, z) \right] M(z). \end{aligned} \quad (2.16)$$

The function $\Delta G(q_t, z)$ is a combination of the Green's function $G(q_t, z, z')$ in $z=z'$ and the subtraction term (2.12d):

$$\Delta G(q_t, z) \equiv G(q_t, z, z')|_{z=z'} - \frac{1}{2q_t}, \quad (2.17)$$

where the Green's function $G(q_t, z, z')$ is the solution of the Schrödinger-like equation

$$\left(-\frac{d^2}{dz^2} + t + \frac{u}{2} M_0(z)^2 + q_t^2 \right) G(q_t, z, z') = \delta(z-z') \quad (2.18)$$

and $M_0(z)$ is the lowest order solution of (2.16), i.e. the solution of the classical Van der Waals equation in the presence of an external field,

$$\frac{d^2}{dz^2} M_0(z) = \left(t + \frac{u}{6} M_0(z)^2 \right) M_0(z) - gz. \quad (2.19)$$

The subtraction in (2.17) coming from δt is sufficient to remove in four dimensions the quadratic divergence of the wavevector integration in (2.16). The expression involving $\Delta G(q_t, z)$ in (2.16) is now a convergent integral for all $d < 4$. For $\epsilon = 4 - d \rightarrow 0$ it starts to diverge logarithmically, leading to a $1/\epsilon$ contribution, which is compensated by another $1/\epsilon$ term in (2.16).

To see the cancellation of the $1/\epsilon$ contribution we use the asymptotic behaviour of $\Delta G(q_t, z)$ for large q_t , which is derived in the next section (see (3.13)),

$$\Delta G(q_t, z) = -\frac{v(z)}{4q_t^3} + \mathcal{O}(q_t^{-5}), \quad (2.20)$$

with $v(z)$ given by

$$v(z) = t + \frac{\mu}{2} M_0(z)^2. \quad (2.21)$$

Thus we write the q_t integral in (2.16) as

$$\begin{aligned} \int_0^\infty q_t^{d-2} \Delta G(q_t, z) dq_t &= \int_0^{q_0} q_t^{d-2} \Delta G(q_t, z) dq_t \\ &+ \int_{q_0}^\infty q_t^{d-2} \left(\Delta G(q_t, z) + \frac{v(z)}{4q_t^3} \right) dq_t + \frac{v(z)}{4(d-4)} q_0^{d-4}, \end{aligned} \quad (2.22)$$

where q_0 can be chosen later. Both integrals are now convergent for $\epsilon \rightarrow 0$. Together with the volume factor S_{d-1} the last term of (2.22) contributes to the last term in (2.16) for small ϵ ,

$$\begin{aligned} \frac{\mu}{2} S_{d-1} \frac{v(z)}{4(-\epsilon)q_0^\epsilon} M(z) &= -\frac{\mu}{2} S_{4-\epsilon} v(z) M(z) \\ &\times \left(\frac{1}{\epsilon} + \frac{1}{2} (1-2 \ln 2) - v(z) \ln q_0 \right), \end{aligned} \quad (2.23)$$

where we have used for d near 4

$$\frac{S_{d-1}}{S_d} = 4 \left(1 + \frac{\epsilon}{2} (1-2 \ln 2) \right) + \mathcal{O}(\epsilon^2). \quad (2.24)$$

One now sees that the $1/\epsilon$ exactly compensates the $1/\epsilon$ contribution of the term containing J in (2.16) when the expression (2.13) for J is inserted.

Combining expressions (2.22), (2.23) and (2.13) and using the special value u^* for u we obtain for (2.16)

$$\begin{aligned} \frac{d^2 M}{dz^2} &= \left(t + \frac{\mu}{6} M(z)^2 \right) M(z) - gz + \frac{1}{6} \epsilon \left(Q(z) - v(z) + 2v(z) \ln q_0 \right) M(z) \\ &+ \mathcal{O}(\epsilon^2), \end{aligned} \quad (2.25)$$

in which $Q(z)$ is defined as

$$Q(z) = 8 \int_0^{q_0} q_t^2 \Delta G(q_t, z) dq_t + 8 \int_{q_0}^{\infty} q_t^2 \left(\Delta G(q_t, z) + \frac{v(z)}{4q_t^3} \right) dq_t - (1 - 2 \ln 2) v(z). \quad (2.26)$$

Obviously $Q(z)$ is not independent of q_0 . However, the combination $Q(z) + 2v(z) \ln q_0$ does not depend on q_0 .

The two expressions (2.25) and (2.26), together with (2.17)-(2.19), define the problem in a form free of divergences.

So far the case with an external field ($g \neq 0$) runs parallel to the field free case ($g=0$)². For $g=0$ eq. (2.19) can be solved exactly as well as the associated equation (2.18). For $g \neq 0$ we must rely on numerical methods together with an asymptotic analysis.

3. Perturbation expansion for $G(q_t, z, z')$ for small gradients

We want to solve (2.18) with the boundary condition

$$\lim_{z \rightarrow \pm \infty} G(q_t, z, z') = 0 \quad (3.1)$$

as a function of the wavevector q_t for all z and z' and for many values of the temperature parameter t . For small q_t and z , respectively z' , this can be done most easily by solving (2.18) numerically. For large q_t and z values, it is advantageous to solve (2.18) analytically, so that we can carry out the q_t integration analytically in a large domain. Therefore we consider the case that $v(z)$, defined in (2.21), is a slowly varying function of z . This happens for large z , where $M_0(z)$ varies slowly and for large q_t where $M_0(z)$ is immaterial. In these regions we make, at a fixed temperature t , an expansion of $v(z) + q_t^2$ around z' ,¹⁴

$$v(z) + q_t^2 = (v(z') + q_t^2) \{ 1 + X_1(z')s + X_2(z')s^2 + \dots \}, \quad (3.2)$$

where

$$s = (v(z') + q_t^2)^{1/2} (z - z') \quad (3.3)$$

and

$$X_n(z') = \frac{v^{(n)}(z')}{(v(z') + q_t^2)^{(n+2)/2}}. \quad (3.4)$$

$v^{(n)}(z')$ denotes the n -th derivative of $v(z)$ with respect to z , taken in $z = z'$.

Substitution of (3.2) into (2.18) yields

$$\left(-\frac{d^2}{ds^2} + (1 + X_1 s + X_2 s^2 + X_3 s^3 + \dots) \right) G(s) = \delta(s), \quad (3.5)$$

where $G(s)$ has been defined as

$$G(s) = (v(s) + q_t^2)^{1/2} G(q_t, z, z'). \quad (3.6)$$

An expansion for $G(s)$ can easily be obtained by substituting the series

$$G(s) = g^{(0)}(s) + X_1 g^{(1,1)}(s) + X_1^2 g^{(1,2)}(s) + X_2 g^{(2,1)}(s) + \dots \quad (3.7)$$

into eq. (3.5)

We obtain now the following set of equations for $g^{(n,m)}(s)$:

$$\begin{aligned} \frac{d^2}{ds^2} g^{(0)}(s) &= g^{(0)}(s), \\ \frac{d^2}{ds^2} g^{(1,1)}(s) &= g^{(1,1)}(s) + s g^{(0)}(s), \\ \frac{d^2}{ds^2} g^{(1,2)}(s) &= g^{(1,2)}(s) + s g^{(1,1)}(s), \\ \frac{d^2}{ds^2} g^{(2,1)}(s) &= g^{(2,1)}(s) + s^2 g^{(0)}(s). \end{aligned} \quad (3.8)$$

These equations can be solved subject to the boundary conditions following from $G(0) = \lambda(q_t, z')$ and $g(\pm\infty) = 0$. The multiplicative factor $\lambda(q_t, z')$ will be chosen later to meet the requirement that the derivative of $G(s)$ with respect to s has a jump 1 in $s=0$. The result is

$$G(s) = \lambda(q_t, z') e^{-s} \left\{ 1 - \frac{1}{4} X_1 (s + s^2) + \frac{1}{96} X_1^2 (15s + 15s^2 + 10s^3 + 3s^4) - \frac{1}{12} X_2 (3s + 3s^2 + 2s^3) + \dots \right\} \quad (s > 0), \quad (3.9a)$$

$$G(s) = \lambda(q_t, z') e^{+s} \left\{ 1 + \frac{1}{4} X_1 (-s + s^2) + \frac{1}{96} X_1^2 (-15s + 15s^2 - 10s^3 + 3s^4) \right\} \quad (s < 0).$$

$$-\frac{1}{12}X_2(-3s+3s^2-2s^3)+\dots\} \quad (s<0), \quad (3.9b)$$

$\lambda(q_i, z')$ follows from the condition that

$$G(0^-)-G(0^+) = 1 \quad (3.10)$$

and can therefore be evaluated to be

$$\lambda(q_i, z') = \frac{1}{2}\left\{1 - \frac{1}{4}X_2 + \frac{5}{32}X_1^2 - \frac{3}{4}X_4 + \frac{21}{32}X_2^2 - \frac{45}{8}X_6 + \dots\right\}. \quad (3.11)$$

The value of interest for us is $G(0)$, because we need $G(q_i, z, z')$ in $z=z'$ as one sees from (2.17). This value is equal to $\lambda(q_i, z')$, given in (3.11). It can be calculated once the zeroth order profile $M_0(z)$ has been determined (numerically) from (2.19) and the values of $X_n(z')$ have been found according to (3.4). Combining (3.6), (3.11) and (2.17) we find

$$\Delta G(q_i, z) = \frac{1}{2(q_i^2 + \nu(z))^{1/2}} \left\{ 1 - \frac{1}{4}X_2 + \frac{5}{32}X_1^2 - \frac{3}{4}X_4 + \frac{21}{32}X_2^2 - \frac{45}{8}X_6 + \dots \right\} - \frac{1}{2q_i}. \quad (3.12)$$

We will use the result (3.12) in the regions of large q_i , and of large z , where the small gradient expansion is valid, to supplement the values, which can be found by direct numerical integration of (2.18). The integration over q_i occurring in (2.26) can be carried out analytically from $q_f(z)$ to infinity. $q_f(z)$ is the value above which the small gradient expansion is valid. The results of the integrations are given in Appendix A.

Note that from (3.12) we have

$$\Delta G(q_i, z) = -\frac{\nu(z)}{4q_i^3} + O(q_i^{-5}) \quad (q_i \text{ large}) \quad (3.13)$$

as we have used in the previous section (see (2.20)). The result (3.12) is generally applicable e.g. in higher order calculations, since the dependence of $\Delta G(q_i, z)$ on $\nu(z)$ occurs only through the $X_n(z')$.

4. Scaling of the equation for $M(z)$

Before we enter into the numerical calculation of $M_0(z)$ and $\Delta G(q_i, z)$ it is convenient to introduce scaled variables $\bar{M}(\bar{z})$, \bar{z} and \bar{t} , such that

$$M = \mu_i \bar{M}, \quad z = \zeta_i \bar{z}, \quad t = \theta_i \bar{t}, \quad (4.1)$$

with

$$\mu_t = \left(\frac{u}{6} \right)^{-3/8 - 3\epsilon/64} g^{1/4 - 3\epsilon/32}, \quad (4.2a)$$

$$\zeta_t = \left(\frac{u}{6} \right)^{-1/8 - \epsilon/64} g^{-1/4 - \epsilon/32}, \quad (4.2b)$$

$$\theta_t = \left(\frac{u}{6} \right)^{1/4 - \epsilon/96} g^{1/2 - \epsilon/48}. \quad (4.2c)$$

This choice of the scaled variables scales out all u dependence of (2.25) up to order ϵ and makes it possible to study the behaviour of the profile $\bar{M}(\bar{z})$ as a function of the temperature-like parameter \bar{t} . In terms of the variables defined by (4.1) eq. (2.25) reads

$$\frac{d^2}{d\bar{z}^2} \bar{M}(\bar{z}) = (\bar{t} + \bar{M}(\bar{z})^2) \bar{M}(\bar{z}) - \bar{z} + \frac{1}{6} \epsilon (\bar{Q}(\bar{z}) - \bar{v}(\bar{z})) \bar{M}(\bar{z}) + O(\epsilon^2), \quad (4.3)$$

where the scaled functions $\bar{v}(\bar{z})$ and $\bar{Q}(\bar{z})$ are defined by

$$\bar{v}(\bar{z}) = \bar{t} + 3\bar{M}_0(\bar{z})^2, \quad (4.4)$$

$$\begin{aligned} \bar{Q}(\bar{z}) = & 8 \int_0^1 \bar{q}_t^2 \Delta \bar{G}(\bar{q}_t, \bar{z}) d\bar{q}_t + 8 \int_1^\infty \bar{q}_t^2 \left(\Delta \bar{G}(\bar{q}_t, \bar{z}) + \frac{\bar{v}(\bar{z})}{4\bar{q}_t^3} \right) d\bar{q}_t \\ & - (1 - 2 \ln 2) \bar{v}(\bar{z}), \end{aligned} \quad (4.5)$$

where $\bar{M}_0(\bar{z})$, $\Delta \bar{G}(\bar{q}_t, \bar{z})$ and $\bar{G}(\bar{q}_t, \bar{z}, \bar{z}')$ are given by the scaled equivalences of (2.19), (2.17) and (2.18), respectively,

$$\frac{d^2}{d\bar{z}^2} \bar{M}_0(\bar{z}) = (\bar{t} + \bar{M}_0(\bar{z})^2) \bar{M}_0(\bar{z}) - \bar{z}, \quad (4.6)$$

$$\left(-\frac{d^2}{d\bar{z}^2} + \bar{v}(\bar{z}) + \bar{q}_t^2 \right) \bar{G}(\bar{q}_t, \bar{z}, \bar{z}') = \delta(\bar{z} - \bar{z}'), \quad (4.7)$$

$$\Delta \bar{G}(\bar{q}_t, \bar{z}) = \bar{G}(\bar{q}_t, \bar{z}, \bar{z}')|_{\bar{z}' = \bar{z}} - \frac{1}{2\bar{q}_t}. \quad (4.8)$$

Note that we have chosen for q_0 which appears in (2.23), the value

$$q_0 = \zeta_t^{-1}. \quad (4.9)$$

The whole problem of finding $\bar{M}(\bar{z})$ is now completely defined by (4.3)-(4.8).

These equations do not depend on u and g , and give rise to universal magnetization profiles $\bar{M}(\bar{z})$ only depending on \bar{z} and \bar{t} .

We can also reduce the number of parameters in eq. (2.29) by scaling out the temperature-like variable t . This scaling is especially suited to study the behaviour of the order-parameter profile in the regime of very small fields.

For this purpose we introduce the scaled variables \bar{M} , \bar{z} and \bar{g} such that

$$M = \mu_g \bar{M}, \quad z = \zeta_g \bar{z}, \quad g = \gamma_g \bar{g} \quad (4.10)$$

with

$$\mu_g = \left(\frac{u}{6}\right)^{-1/2} |t|^{1/2 - \epsilon/6}, \quad (4.11a)$$

$$\zeta_g = |t|^{-1/2 + \epsilon/12} \quad (4.11b)$$

$$\gamma_g = \left(\frac{u}{6}\right) |t|^{2 + \epsilon/48}. \quad (4.11c)$$

Substitution of (4.10) into (2.25) yields the scaled equation for the profile $\bar{M}(\bar{z})$ which is independent of t and u ,

$$\begin{aligned} \frac{d^2}{d\bar{z}^2} \bar{M}(\bar{z}) = & (-1 + \bar{M}(\bar{z})^2) \bar{M}(\bar{z}) - \bar{g} \bar{z} + \frac{1}{6} \epsilon (\bar{Q}(\bar{z}) - \bar{v}(\bar{z})) \bar{M}(\bar{z}) \\ & + O(\epsilon^2) \quad (t < 0), \end{aligned} \quad (4.12)$$

where

$$\bar{v}(\bar{z}) = -1 + 3\bar{M}_0(\bar{z})^2, \quad (4.13)$$

$$\begin{aligned} \bar{Q}(\bar{z}) = & 8 \int_0^1 \bar{q}_t^2 \Delta \bar{G}(\bar{q}_t, \bar{z}) d\bar{q}_t + 8 \int_1^{+\infty} \bar{q}_t^2 \left[\Delta \bar{G}(\bar{q}_t, \bar{z}) + \frac{\bar{v}(\bar{z})}{4\bar{q}_t^3} \right] d\bar{q}_t \\ & - (1 - 2 \ln 2) \bar{v}(\bar{z}) \end{aligned} \quad (4.14)$$

and $\bar{M}_0(\bar{z})$, $\Delta \bar{G}(\bar{q}_t, \bar{z})$ and $\bar{G}(\bar{q}_t, \bar{z}, \bar{z}')$ follow from

$$\frac{d^2}{d\bar{z}^2} \bar{M}_0(\bar{z}) = (-1 + \bar{M}_0(\bar{z})^2) \bar{M}_0(\bar{z}) - \bar{g} \bar{z}, \quad (4.15)$$

$$\left[-\frac{d^2}{d\bar{z}^2} + \bar{v}(\bar{z}) + \bar{q}_t^2 \right] \bar{G}(\bar{q}_t, \bar{z}, \bar{z}') = \delta(\bar{z} - \bar{z}'), \quad (4.16)$$

$$\Delta \bar{G}(\bar{q}_t, \bar{z}) = \bar{G}(\bar{q}_t, \bar{z}, \bar{z}') \Big|_{\bar{z}' = \bar{z}} - \frac{1}{2\bar{q}_t}. \quad (4.17)$$

Here we have taken for q_0 the value

$$q_0 = \zeta_g^{-1} \quad (4.18)$$

The results of the scaling using \bar{t} can easily be converted into the results for the scaling with \bar{g} as parameter by the formulae

$$\bar{M} = \bar{t}^{-1/2} \bar{M} \left(1 + \frac{\epsilon}{6} \ln \bar{t} \right) + \mathcal{O}(\epsilon^2), \quad (4.19a)$$

$$\bar{z} = \bar{t}^{1/2} \bar{z} \left(1 + \frac{\epsilon}{12} \ln \bar{t} \right) + \mathcal{O}(\epsilon^2), \quad (4.19b)$$

$$\bar{g} = \bar{t}^{-2} \left(1 - \frac{\epsilon}{48} \ln \bar{t} \right) + \mathcal{O}(\epsilon^2). \quad (4.19c)$$

For $\bar{g}=0$ we can compare our results to the analytical results of Ohta and Kawasaki².

5. The classical order-parameter profile

Using the scaled variables defined in (4.1) the mean field magnetization profile is given as a solution of differential equation (4.6). For large \bar{z} this solution behaves as

$$\begin{aligned} \bar{M}_0(\bar{z}) = & \bar{z}^{1/3} + \left(\frac{\bar{t}}{3} \right) \bar{z}^{-1/3} - \frac{1}{3} \left(\frac{\bar{t}}{3} \right)^3 \bar{z}^{-5/3} + \frac{1}{3} \left[\left(\frac{\bar{t}}{3} \right)^4 - \frac{2}{9} \right] \bar{z}^{-7/3} \\ & + \frac{2}{9} \left(\frac{\bar{t}}{3} \right) \bar{z}^{-9/3} - \frac{4}{9} \left[\left(\frac{\bar{t}}{3} \right)^6 - \frac{1}{3} \left(\frac{\bar{t}}{3} \right)^2 \right] \bar{z}^{-11/3} \\ & + \mathcal{O}(\bar{z}^{-13/3}), \quad (\bar{z} \text{ large}). \end{aligned} \quad (5.1)$$

For large \bar{t} however the series (5.1) is slowly converging and we can use this asymptotic formula only for very large \bar{z} . For smaller \bar{z} the magnetization profile $\bar{M}_0(\bar{z})$ can best be calculated numerically from (4.6) for a fixed temperature \bar{t} . The solution is found by a trial and error method. For a guessed initial slope (4.6) is integrated forward, and the guess is adjusted, until the profile and its first derivative are well behaved for all \bar{z} values that we can reach (limited by numerical precision). When the proper limiting profile (5.1) was not reached, we have extended the solution by calculating $\bar{M}_0(\bar{z})$ as a small distortion of the locally homogeneous profile $\bar{M}_0^0(\bar{z})$, which is a solution of

$$0 = (\bar{t} + \bar{M}_0^0(\bar{z})^2) \bar{M}_0^0(\bar{z}) - \bar{z}. \quad (5.2)$$

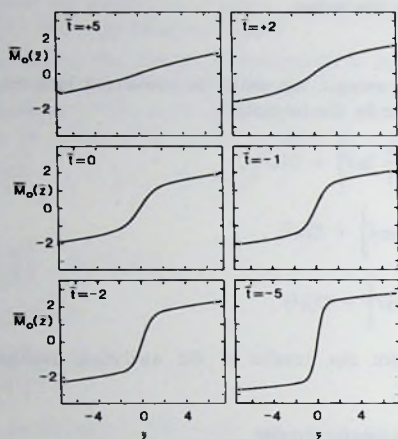


Fig. 2. The classical order-parameter profiles $\bar{M}_0(\bar{z})$ for temperatures above ($\bar{t}=+5, +2$) and below ($\bar{t}=-1, -2, -5$) the critical temperature ($\bar{t}=0$)

We then find $\bar{M}_0(\bar{z})$ as

$$\bar{M}_0(\bar{z}) = \bar{M}_0^0(\bar{z}) \left\{ 1 - \frac{6}{(\bar{t} + 3\bar{M}_0^0(\bar{z})^2)^4} + \dots \right\}. \quad (5.3)$$

As one sees from (4.4), the profiles are antisymmetric around $\bar{z}=0$, so we only have to determine them for positive \bar{z} values.

In fig. 2 we have plotted the zeroth order density profiles for a few selected \bar{t} values, both below and above the critical temperature. When the temperature is lowered, the interface width decreases as could be expected. At $\bar{t}=0$ the zeroth order profile does not vanish, as is the case without an external field present, but this profile is completely induced by the field. For the same reason a profile persists above T_c .

Using the scaling defined by (4.10) we have also calculated the zeroth order profiles for a few values of \bar{g} below the critical temperature (fig. 3). For $\bar{g}=0$ the differential equation (4.15) can be solved analytically yielding the classical van der Waals hyperbolic tangent profile

$$\bar{M}_0(\bar{z}) = \tanh(\bar{z}/\sqrt{2}), \quad \bar{g}=0. \quad (5.4)$$

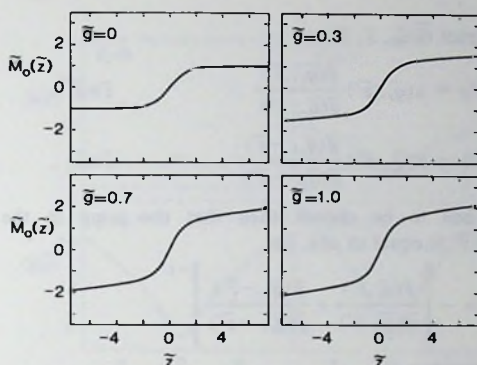


Fig. 3. The classical order-parameter profiles $\bar{M}_0(\bar{z})$ for some values of \bar{g} ($\bar{g}=0, 0.3, 0.7$ and 1).

6. Numerical solution for the Green's function

Now that the zeroth order profile $\bar{M}_0(\bar{z})$ has been calculated we can solve the Green's function $\bar{G}(\bar{q}_t, \bar{z}, \bar{z}')$ and $\Delta\bar{G}(\bar{q}_t, \bar{z})$ from eqs. (4.7)-(4.8), with the aid of an auxiliary function $\bar{g}(\bar{q}_t, \bar{z})$. Following Van Leeuwen and Sengers¹⁴ we consider

$$\left\{ -\frac{d^2}{d\bar{z}^2} + \bar{v}(\bar{z}) + \bar{q}_t^2 \right\} \bar{g}(\bar{q}_t, \bar{z}) = 0, \quad (6.1)$$

with boundary conditions

$$\lim_{\bar{z} \rightarrow -\infty} \bar{g}(\bar{q}_t, \bar{z}) = 0, \quad (6.2)$$

$$\bar{g}(\bar{q}_t, 0) = 1. \quad (6.3)$$

The boundary conditions and the absence of a jump in the derivative are the only differences from $\bar{g}(\bar{q}_t, \bar{z})$ with respect to $\bar{G}(\bar{q}_t, \bar{z}, \bar{z}')$. The solution of (6.1) will diverge exponentially for $\bar{z} \rightarrow -\infty$. The procedure to find $\bar{g}(\bar{q}_t, \bar{z})$ numerically is as follows. First guess a trial slope $\bar{g}'(\bar{q}_t, 0)$ and integrate (6.1) numerically from $\bar{z}=0$ towards both smaller and larger \bar{z} . In general the solution will not satisfy the condition (6.2), but diverges exponentially. When $\bar{g}_1(\bar{q}_t, \bar{z})$ however is a solution of (6.1) then $\bar{g}_1(\bar{q}_t, -\bar{z})$ satisfies (6.1) also. We obtain a solution satisfying the boundary condition (6.2) as the linear combination of $\bar{g}_1(\bar{q}_t, \bar{z})$ and $\bar{g}_1(\bar{q}_t, -\bar{z})$ which cancels out the exponential divergences for $\bar{z} \rightarrow -\infty$. Once we have determined

$\bar{g}(\bar{q}_t, \bar{z})$ we construct $\bar{G}(\bar{q}_t, \bar{z}, \bar{z}')$ as

$$\bar{G}(\bar{q}_t, \bar{z}, \bar{z}') = \lambda(\bar{q}_t, \bar{z}') \frac{\bar{g}(\bar{q}_t, \bar{z})}{\bar{g}(\bar{q}_t, \bar{z}')} , \quad \bar{z} \geq \bar{z}' , \quad (6.4a)$$

$$\bar{G}(\bar{q}_t, \bar{z}, \bar{z}') = \lambda(\bar{q}_t, \bar{z}') \frac{\bar{g}(\bar{q}_t, -\bar{z})}{\bar{g}(\bar{q}_t, -\bar{z}')} , \quad \bar{z} \leq \bar{z}' , \quad (6.4b)$$

where $\lambda(\bar{q}_t, \bar{z}')$ has to be chosen such that the jump in the derivative of $\bar{G}(\bar{q}_t, \bar{z}, \bar{z}')$ in $\bar{z} = \bar{z}'$ is equal to one, i.e.

$$\lambda(\bar{q}_t, \bar{z}') = - \left[\frac{\bar{g}'(\bar{q}_t, \bar{z}')}{\bar{g}(\bar{q}_t, \bar{z}')} + \frac{\bar{g}'(\bar{q}_t, -\bar{z}')}{\bar{g}(\bar{q}_t, -\bar{z}')} \right]^{-1} . \quad (6.5)$$

From (4.8) one sees that

$$\Delta \bar{G}(\bar{q}_t, \bar{z}) = \lambda(\bar{q}_t, \bar{z}) - \frac{1}{2\bar{q}_t} . \quad (6.6)$$

For large \bar{z} , or large \bar{q}_t , the calculation of $\lambda(\bar{q}_t, \bar{z})$ becomes numerically inaccurate. Fortunately in these regions the small gradient expansion developed in section 3 is valid. To be specific we calculate $\Delta \bar{G}(\bar{q}_t, \bar{z})$ for a selected temperature and \bar{z}

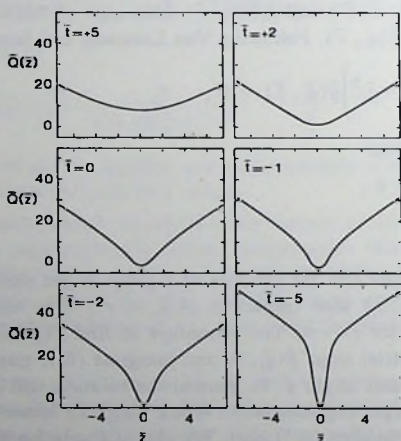


Fig. 4. The function $\bar{Q}(\bar{z})$ for the temperatures $\bar{t} = +5, +2, 0, -1, -2$ and -5 .

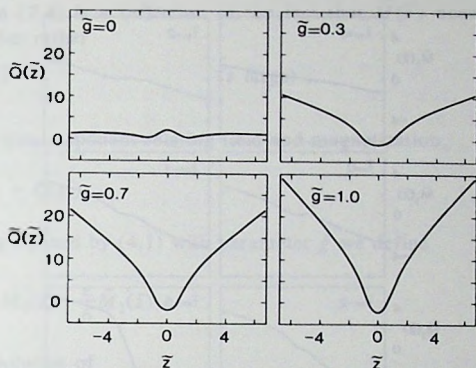


Fig. 5. The function $\bar{Q}(\bar{z})$ for $\bar{g}=0, 0.3, 0.7$ and 1 .

up to the wavenumber $\bar{q}_f(\bar{z})$ numerically, whereas for larger \bar{z} , $\bar{q}_f(\bar{z})$ is smaller, until at a certain value of \bar{z} , $\Delta\bar{G}(\bar{q}_t, \bar{z})$ can be calculated using the asymptotic expansion only. Next we do the integrations over \bar{q}_t occurring in (4.5). For any \bar{z} the integration has to be carried out numerically for \bar{q}_t smaller than $\bar{q}_f(\bar{z})$ and analytically for larger values of \bar{q}_t . The resulting functions $\bar{Q}(\bar{z})$ are shown in fig. 4 for the same selected temperatures as for which the zeroth order profiles $\bar{M}_0(\bar{z})$ are shown in fig. 2.

The functions $\bar{Q}(\bar{z})$ in the scaling with parameter \bar{g} can be calculated similar to the calculation of $\bar{Q}(\bar{z})$. The results for various \bar{g} are shown in fig. 5. In the limit of no external field we reproduce the result of Ohta and Kawasaki.

7. The order-parameter profile to first order in ϵ

We can find the magnetization profile up to order ϵ from (4.3), using the zeroth order profile $\bar{M}_0(\bar{z})$ and the function $\bar{Q}(\bar{z})$, calculated in the previous section. Because eq. (4.3) is only correct up to first order in ϵ , it is consistent to present the magnetization profile $\bar{M}(\bar{z})$ as a series in ϵ .

$$\bar{M}(\bar{z}) = \bar{M}_0(\bar{z}) - \frac{\epsilon}{6} \bar{M}_1(\bar{z}) + \mathcal{O}(\epsilon^2). \quad (7.1)$$

By substitution of (7.1) in (4.3) we obtain the equation for the first order profile $\bar{M}_1(\bar{z})$,

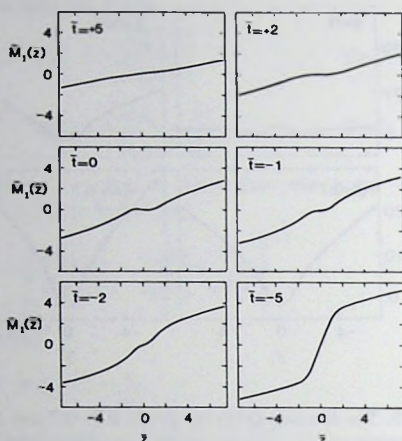


Fig. 6. The first-order profiles $\bar{M}_1(\bar{z})$ for $\bar{t} = +5, +2, 0, -2$ and -5 .

$$\frac{d^2}{d\bar{z}^2} \bar{M}_1(\bar{z}) = \bar{v}(\bar{z})(\bar{M}_1(\bar{z}) + \bar{M}_0(\bar{z})) - \bar{Q}(\bar{z})\bar{M}_0(\bar{z}). \quad (7.2)$$

Eq. (7.2) is solved in the same way as we have determined $\bar{M}_0(\bar{z})$. In fig. 6 the resulting first-order profiles $\bar{M}_1(\bar{z})$ are shown for the same \bar{t} values used previously.

The asymptotic behaviour of $\bar{M}_1(\bar{z})$ can be found easily from the asymptotic behaviour of $\bar{Q}(\bar{z})$. For large \bar{z} the value $\bar{q}_f(\bar{z}) = 0$ (for $\bar{q}_t > \bar{q}_f(\bar{z})$ the small gradient expansion is valid). Thus we can do the integration over \bar{q}_t analytically yielding

$$\bar{Q}(\bar{z}) = \bar{v}(\bar{z}) \ln \bar{v}(\bar{z}) \quad (\bar{z} \text{ large}). \quad (7.3)$$

As $d^2 \bar{M}_1 / d\bar{z}^2 \rightarrow 0$ for large \bar{z} , $\bar{M}_1(\bar{z})$ will behave as

$$\bar{M}_1(\bar{z}) = \bar{M}_0(\bar{z})(\ln \bar{v}(\bar{z}) - 1) \quad (\bar{z} \text{ large}). \quad (7.4)$$

The logarithm in (7.4) is a reflection of the fact that $\bar{M}(\bar{z})$ does not follow the behaviour (5.1) but rather

$$\bar{M}(\bar{z}) \approx \bar{z}^{1/\delta} \quad (\bar{z} \text{ large}), \quad (7.5)$$

where δ is the critical exponent relating field and magnetization,

$$\delta = 3 + \epsilon + \mathcal{O}(\epsilon^2). \quad (7.6)$$

Using the scaling defined by (4.1) with parameter \bar{g} we define

$$\tilde{M}(\tilde{z}) = \tilde{M}_0(\tilde{z}) - \frac{\epsilon}{6} \tilde{M}_1(\tilde{z}). \quad (7.7)$$

$\tilde{M}_1(\tilde{z})$ is now a solution of

$$\frac{d^2}{d\tilde{z}^2} \tilde{M}_1(\tilde{z}) = \tilde{v}(\tilde{z})(\tilde{M}_1(\tilde{z}) + \tilde{M}_0(\tilde{z})) - \tilde{Q}(\tilde{z})\tilde{M}_0(\tilde{z}). \quad (7.8)$$

In fig. 7 the profiles $\tilde{M}(\tilde{z})$ are shown, calculated from (7.8). For $\bar{g}=0$ we get a result that is equivalent up to order ϵ to the result of Ohta and Kawasaki.

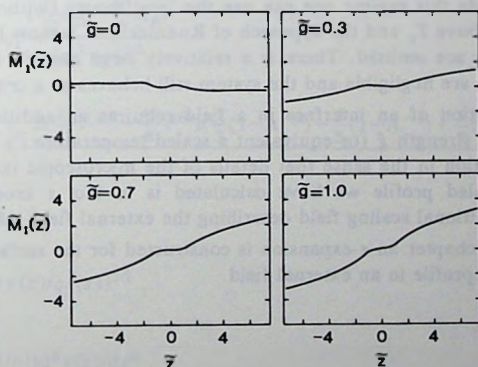


Fig. 7. The first-order profiles $\tilde{M}_1(\tilde{z})$ for $\bar{g}=0, 0.3, 0.7$ and 1 .

8. Discussion

In this chapter we have given a calculation of the order-parameter profile in an external field, following the calculation of Ohta and Kawasaki in the field free system. For $d < 4$ the theory is finite as a result of the same subtractions we need in the homogeneous renormalized system. The divergences arising when we let $\epsilon = 4 - d \rightarrow 0$ are canceled exactly by a subtraction term with the same divergences.

When we formally set $\epsilon = 1$ to get the three dimensional case, everything stays finite even in the zero field case. The divergence of the interfacial width due to the capillary waves is lost in an intermediate stage of the calculation, namely when integrating over q_i in $4 - \epsilon$ dimensions we suppress the capillary waves. Clearly the integration over q_i in three dimensions would lead to a $\ln g$ capillary divergence of the profile width below the critical temperature.

For any finite value of g the capillary waves are suppressed by the field, and no divergence of the interface width occurs⁷ in any dimension.

The transition from the interface below T_c to the field induced magnetization profile above T_c is smooth. The smoothness results from the high susceptibility of the systems with respect to the field, which distorts the interface and keeps it finite even at criticality.

The region where these distortion effects occur is a rather narrow temperature regime around T_c and a rather narrow band around the critical layer $z = 0$ (where $M(0) = 0$). Outside this regime one can use the local theory (without the squared-gradient term) above T_c and the approach of Rudnick and Jasnow below T_c , where distortion effects are omitted. There is a relatively large domain below T_c where distortion effects are negligible and the system still behaves as a critical system.

The description of an interface in a field requires an additional parameter, namely the field strength \bar{g} (or equivalent a scaled temperature \bar{t}) but is otherwise a universal function in the sense that details of the microscopic interaction do not matter. The scaled profile we have calculated is in fact a cross-over function involving an additional scaling field describing the external field influence.

In the next chapter an ϵ -expansion is constructed for the surface tension of an order-parameter profile in an external field.

Appendix A

In this appendix we give the results of the analytical integration over q_i of the

terms appearing in the small gradient expansion of section 3:

$$2 \int_{q_f}^{\infty} q_t^2 dq_t \left(\frac{1}{(q_t^2 + \nu)^{1/2}} - \frac{1}{q_t} + \frac{\nu}{2q_t^3} \right) \\ = \frac{1}{2} \nu (1 - 2 \ln 2) + \nu \ln(1+A) + (1-A) q_f^2. \quad (\text{A.1})$$

$$-2 \int_{q_f}^{\infty} q_t^2 dq_t \frac{\frac{1}{4} X_2}{(q_t^2 + \nu)^{1/2}} = -\frac{\frac{1}{6} \nu^{(2)} (1-A^{-3})}{\nu}. \quad (\text{A.2})$$

$$2 \int_{q_f}^{\infty} q_t^2 dq_t \frac{(\frac{5}{32} X_1^2 - \frac{3}{4} X_4)}{(q_t^2 + \nu)^{1/2}} \\ = \frac{2(\frac{5}{32} \nu^{(1)2} - \frac{3}{4} \nu^{(4)}) (\frac{1}{3} (1-A^{-3}) - \frac{1}{5} (1-A^{-5}))}{\nu^2}, \quad (\text{A.3})$$

$$2 \int_{q_f}^{\infty} q_t^2 dq_t \frac{(\frac{21}{32} X_2^2 - \frac{45}{8} X_6)}{(q_t^2 + \nu)^{1/2}} \\ = \frac{2(\frac{21}{32} \nu^{(2)2} - \frac{45}{8} \nu^{(6)}) (\frac{1}{3} (1-A^{-3}) - \frac{2}{5} (1-A^{-5}) + \frac{1}{7} (1-A^{-7}))}{\nu^3}, \quad (\text{A.4})$$

where

$$A = (1 + \nu(z)/q_f^2(z))^{1/2}, \quad (\text{A.5})$$

and

$$\nu^{(n)} = (1/n!) d^n \nu(z)/dz^n. \quad (\text{A.6})$$

References

- 1) D. Jasnow, Rep. Progr. Phys. **47** (1984) 1059 and references therein.
- 2) T. Ohta and K. Kawasaki, Progress of Theor. Phys. **58** (1977) 467.
- 3) E. Brézin and S. Feng, Phys. Rev. B **29** (1984) 472.
- 4) F.P. Buff, R.A. Lovett and F.H. Stillinger, Phys. Rev. Lett. **15** (1965) 621.
- 5) D. Jasnow and J. Rudnick, Phys. Rev. Lett. **41** (1978) 698.
- 6) J.V. Sengers and J.M.J. van Leeuwen, Physica **116A** (1982) 345.
- 7) J.M.J. van Leeuwen and J.V. Sengers, Physica **132A** (1985) 207.
- 8) D.J. Amit, Field Theory, *The Renormalization Group and Critical Phenomena* (McGraw-Hill, New York, 1978).
- 9) E. Brézin, J.C. LeGuillou and J. Zinn-Justin, in *Phase Transitions and Critical Phenomena*, vol.6, C. Domb and M.S. Green, eds. (Academic Press, New York, 1976), p. 125.
- 10) D.J. Wallace, in *Phase Transitions and Critical Phenomena*, vol. 6, C. Domb and M.S. Green, eds. (Academic Press, New York, 1976), p. 293.
- 11) E. Brézin, D.J. Wallace and K. Wilson, Phys. Rev. B **7** (1972) 232.
- 12) J. Rudnick and D.R. Nelson, Phys. Rev B **13** (1976) 2208.
- 13) E. Brézin, J.C. LeGuillou and J. Zinn-Justin, Phys. Rev. D **8** (1973) 434.
- 14) J.M.J. van Leeuwen and J.V. Sengers, Physica **128A** (1984) 99.

CHAPTER III

**AN ϵ -EXPANSION OF THE SURFACE TENSION
IN AN EXTERNAL FIELD**

ABSTRACT

A system near criticality is considered in a linearly varying potential. With the order-parameter profile, whether induced by the field ($T > T_c$) or spontaneously formed ($T < T_c$), a surface tension can be associated as the difference of the actual free energy and a reference free energy. The reference free energy is taken as that of a locally homogeneous system with varying field strength, which leads to a convergent ϵ -expansion for the surface tension. This surface tension is a universal function of temperature and field strength and is evaluated to first order in ϵ .

1. Introduction

The calculation of the surface tension σ is a problem closely related to the calculation of the interfacial profile between two coexisting phases. Whereas the actual profile only can be measured indirectly, the surface tension σ of an interface is a quantity directly accessible for experiments. Therefore much effort, both experimentally and theoretically, has been given to obtain σ . From experiments it is known that the surface tension in the vicinity of the critical point decreases as a function of temperature, with a universal exponent defined as

$$\sigma(t) = s_0 |t|^\mu \quad (t = (T - T_c)/T_c) \quad (t < 0), \quad (1.1)$$

where $\mu \approx 1.26$.

A calculation of $\sigma(t)$ in the ϵ -expansion has been given by Ohta and Kawasaki¹, and also by Brézin and Feng². In the spirit of their evaluation, we discuss the effects of an external field on the surface tension of interfaces in that field. In our calculation we use the results of the preceding chapter³ on the effects of an external field with respect to the interfacial profile.

The notion of the surface tension on an interface is not unique when an external field is present. In the field-free case the surface tension is defined in terms of the difference in free energy between the actual system and two bulk phases separated by the Gibbs dividing surface⁴. An external field deforms the interfacial profile, but also influences the bulk phases far away from the interface⁵. What one would attribute to the surface tension is to a certain extent a matter of taste and effectiveness in describing the experiments. The issue comes up clearly when one considers an interface in an external field and increases the temperature T , through the critical point T_c to a $T > T_c$. Then the distinction between the coexisting phases forming the interface has disappeared, but a profile induced by the field remains. Should one speak about the surface tension of such an induced "interface" or opt for a definition of surface tension which disappears when the distinction between the interfaces disappears.

Van Leeuwen and Sengers⁶ have proposed a definition on the basis of the squared-gradient theory for the interface. They defined the surface tension as the free-energy difference between the actual system and a hypothetical system in which two bulk phases are joined by a dividing surface with a jump in the order-parameter. This jump is twice the spontaneous order-parameter in a field-free system. Such a definition has the advantage that the actual system may be replaced by the hypothetical system augmented by the surface tension. The effect of the field on the interface is then thought of as a surface tension associated with a sharp dividing surface. The distortion of the bulk phases, being also present in the hypothetical system, is not included in the surface tension and above T_c this

surface tension vanishes, because of the spontaneous jump in the order-parameter vanishes above T_c . This proposal may have advantages in discussing experiments, such as capillary rise, but the main drawback is that the definition is restricted to an approximate theory. In the squared-gradient theory the condition of a jump can easily be implemented as a boundary condition in the differential equation from which the profile is calculated.

In general, there is no local equation of state from which the interface can be calculated as in the squared-gradient theory. We have attempted to follow the definition of the surface tension, sketched above, in the context of the ϵ -expansion, but were led to divergent expressions not compensated by subtractions, due to the non-locality of the equation of state.

Therefore we adopt in this chapter a different reference system for the surface tension which is discussed below.

In this chapter, as in chapter II, we adopt the magnetic language, which is most commonly used in the renormalization theory^{7,8} of critical phenomena, although our main interest is to study the interfacial properties of a liquid-vapour coexisting system in a gravitational field. The connection of the magnetic system (via the lattice gas) with a fluid system is simple:

local magnetization density $M(\mathbf{r})$	- local number density $\rho(\mathbf{r})$;
local free-energy density $\mathcal{F}(\mathbf{r})$	- local pressure $p(\mathbf{r})$;
external field $H(\mathbf{r})$	- chemical potential $\mu(\mathbf{r})$.

In a fluid the gravitational field only changes the chemical potential μ into an effective potential $\mu_{eff}(\mathbf{r})$.

A result of the ϵ -expansion is the possibility to evaluate the free-energy density of a bulk system in a homogeneous external field. Also the equation of state can be evaluated easily in a systematic way and thereby the bulk magnetization of a system in a homogeneous field^{9,10}. We use these known facts to construct a reference system for the actual magnetization profile. For each z , which is the direction along which the external field varies, we compare the free-energy density of the actual system, to that of a bulk system in a homogeneous external field. The value of this homogeneous external field at z is taken to be equal to the value the real external field has locally at z . The magnetization densities associated with this homogeneous field can then be obtained for each z from the equation of state. The reference profile thus formed is called the locally homogeneous profile. For large z or for temperatures above the critical point the gradients in the actual profile are very small, and the locally homogeneous profile is a good approximation for the real profile. Consequently in these regions the free-energy densities do not differ very much, and deviations are restricted to the interfacial region. We define the

surface tension as the integral over z of the free-energy density difference of the actual and the reference system:

$$\frac{\sigma}{k_B T} = \int_{-\infty}^{+\infty} dz \left[\mathcal{F}(z) - \mathcal{F}^B(z) \right], \quad (1.2)$$

where $\mathcal{F}(z)$ is the free-energy density of the actual profile at z , and $\mathcal{F}^B(z)$ is the free-energy density of the reference system at z (the superscript B denotes that \mathcal{F}^B is the free energy of a bulk system). With this definition of the surface tension, we easily see that for zero external field it reduces to the usual definition⁴. One also sees that the surface tension does not vanish above the critical point, but remains finite, but very small, at any temperature, because of the existence of small gradients in the actual interface.

The ϵ -expansion provides a way to calculate both $\mathcal{F}(z)$ and $\mathcal{F}^B(z)$ systematically, leading to a systematic and universal expansion of the surface tension.

The remainder of this chapter is organized as follows: In section 2 we give explicit formulae from which we can calculate σ up to first order in ϵ . In section 3 we scale all non-essential quantities out of these formulae and show that there remains a universal $\sigma(t)$. In section 4 the results of the numerical calculation of σ are presented. The chapter closes with a discussion of the results.

2. The surface tension

In this section we show that the choice of the locally homogeneous profile as a reference profile leads to a consistent definition of the surface tension σ . We will demonstrate that all divergences occurring in the ϵ -expansion of σ can be compensated and that the resulting σ is finite. The surface tension has been defined in (1.1) as the integral over z of the difference of the actual free-energy density and the free energy of the reference profile. The free-energy densities associated with the profiles are calculated from the Ginzburg-Landau-Wilson Hamiltonian defined in chapter II. In the one-loop approximation (which gives results correct up to first order in $\epsilon=4-d$ in the ϵ -expansion) we get

$$\begin{aligned} \mathcal{F}(z) = & \left\{ \frac{Z}{2} \left[\frac{dM(z)}{dz} \right] + \frac{1}{2} (t Z_2 + \delta t) M(z)^2 + \frac{\mu}{4!} Z_4 M(z)^4 - g z M(z) \right\} \\ & + \frac{1}{2} \frac{\text{Tr}}{V^{d-1}} \ln \left[\mathcal{H}^{(2)} \right] \end{aligned} \quad (2.1)$$

and

$$\mathcal{F}^B(z) = \left\{ \frac{1}{2} (t Z_2 + \delta t) M^B(z)^2 + \frac{\mu}{4!} Z_4 M^B(z)^4 - g z M^B(z) \right\}$$

$$+ \frac{1}{V^{d-1}} \text{Tr} \ln \left[\mathcal{H}^{B(2)} \right], \quad (2.2)$$

where $M(z)$ is the actual magnetization profile and $M^B(z)$ is the magnetization which (as a function of z) forms the reference profile. V^{d-1} is the area of the plane transverse to the field direction. $\mathcal{H}^{(2)}(r, r')$ and $\mathcal{H}^{B(2)}(r, r')$ are given by

$$\mathcal{H}^{(2)}(r, r') = \left\{ -Z \nabla^2 + \delta t + t Z_2 + \frac{u}{2} Z_4 M(z)^2 \right\} \delta(r - r') \quad (2.3)$$

and

$$\mathcal{H}^{B(2)}(r, r') = \left\{ -Z \nabla^2 + \delta t + t Z_2 + \frac{u}{2} Z_4 M^B(z')^2 \right\} \delta(r - r'). \quad (2.4)$$

As in chapter II the parameters Z, Z_2, Z_4 and δt are renormalization constants which have been evaluated as¹¹

$$Z = 1 + \mathcal{O}(u^2), \quad (2.5)$$

$$Z_2 = 1 + \frac{u}{2} J + \mathcal{O}(u^2), \quad (2.6)$$

$$Z_4 = 1 + \frac{3}{2} u J + \mathcal{O}(u^2), \quad (2.7)$$

$$\delta t = -\frac{u}{2} \int \frac{1}{q^2} = -\frac{u}{2} S_{3-\epsilon} \int_0^{+\infty} dq_t \frac{q_t^{2-\epsilon}}{2q_t}, \quad (2.8)$$

with

$$J = \frac{S_{4-\epsilon}}{\epsilon} \left(1 - \frac{\epsilon}{2} + \mathcal{O}(\epsilon^2) \right) \quad (2.9)$$

and

$$S_d = \frac{2\pi^{d/2}}{\Gamma(d/2)} \frac{1}{(2\pi)^d}. \quad (2.10)$$

For the coupling constant u we take the fixed point value u^* ,⁸

$$u^* S_{4-\epsilon} = \frac{2}{3} \epsilon + \mathcal{O}(\epsilon^2). \quad (2.11)$$

In I we have calculated the profiles $M(z)$ in an ϵ -expansion as

$$M(z) = M_0(z) + \frac{\epsilon}{6} M_1(z) + \mathcal{O}(\epsilon^2). \quad (2.12)$$

$M_0(z)$ fulfills the mean-field equation in a field gz ,

$$\frac{d^2}{dz^2} M_0(z) = (t + M_0^2(z)) M_0(z) - gz. \quad (2.13)$$

Similarly the reference profile can be expanded in ϵ ,

$$M^B(z) = M_0^B(z) + \frac{\epsilon}{6} M_1^B(z) + O(\epsilon^2), \quad (2.14)$$

where $M_0^B(z)$ obeys the locally homogeneous mean-field equation of state,

$$0 = (t + M_0^B(z)^2) M_0^B(z) - gz, \quad (2.15)$$

i.e. $M_0^B(z)$ is calculated as if the field gz is not dependent on z and thus the second derivative on the left-hand side in (2.13) is set equal to zero. The profile-corrections $M_1(z)$ and $M_1^B(z)$ are not necessary for the computation of σ to first order in ϵ due to the stationarity of the free energy functionals.

The ϵ -expansion for σ ,

$$\sigma/k_B T = \sigma_0/k_B T + \epsilon \sigma_1/k_B T + \dots, \quad (2.16)$$

is then obtained by substituting the renormalization constants (2.5)-(2.9) into (2.1) and (2.2) together with the lowest order profiles $M_0(z)$ and $M_0^B(z)$. Then σ_0 becomes

$$\begin{aligned} (\sigma_0/k_B T) = & \int_{-\infty}^{+\infty} dz \left\{ \frac{1}{2} \left(\frac{dM_0(z)}{dz} \right)^2 + \frac{1}{2} t (M_0(z)^2 - M_0^B(z)^2) \right. \\ & \left. + \frac{u}{4!} (M_0(z)^4 - M_0^B(z)^4) - gz (M_0(z) - M_0^B(z)) \right\} \end{aligned} \quad (2.17)$$

and σ_1 is obtained as

$$\begin{aligned} (\sigma_1/k_B T) = & \lim_{\epsilon \rightarrow 0} \frac{1}{\epsilon} \left\{ \frac{1}{2} S_{3-\epsilon} \int_{-\infty}^{\infty} dz \int_0^{+\infty} dq_t q_t^{2-\epsilon} \left[\ln [\mathcal{H}^{(2)}] - \ln [\mathcal{H}^{B(2)}] \right. \right. \\ & \left. \left. - \frac{(v(z) - v^B(z))}{2q_t} \right] - \frac{1}{4} S_{4-\epsilon} \left[\frac{1}{2} - \frac{1}{\epsilon} \right] \int_{-\infty}^{\infty} dz (v(z)^2 - v^B(z)^2) \right\}. \end{aligned} \quad (2.18)$$

The functions $v(z)$ and $v^B(z)$ are defined as

$$v(z) = t + \frac{u}{2} M_0(z)^2 \quad (2.19)$$

$$v^B(z) = t + \frac{u}{2} M_0^B(z)^2. \quad (2.20)$$

The integration over z in (2.17) is convergent although not very rapidly, due to the behaviour of $M_0(z)$ for large z

$$M_0(z) \sim z^{1/3} \quad (z \text{ large}). \quad (2.21)$$

The integration over q_i in (2.18) also converges for any $\epsilon > 0$. For $\epsilon \rightarrow 0$ however the integral starts to diverge, leading to an $1/\epsilon$ -contribution. This $1/\epsilon$ -contribution is compensated exactly by the other $1/\epsilon$ -term in (2.18). Before showing this, we first integrate (2.18) by parts, what results into

$$\begin{aligned} (\sigma_1/k_B T) = & -\lim_{\epsilon \rightarrow 0} \frac{1}{\epsilon} \left[2S_{3-\epsilon} \int_0^{+\infty} dz \frac{1}{(3-\epsilon)} \int_0^{+\infty} dq_i q_i^{4-\epsilon} \Delta G'(q_i, z) \right. \\ & \left. - \frac{1}{2} S_{4-\epsilon} \left[\frac{1}{2} - \frac{1}{\epsilon} \right] \int_0^{+\infty} (v(z)^2 - v^B(z)^2) dz \right]. \end{aligned} \quad (2.22)$$

In (2.22) we have used the antisymmetry of $M_0(z)$ and $M_0^B(z)$ which is apparent from (2.13) and (2.15). $\Delta G'(q_i, z)$ is defined as

$$\Delta G'(q_i, z) = \left[G(q_i, z, z') - G^B(q_i, z, z') \right]_{z=z'} + \left(\frac{v(z) - v^B(z)}{4q_i^3} \right). \quad (2.23)$$

$G(q_i, z, z')$ and $G^B(q_i, z, z')$ are the Green's functions given implicitly as solutions of the equations

$$\left(-\frac{d^2}{dz^2} + q_i^2 + v(z) \right) G(q_i, z, z') = \delta(z - z') \quad (2.24)$$

$$\left(-\frac{d^2}{dz^2} + q_i^2 + v^B(z') \right) G^B(q_i, z, z') = \delta(z - z'). \quad (2.25)$$

Eq. (2.25) for the locally homogeneous Green's function $G^B(q_i, z, z')$ can be solved analytically giving

$$G^B(q_i, z, z') = \frac{e^{-\sqrt{q_i^2 + v^B(z')} |z - z'|}}{2(q_i^2 + v^B(z'))^{1/2}}. \quad (2.26)$$

To see the cancellation of the $1/\epsilon$ -term in (2.22) we use the large q_i expansion of $G(q_i, z, z')$ developed in chapter II, together with the large q_i expansion of (2.26) for $z = z'$. Then $\Delta G'(q_i, z)$ becomes

$$\Delta G'(q_t, z) = \frac{3}{16} \left(\frac{v(z)^2 - v^B(z)^2}{q_t^5} \right) - \frac{1}{16} \frac{v^{(2)}(z)}{q_t^5} + \mathcal{O}(q_t^{-7}) \quad (q_t \text{ large}), \quad (2.27)$$

where $v^{(n)}(z)$ denotes the n -th derivative of $v(z)$ with respect to z . We now rewrite (2.22) as

$$\begin{aligned} (\sigma_1 / k_B T) = \lim_{\epsilon \rightarrow 0} \frac{1}{\epsilon} & \left[-2S_{3-\epsilon} \int_0^{+\infty} dz \frac{1}{(3-\epsilon)} \int_0^{q_0} dq_t q_t^{4-\epsilon} \Delta G'(q_t, z) \right. \\ & - 2S_{3-\epsilon} \int_0^{+\infty} dz \frac{1}{(3-\epsilon)} \int_{q_0}^{\infty} dq_t q_t^{4-\epsilon} \left\{ \Delta G'(q_t, z) + \frac{1}{16} \frac{v^{(2)}(z)}{q_t^5} \right. \\ & \left. \left. - \frac{3}{16} \left(\frac{v(z)^2 - v^B(z)^2}{q_t^5} \right) \right\} \right. \\ & - \frac{3}{8} S_{3-\epsilon} \frac{q_0^{-\epsilon}}{\epsilon(3-\epsilon)} \int_0^{+\infty} dz (v(z)^2 - v^B(z)^2) \\ & \left. + \frac{1}{2} S_{4-\epsilon} \left(\frac{1}{\epsilon} - \frac{1}{2} \right) \int_0^{+\infty} dz (v(z)^2 - v^B(z)^2) \right]. \quad (2.28) \end{aligned}$$

The cutoff parameter q_0 will be chosen later. Using that

$$S_{3-\epsilon} = 4S_{4-\epsilon} \left(1 + \epsilon \left(\frac{1}{2} - \ln 2 \right) + \mathcal{O}(\epsilon^2) \right) \quad (2.29)$$

and the expansion

$$-\frac{3}{8} \frac{q_0^{-\epsilon}}{\epsilon(3-\epsilon)} S_{3-\epsilon} = -\frac{1}{2} S_{4-\epsilon} \left(\frac{1}{\epsilon} + \frac{1}{3} + \left(\frac{1}{2} - \ln 2 \right) - \ln q_0 + \mathcal{O}(\epsilon) \right), \quad (2.30)$$

we see the $1/\epsilon$ -part of the last term on the right hand side of (2.28) exactly cancels the $1/\epsilon$ -term of (2.30). The remaining integrals over q_t are finite as well as the integration over z .

With the fixed point value of u given in (2.11) the resulting expression for σ_1 is

$$(u\sigma_1 / k_B T) = -\frac{16}{9} \int_0^{+\infty} dz \int_0^{q_0} dq_t q_t^4 \Delta G'(q_t, z) - \frac{16}{9} \int_0^{+\infty} dz \int_{q_0}^{\infty} dq_t q_t^4$$

$$\begin{aligned}
& \times \left(\Delta G'(q_i, z) + \frac{1}{16} \frac{v^{(2)}(z)}{q_i^5} - \frac{3}{16} \left(\frac{v(z)^2 - v^B(z)^2}{q_i^5} \right) \right) \\
& - \left(\frac{5}{18} + \frac{1}{3} \left(\frac{1}{2} - \ln 2 \right) - \frac{8}{9} \ln q_0 \right) \int_0^{+\infty} dz (v(z)^2 - v^B(z)^2) .
\end{aligned} \tag{2.31}$$

The integrations in (2.31) can be carried out numerically using the same techniques as have been used in chapter II.

3. Scaling of the surface tension

Before we calculate $\bar{\sigma}_0$ and $\bar{\sigma}_1$ we first introduce scaled variables $\bar{M}(\bar{z})$, \bar{z} , and \bar{t} , by which all parameters, which are not essential to the problem, are scaled out:

$$M = \mu_t \bar{M}, \quad z = \zeta_t \bar{z}, \quad t = \theta_t \bar{t}, \tag{3.1}$$

with

$$\mu_t = \left(\frac{u}{6} \right)^{-3/8 - (3/64)\epsilon} g^{1/4 - (3/32)\epsilon}, \tag{3.2}$$

$$\zeta_t = \left(\frac{u}{6} \right)^{-1/8 - (1/64)\epsilon} g^{-1/4 - (1/32)\epsilon}, \tag{3.3}$$

$$\theta_t = \left(\frac{u}{6} \right)^{1/4 - (1/96)\epsilon} g^{1/2 - (1/48)\epsilon}. \tag{3.4}$$

In eqs. (2.13) and (2.15) for the actual, respectively the reference profile all u dependence scales out up to order ϵ , yielding

$$\frac{d^2 \bar{M}_0(\bar{z})}{d\bar{z}^2} = (\bar{t} + \bar{M}_0(\bar{z})^2) \bar{M}_0(\bar{z}) - \bar{z} \tag{3.5}$$

and

$$0 = (\bar{t} + \bar{M}_0^B(\bar{z})^2) \bar{M}_0^B(\bar{z}) - \bar{z}. \tag{3.6}$$

The scaled expression for σ is easily found to be

$$\left(\frac{\sigma}{k_B T} \right) = \left(\frac{u}{6} \right)^{-5/8 - (5/64)\epsilon} g^{3/4 - (5/32)\epsilon} \bar{\sigma}, \tag{3.7}$$

where

$$\bar{\sigma} = \bar{\sigma}_0 + \epsilon \bar{\sigma}_1 \quad (3.8)$$

and

$$\begin{aligned} \bar{\sigma}_0 = 2 \int_0^{+\infty} d\bar{z} \left\{ \frac{1}{2} \left(\frac{d\bar{M}_0(\bar{z})}{d\bar{z}} \right)^2 + \frac{1}{2} \bar{t} (\bar{M}_0(\bar{z})^2 - \bar{M}_0^B(\bar{z})^2) \right. \\ \left. + \frac{1}{4} (\bar{M}_0(\bar{z})^4 - \bar{M}_0^B(\bar{z})^4) - \bar{z} (\bar{M}_0(\bar{z}) - \bar{M}_0^B(\bar{z})) \right\} \end{aligned} \quad (3.9)$$

and

$$\begin{aligned} \bar{\sigma}_1 = -\frac{8}{27} \int_0^{+\infty} d\bar{z} \int_0^1 d\bar{q}_t \bar{q}_t^4 \Delta \bar{G}'(\bar{q}_t, \bar{z}) \\ - \frac{8}{27} \int_0^{+\infty} d\bar{z} \int_1^{\infty} d\bar{q}_t \bar{q}_t^4 \left(\Delta \bar{G}'(\bar{q}_t, \bar{z}) \right. \\ \left. + \frac{1}{16} \frac{\bar{v}^{(2)}(\bar{z})}{\bar{q}_t^5} - \frac{3}{16} \left(\frac{\bar{v}(\bar{z})^2 - \bar{v}^B(\bar{z})^2}{\bar{q}_t^5} \right) \right) \\ - \frac{1}{54} \left(\frac{5}{2} + 3 \left(\frac{1}{2} - \ln 2 \right) \right) \int_0^{+\infty} d\bar{z} (\bar{v}(\bar{z})^2 - \bar{v}^B(\bar{z})^2). \end{aligned} \quad (3.10)$$

We have chosen q_0 in (2.31) equal to

$$q_0 = \zeta_t^{-1}. \quad (3.11)$$

$\bar{v}(\bar{z})$, $\bar{v}^B(\bar{z})$, $\bar{v}^{(n)}(\bar{z})$, $\Delta \bar{G}'(\bar{q}_t, \bar{z})$, $\bar{G}(\bar{q}_t, \bar{z}, \bar{z}')$ and $\bar{G}^B(\bar{q}_t, \bar{z}, \bar{z}')$ are given respectively by

$$\bar{v}(\bar{z}) = \bar{t} + 3\bar{M}_0(\bar{z})^2, \quad (3.12)$$

$$\bar{v}^B(\bar{z}) = \bar{t} + 3\bar{M}_0^B(\bar{z})^2, \quad (3.13)$$

$$\bar{v}^{(n)}(\bar{z}) = \frac{d^n}{d\bar{z}^n} \bar{v}(\bar{z}) \quad (3.14)$$

and

$$\left(-\frac{d^2}{d\bar{z}^2} + \bar{q}_t^2 + \bar{v}(\bar{z}) \right) \bar{G}(\bar{q}_t, \bar{z}, \bar{z}') = \delta(\bar{z} - \bar{z}'), \quad (3.15)$$

$$\bar{G}^B(\bar{q}_t, \bar{z}, \bar{z}') = \frac{e^{-\sqrt{\bar{q}_t^2 + \bar{v}^B(\bar{z}')} |\bar{z} - \bar{z}'|}}{2(\bar{q}_t^2 + \bar{v}^B(\bar{z}'))^{1/2}}, \quad (3.16)$$

together with

$$\Delta \bar{G}'(\bar{q}_t, \bar{z}) = \left[\bar{G}(\bar{q}_t, \bar{z}, \bar{z}') - \bar{G}^B(\bar{q}_t, \bar{z}, \bar{z}') \right]_{\bar{z}=\bar{z}'} + \frac{(\bar{v}(\bar{z}) - \bar{v}^B(\bar{z}))}{4\bar{q}_t^3} \quad (3.17)$$

Eqs. (3.5)-(3.16) define the problem of calculating the scaled surface tension as a function of the temperature-like parameter \bar{t} . Similar to the order-parameter profile $\bar{M}(\bar{z})$, the surface tension $\bar{\sigma}$ in an external field is a universal quantity.

From (3.4) we see that the limit of a small external field ($g \rightarrow 0$) is equivalent to the region of very large \bar{t} . For \bar{t} large the surface tension that we have calculated using (3.9) and (3.10), approaches asymptotically to the result evaluated by Ohta and Kawasaki¹ (and also by Brézin and Feng²), which is in our scaled units

$$\bar{\sigma} = \frac{2}{3} \sqrt{2} |\bar{t}|^{3/2} \left\{ 1 - \frac{1}{4} \epsilon \left[\ln(2|\bar{t}|) - 2 + \frac{\sqrt{3}}{9} \pi \right] \right\} \quad (T < T_c) \quad (3.18)$$

in appendix B we have made a similar asymptotic analysis for large \bar{t} and $T > T_c$ which leads to the expression (see (B.4) and (B.10))

$$\bar{\sigma} = -\frac{\pi}{6} \sqrt{3} \bar{t}^{-1/2} \left\{ 1 + \epsilon \left[\frac{1}{3} \ln |\bar{t}| - \frac{5}{36} + \frac{2}{3} \ln 2 \right] \right\} \quad (T > T_c) \quad (3.19)$$

4. Numerical evaluation of $\bar{\sigma}$

Once the profiles $\bar{M}_0(\bar{z})$ and $\bar{M}_0^B(\bar{z})$ are known, we can compute $\bar{\sigma}$ using (3.8)-(3.16). In chapter II we have given the results for $\bar{M}_0(\bar{z})$ for several selected temperatures \bar{t} , so now we confine ourselves showing the profiles in fig. 1. The locally homogeneous or reference profile $\bar{M}^B(\bar{z})$ is solved easily from (3.6) and is shown also in fig. 1. For $\bar{t} < 0$ the reference profile has a jump in $\bar{z} = 0$ equal to twice the spontaneous magnetization. For $\bar{t} \geq 0$ $\bar{M}^B(\bar{z})$ is continuous everywhere.

The Green's function $\bar{G}(\bar{q}_t, \bar{z}, \bar{z}')$ has also been calculated in chapter II. The computation of this function for small values of \bar{q}_t and \bar{z}' has been supplemented by an analytical expansion valid for small gradients, which is correct for large \bar{q}_t and also for large \bar{z}' . In this region we have (see chapter II)

$$\begin{aligned} \Delta \bar{G}'(\bar{q}_t, \bar{z}) = & \frac{1}{2} \left((\bar{q}_t^2 + \bar{v}(\bar{z}))^{-1/2} - (\bar{q}_t^2 + \bar{v}^B(\bar{z}))^{-1/2} \right) + \frac{(\bar{v}(\bar{z}) - \bar{v}^B(\bar{z}))}{4\bar{q}_t^3} \\ & + \frac{1}{2} (\bar{q}_t^2 + \bar{v}(\bar{z}))^{-1/2} \left(-\frac{1}{4} X_2 + \frac{5}{32} X_1^2 - \frac{3}{4} X_4 \right. \\ & \left. + \frac{21}{32} X_2^2 - \frac{45}{8} X_6 + \dots \right) \quad (\bar{q}_t \text{ large or } \bar{z} \text{ large}), \end{aligned} \quad (4.1)$$

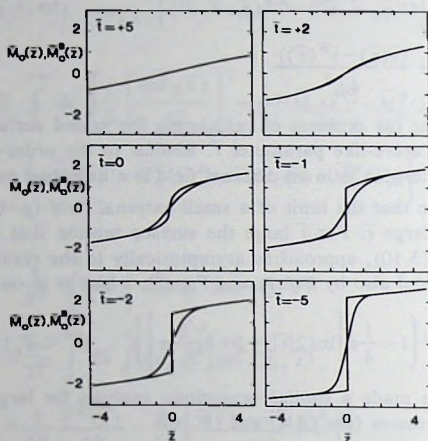


Fig. 1. The actual magnetization profile $\bar{M}_0(\bar{z})$ and the reference profile $\bar{M}_0^B(\bar{z})$ for a few selected temperatures around T_c . ($\bar{t} = +5, +2, 0, -1, -2, -5$).

where the X_n are defined as

$$X_n = \frac{1}{n!} \frac{\bar{v}^{(n)}(\bar{z})}{(\bar{q}_t^2 + \bar{v}(\bar{z}))^{(n+2)/2}}. \quad (4.2)$$

As in chapter II, for each \bar{z} , we carry out the integration over \bar{q}_t in (3.10) numerically up to the value $\bar{q}_f(\bar{z})$, above which the small gradient expansion of (4.1) is valid. For larger \bar{q}_t we perform the integration over \bar{q}_t by integrating analytically over the terms of the expansion (4.1) (see appendix A). Finally we have to do the integration over \bar{z} in (3.9) and (3.10). For all (small) values of \bar{z} for which we know $\bar{M}_0(\bar{z})$ with sufficient accuracy we carry out this integration numerically. For large \bar{z} the first term on the right-hand side of (3.9) still gives a significant contribution to $\bar{\sigma}_0$. Also some terms of (4.1) give a large \bar{z} contribution to $\bar{\sigma}_1$. We can do an exact calculation of these contribution, by considering $\bar{M}_0(\bar{z})$ as a small deviation of $\bar{M}_0^B(\bar{z})$. For details see appendix B, where also the asymptotic behaviour of $\bar{\sigma}$ above T_c is calculated.

The resulting functions $\bar{\sigma}_0(\bar{t})$ and $\bar{\sigma}_1(\bar{t})$, together with their asymptotic behaviour, are shown in figs. 2 and 3 respectively.

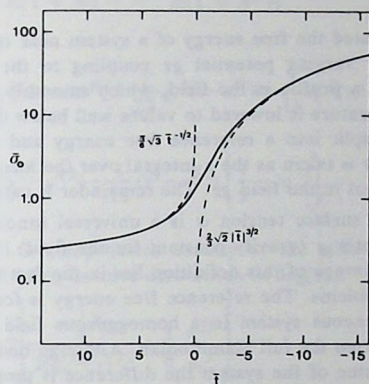


Fig. 2. The zeroth-order contribution to the surface tension as a function of temperature, together with the asymptotic behaviour both above and below T_c .

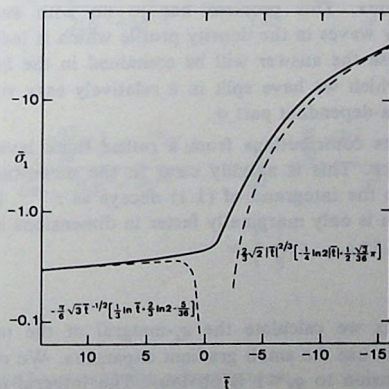


Fig. 3. The first-order contribution to the surface tension as a function of temperature. The dashed lines indicate the asymptotic behaviour of $\bar{\sigma}_1$.

5. Discussion

We have calculated the free energy of a system near criticality which is influenced by a linearly varying potential gz coupling to the order-parameter. The order-parameter has a profile in the field, which smoothly develops into an interface when the temperature is lowered to values well below the critical temperature. The free energy is split into a reference free energy and a surface tension. The reference free energy is taken as the z -integral over the local free-energy density of a homogeneous system in the field gz . The remainder is called the surface tension.

The so defined surface tension σ is a universal function of the temperature and the field parameter g (gravity constant for the fluid). σ is calculated to first order in ϵ . The advantage of this definition lies in the fact that it requires to solve two well-defined problems. The reference free energy is found from the bulk free energy in a homogeneous system in a homogeneous field. The true free energy must be calculated from the full Hamiltonian. Although both free energies are proportional to the volume of the system the difference is proportional to the area in the transverse plane.

The consequence of this definition is that we have a non-vanishing surface tension below and above the critical point T_c . Well below T_c the usual surface tension is recovered varying as $|\bar{t}|^\mu$ (see 3.18)) where \bar{t} measures the temperature difference. Above T_c the surface tension decays as $|\bar{t}|^{\beta-2\nu}$ (see (3.19))¹².

One may ask whether this definition of σ leads to a useful quantity in explaining experiments. This problem has to do with such questions as the existence of capillary waves in the density profile which is induced by the field just above T_c . In any case the answer will be contained in the full free energy of the system in a field, which we have split in a relatively easy volume-dependent part and a remaining area-dependent part σ .

Our σ draws its contributions from a rather thick layer around the central plane of the interface. This is already clear in the mean-field picture where the main contribution to the integrand of (1.1) decays as $z^{-5/3}$. In general this power will be $z^{-2+1/\delta}$ which is only marginally faster in dimensions lower than $d=4$.

Appendix A

In this appendix we calculate the q_t -integral of the terms of (4.1) in the regions where we can use the small gradient expansion. We only give the integrals for $q_f > 1$. The extension to $q_f < 1$ is obvious. The integral over the first term of (4.1) gives

$$-\frac{8}{27} \int_{q_f}^{+\infty} dq_t q_t^4 \left[\frac{1}{2(q_t^2 + \nu)^{1/2}} - \frac{1}{2(q_t^2 + \nu^B)^{1/2}} + \left(\frac{\nu - \nu^B}{4q_t^3} \right) - \frac{3}{16} \left(\frac{\nu^2 - \nu^{B2}}{q_t^5} \right) \right]$$

$$\begin{aligned}
&= \frac{1}{18} (v^2 \ln(1+A) - v^{B^2} \ln(1+A^B)) \\
&\quad - \frac{1}{27} q_f^4 (A - A^B) + \frac{1}{27} q_f^2 (v - v^B) - \frac{1}{18} q_f^2 (vA - v^B A^B) \\
&\quad + \frac{1}{108} (v^2 - v^{B^2}) - \frac{1}{18} (v^2 - v^{B^2}) \left(\frac{1}{2} - \ln 2 \right). \quad (A.1)
\end{aligned}$$

The last term in (A.1) is compensated exactly by the same term in (3.10). The remaining terms in (4.1) only involve derivatives of $M_0(z)$:

$$\begin{aligned}
& - \frac{8}{27} \int_{q_f}^{+\infty} dq_t q_t^4 \left[\frac{-\frac{1}{4} X_2}{2(q_t^2 + v)^{1/2}} + \frac{1}{8} \frac{v^{(2)}}{q_t^5} \right] \\
&= - \frac{1}{27} \left(1 + \frac{1}{3} - \ln 2 - A^{-1} - \frac{1}{3} A^{-3} + \ln(1+A) \right) v^{(2)}, \quad (A.2)
\end{aligned}$$

$$- \frac{8}{27} \int_{q_f}^{+\infty} dq_t q_t^4 \frac{(\frac{5}{32} X_1^2 - \frac{3}{4} X_4)}{2(q_t^2 + v)^{1/2}} = - \frac{4}{135} \frac{(\frac{5}{32} v^{(1)2} - \frac{3}{4} v^{(4)})}{v} (1 - A^{-5}) \quad (A.3)$$

and

$$\begin{aligned}
& - \frac{8}{27} \int_{q_f}^{+\infty} dq_t q_t^4 \frac{(\frac{21}{32} X_2^2 - \frac{45}{8} X_6)}{2(q_t^2 + v)^{1/2}} = - \frac{4}{27} \frac{(\frac{21}{32} v^{(2)2} - \frac{45}{8} v^{(6)})}{v^2} \\
&\quad \times \left(\frac{1}{5} (1 - A^{-5}) - \frac{1}{7} (1 - A^{-7}) \right), \quad (A.4)
\end{aligned}$$

etc.

In (A.1)-(A.4) we have used the abbreviations

$$A = \left(1 + \frac{v(z)}{q_f^2} \right)^{1/2},$$

$$A^B = \left(1 + \frac{v^B(z)}{q_f^2} \right)^{1/2},$$

and $v^{(n)} = (1/n!)d^n v(z) / dz^n$.

Appendix B

In this appendix we perform the large \bar{z} -part of the \bar{z} integration in (3.9) and (3.10). For large \bar{z} the difference between the actual and the reference profile is very small and we can find $\bar{M}_0(\bar{z})$ as a small deviation of $\bar{M}_0^B(\bar{z})$:

$$\bar{M}_0(\bar{z}) = \bar{M}_0^B(\bar{z}) \left[1 - \frac{6}{\bar{v}^B(\bar{z})^4} + \dots \right] \quad (\text{for } \bar{z} > \bar{z}_f(\bar{r})), \quad (\text{B.1})$$

when $\bar{z}_f(\bar{r})$ is sufficiently large. The derivatives of $\bar{M}_0(\bar{z})$ in this region are very well given by the derivatives of $\bar{M}_0^B(\bar{z})$,

$$\frac{d\bar{M}_0(\bar{z})}{d\bar{z}} = \frac{1}{\bar{v}^B(\bar{z})} + \dots, \quad (\text{B.2})$$

etc. We continue with the formulae for $\bar{r} > 0$. In the case of $\bar{r} < 0$ everything is similar.

For $\bar{z} > \bar{z}_f(\bar{r})$ the only term contributing to (3.9) is

$$2 \int_{\bar{z}_f}^{+\infty} \frac{1}{2} \left(\frac{d\bar{M}_0(\bar{z})}{d\bar{z}} \right)^2 d\bar{z} = \frac{\bar{r}^{-1/2}}{\sqrt{3}} \int_{x_f}^{+\infty} \frac{1}{x^2+1} dx = \frac{\bar{r}^{-1/2}}{\sqrt{3}} \left(\frac{\pi}{2} - \arctan x_f \right), \quad (\text{B.3})$$

where $x_f = \sqrt{3} \bar{r}^{-1/2} \bar{M}(\bar{z})$.

For \bar{r} above T_c the profiles $\bar{M}_0(\bar{z})$ and $\bar{M}_0^B(\bar{z})$ differ very little (see fig. 1) for all \bar{z} , so we may put $\bar{z}_f=0$ and obtain asymptotically

$$\bar{\sigma}_0 = \frac{\pi}{6} \sqrt{3} \bar{r}^{-1/2} \quad (\bar{r} \text{ large, } \bar{r} > 0). \quad (\text{B.4})$$

The $\bar{\sigma}_1$ -contributions of the large \bar{z} region come from the terms calculated in appendix A where we may set $\bar{q}_f=0$. From (A.1) for $\bar{q}_f=0$ we get

$$\begin{aligned} & \frac{1}{36} \int_{\bar{z}_f}^{+\infty} d\bar{z} (\bar{v}(\bar{z})^2 \ln \bar{v}(\bar{z}) - \bar{v}^B(\bar{z})^2 \ln \bar{v}^B(\bar{z})) \\ &= -\frac{\pi \bar{r}^{-1/2}}{2\sqrt{3}} \left\{ \frac{1}{3} \ln \bar{r} + \frac{1}{3} + \frac{2}{3} \ln 2 - \frac{2}{3\pi} \ln \bar{r} \left(\arctan x_f - \frac{x_f}{(1+x_f^2)} \right) \right\} \end{aligned}$$

$$-\frac{2}{3\pi} \left\{ \arctan x_f - \frac{x_f}{(1+x_f^2)} - \frac{x_f}{(1+x_f^2)} \ln(1+x_f^2) + I(x_f) \right\} \quad (\text{B.5})$$

and (combined with the $(v^2 - \bar{v}^B(\bar{z})^2)$ term in (3.10))

$$\begin{aligned} & -\frac{1}{27} \int_{\bar{z}_f}^{+\infty} d\bar{z} (\bar{v}(\bar{z})^2 - \bar{v}^B(\bar{z})^2) \\ & = -\frac{\pi \bar{t}^{-1/2}}{2\sqrt{3}} \left\{ -\frac{4}{9} + \frac{8}{9\pi} \left(\arctan x_f - \frac{x_f}{(1+x_f^2)} \right) \right\}. \end{aligned} \quad (\text{B.6})$$

The function $I(x_f)$ in (B.5) is defined as

$$I(x_f) = \int_0^{x_f} \frac{\ln(1+x^2)}{(1+x^2)} dx. \quad (\text{B.7})$$

From (A.2) and (A.3) we obtain respectively the contributions

$$\begin{aligned} & -\frac{1}{108} \int_{\bar{z}_f}^{+\infty} d\bar{z} \bar{v}^{(2)}(\bar{z}) \ln \bar{v}(\bar{z}) = -\frac{\pi \bar{t}^{-1/2}}{2\sqrt{3}} \left\{ -\frac{1}{18} - \frac{1}{9\pi} \ln |\bar{t}| \left(\frac{x_f}{1+x_f^2} \right) \right. \\ & \left. + \frac{1}{9\pi} \left(-\frac{x_f}{(1+x_f^2)} \ln(1+x_f^2) + \arctan x_f - \frac{x_f}{(1+x_f^2)} \right) \right\} \end{aligned} \quad (\text{B.8})$$

and

$$-\frac{1}{216} \int_{\bar{z}_f}^{+\infty} d\bar{z} \frac{\bar{v}^{(1)}(\bar{z})^2}{\bar{v}(\bar{z})} = -\frac{\pi \bar{t}^{-1/2}}{2\sqrt{3}} \left\{ \frac{1}{36} + \frac{1}{18\pi} \left(\frac{x_f}{(1+x_f^2)} - \arctan x_f \right) \right\}. \quad (\text{B.9})$$

The contributions for large \bar{z} of (A.4) and further terms in the expansion of $\bar{\sigma}_1$ are negligible.

For $\bar{t} > 0$ we find asymptotically from (B.5)-(B.9)

$$\bar{\sigma}_1 = -\frac{\pi\sqrt{3}}{6} \bar{t}^{-1/2} \left(\frac{1}{3} \ln |\bar{t}| - \frac{5}{36} + \frac{2}{3} \ln 2 \right) \quad (\bar{t} \text{ large, } \bar{t} > 0). \quad (\text{B.10})$$

References

- 1) T. Ohta and K. Kawasaki, *Progress of Theor. Phys.* **58** (1977) 467.
- 2) E. Brézin and S. Feng, *Phys. Rev. B* **29** (1984) 472.
- 3) J.H. Sikkenk and J.M.J. van Leeuwen, *Physica* **137A** (1986) 156.
- 4) J.S. Rowlinson and B. Widom, *Molecular Theory of Capillarity* (Clarendon, Oxford, 1982).
- 5) J.V. Sengers and J.M.J. van Leeuwen, *Physica* **116A** (1982) 345.
- 6) J.M.J. van Leeuwen and J.V. Sengers, *Physica* **132A** (1985) 207.
- 7) D.J. Amit, *Field Theory, The Renormalization Group and Critical Phenomena* (McGraw-Hill, New York, 1978).
- 8) D.J. Wallace, in *Phase Transitions and Critical Phenomena*, vol. 6, C. Domb and M.S. Green, eds (Academic Press, New York, 1976), p. 293.
- 9) E. Brézin, D.J. Wallace and K. Wilson, *Phys. Rev. B* **7** (1972) 232.
- 10) J. Rudnick and D.R. Nelson, *Phys. Rev. B* **13** (1976) 2208.
- 11) E. Brézin, J.C. LeGuillou and J. Zinn-Justin, *Phys. Rev. D* **8** (1973) 434.
- 12) J.M.J. van Leeuwen and J.V. Sengers, *Physica* **138 A** (1986) 1.

CHAPTER IV

**GRAVITY EFFECTS ON THE FLUCTUATIONS OF
A LIQUID-VAPOUR INTERFACE CLOSE TO
THE CRITICAL TEMPERATURE**

ABSTRACT

In this chapter we consider the effects of gravity on the density fluctuations in and near the liquid-vapour interface of a fluid very close to the critical temperature. The results complement those of a previous analysis of the gravity effects on the fluctuations in the one-phase region above the critical temperature. The correlation function is anisotropic and we distinguish between a longitudinal and a transverse correlation length which are height dependent. The longitudinal correlation length profiles exhibit maxima above and below the critical temperature. The transverse correlation length increases with decreasing temperature and its value at the dividing surface approaches the capillary length at temperatures well below the critical temperature.

1. Introduction

The state of a system near a critical point is very sensitive to small changes in the ordering field. As a consequence, fluids near the liquid-vapour critical point are strongly affected by the presence of a gravitational field. In the one-phase region gravity induces an inhomogeneous density distribution and all thermophysical properties become functions of height. In evaluating the effects of gravity one usually assumes that the local properties of the fluid at a given level can still be identified with those of a locally homogeneous fluid¹⁻³. However, very close to the critical point the gravitationally induced density gradients become so large that the assumption of local homogeneity ceases to be valid. Then the presence of gravity leads also to intrinsic effects which modify the local fluid properties themselves and change the nature of the critical point phase transition. In the two-phase region below the critical temperature the (inhomogeneous) liquid and vapour phases are separated by an interface. While the gravitational field acts as a pinning potential for the location of the dividing surface, it is normally considered to have in practice only a minor influence on the interfacial density profile⁴. Again the situation changes very close to the critical temperature, where gravity will affect the structure of the interface because of the large compressibility of the two coexisting phases.

In a series of recent publications⁵⁻⁷ Van Leeuwen and Sengers have presented an analysis of some of these intrinsic gravity effects that occur very close to the critical point. In the first paper of this series⁵, to be referred to as I, they determined the density profiles induced by the gravity in the one-phase region at temperatures above and equal to the critical temperature T_c and demonstrated that the density gradient remains finite at the critical temperature even at the level where the density equals the critical density ρ_c . In the second paper⁶, to be referred to as II, the effects of gravity on the critical fluctuations were investigated. In the presence of a gravitational field the order-parameter correlation function becomes anisotropic, but it was found that the correlation length remains finite in all directions. In the third paper⁷, to be referred to as III, they determined the interfacial density profiles below T_c in the presence of gravity. The gravitational force prevents the interface thickness from growing indefinitely when the critical temperature is approached from below and the interfacial density profiles below T_c are smoothly connected with the density profiles induced by gravity in the one-phase region.

It is the purpose of this chapter to discuss the effects of gravity on the order-parameter correlation function in and near the interface. Specifically, we have determined the transverse and longitudinal correlation lengths as a function of height. These correlation length profiles are smoothly connected with the profiles

found in II for the correlation length perpendicular and parallel to the gravitational field in the one-phase region above T_c .

Our evaluation of the intrinsic gravity effects is based on the squared-gradient theory of van der Waals⁴. As discussed in I-III the squared-gradient theory has a number of shortcomings. First, the squared-gradient theory cannot deal consistently with the small deviations of the correlation function of the homogeneous system from the Ornstein-Zernike form^{5,8}. Secondly, it requires the use of a phenomenological interpolation function for the equation of state at the densities between those of the bulk liquid and vapour phases^{4,7}. The effects of these approximations are expected to be small. In addition, however, the squared-gradient theory does not account appropriately for the presence of capillary waves in the liquid-vapour interface⁹⁻¹². Nevertheless, by restricting ourselves to temperatures sufficiently close to T_c where compressibility effects become dominant, we expect to obtain an essentially correct picture of the nature of the intrinsic gravity effects on the critical phenomena in fluids^{7,13}.

2. Differential equation for the correlation function

According to the squared-gradient theory, the density $\rho(z)$ as a function of the height z in the presence of a gravitational potential gz satisfies a differential equation of the form^{4,5} (see chapter I)

$$A \frac{d^2 \rho}{dz^2} = \mu(\rho(z)) - \mu(\rho_c) + gz, \quad (2.1)$$

with

$$A = \xi^2(\rho(z)) / \chi(\rho(z)). \quad (2.2)$$

The quantities $\mu(\rho(z))$, $\chi(\rho(z))$ and $\xi(\rho(z))$ are the chemical potential μ , the symmetrized compressibility $\chi = (\partial \rho / \partial \mu)_T$ and the correlation length ξ , respectively, of a spatially homogeneous system with uniform density $\rho = \rho(z)$ at the given temperature T . The height z is taken to increase in the direction opposite to the gravitational field and the level $z=0$ is chosen as the level where $\rho(0) = \rho_c$. Differentiating (2.1) with respect to z and neglecting the weak dependence of A on z through $\rho(z)$ as discussed in I, we also note that the density gradient $\Phi(z) = d\rho/dz$ satisfies the equation

$$\left[\frac{d^2}{dz^2} - V(z) \right] \Phi(z) = gA^{-1}, \quad (2.3)$$

where the potential $V(z)$ is given by

$$V(z) = \xi^{-2}(\rho(z)). \quad (2.4)$$

Let $n(r)$ be the number density of molecules at position $r=(x, y, z)$ and $n(r, R)$ the density of pairs of molecules at $r=(x, y, z)$ and $R=(X, Y, Z)$. We define a pair correlation function $G(r, R)$ as

$$G(r, R) = n(r, R) - n(r)n(R). \quad (2.5)$$

In a spatially homogeneous system the correlation function $G(r, R)$ depends only on the distance $|r-R|$. In an inhomogeneous system, however, $G(r, R)$ depends on r and R separately. Here we consider $G(r, R)$ as a function of r or $r-R$ for given R and thus for a given level Z . As shown in chapter I, for given R , the function $G(r, R)$ satisfies the differential equation⁶

$$[\nabla^2 - V(z)]G(r, R) = 0. \quad (2.6)$$

We note that this differential equation does not depend on the gravitational acceleration constant g explicitly, but only implicitly through the density profile $\rho(z)$ determined from (2.1).

The differential equation (2.6) is valid for positions r such that the distance $|r-R|$ is large compared to the intermolecular distances. In the spatially homogeneous case the correlation length ξ is independent of z and the correlation function $G(r, R)$ should reduce to the Ornstein-Zernike form¹⁵

$$G_{OZ}(r-R) \propto \frac{e^{-|r-R|/\xi}}{|r-R|}, \quad (2.7)$$

which satisfies the differential equation

$$(\nabla^2 - \xi^{-2})G_{OZ}(r-R) = C\delta(r-R), \quad (2.8)$$

where C is a for our purposes arbitrary constant which we take to be unity. Near the critical point the correlation length ξ is very large and we do not need to consider deviations from the Ornstein-Zernike behaviour at molecular distances. Hence, to obtain a nontrivial solution from (2.6) we can formally extend it to all distances $|r-R|$ as

$$[\nabla^2 - V(z)]G(r, R) = \delta(r-R). \quad (2.9)$$

Rather than the correlation function itself, we consider its Fourier transform, the structure factor. Because of the special role of the Z -direction along the gravitational field, it is convenient to first define the partial Fourier transform

$$\hat{G}(k_x, k_y; z, Z) = \int_{-\infty}^{+\infty} dx \int_{-\infty}^{+\infty} dy e^{i[k_x(x-X) + k_y(y-Y)]} G(r, R), \quad (2.10)$$

which satisfies the equation

$$\left[\frac{d^2}{dz^2} - \{k_x^2 + k_y^2 + V(z)\} \right] \hat{G}(k_x, k_y; z, Z) = \delta(z-Z), \quad (2.11)$$

and the the full Fourier transform

$$\hat{G}(\mathbf{k}; Z) = \int d\mathbf{r} e^{i\mathbf{k}(\mathbf{r}-\mathbf{R})} G(\mathbf{r}, \mathbf{R}) = \int_{-\infty}^{+\infty} dz e^{i\mathbf{k}_z(z-Z)} \hat{G}(k_x, k_y; z, Z). \quad (2.12)$$

Because of the translational symmetry perpendicular to the gravitational field, the structure factor $\hat{G}(\mathbf{k}; Z)$ only depends on the reference position \mathbf{R} through the height Z . We are interested in the behaviour of the correlation function for large distances $|\mathbf{r}-\mathbf{R}|$ and hence in the behaviour of the structure factor for small wave numbers \mathbf{k} . We expand $\hat{G}(\mathbf{k}; Z)$ for small \mathbf{k} , retain the terms up to those quadratic in k_x, k_y and k_z and obtain⁶

$$\hat{G}(k_x, k_y; z, Z) = g(z, Z) - (k_x^2 + k_y^2) h(z, Z) + \dots \quad (2.13)$$

and

$$\hat{G}(\mathbf{k}; Z) = \hat{G}(0; Z) [1 + iak_z + (k_x^2 + k_y^2)\xi_z^2 + k_z^2\xi_l^2] + \dots, \quad (2.14)$$

with

$$\hat{G}(0; Z) = \int_{-\infty}^{+\infty} dz g(z, Z), \quad (2.15)$$

$$a(Z) = \int_{-\infty}^{+\infty} dz (z-Z) g(z, Z) / \hat{G}(0; Z), \quad (2.16)$$

$$\xi_l^2(Z) = \frac{1}{2} \int_{-\infty}^{+\infty} dz (z-Z)^2 g(z, Z) / \hat{G}(0; Z), \quad (2.17)$$

$$\xi_z^2(Z) = \int_{-\infty}^{+\infty} dz h(z, Z) / \hat{G}(0; Z). \quad (2.18)$$

Here ξ_l represents the longitudinal correlation length, i.e. the range of the correlation function in the direction parallel to the gravitational field and ξ_z represents the transverse correlation length, i.e. the range of the correlation function perpendicular to the gravitational field. As discussed in II, the coefficient a is a length which measures the asymmetry of the correlation function in the $+z$ and $-z$ directions. From (2.11) and (2.13) it follows that the functions $g(z, Z)$ and $h(z, Z)$ satisfy the differential equations

$$\left[\frac{d^2}{dz^2} - V(z) \right] g(z, Z) = \delta(z-Z), \quad (2.19)$$

$$\left[\frac{d^2}{dz^2} - V(z) \right] h(z, Z) = -g(z, Z). \quad (2.20)$$

We note in passing that the functions $g(z, Z)$ and $h(z, Z)$ are related to the functions $f_0(z-Z; Z)$ and $f_1(z-Z; Z)$ evaluated in II by

$$f_0(z-Z; Z) = g(z, Z) / g(Z, Z), \quad (2.21)$$

$$f_1(z-Z; Z) = h(z, Z) / g(Z, Z), \quad (2.22)$$

3. Scaling laws and universality

As shown in I-III the differential equation (2.1) for the density profile and the differential equation (2.9) for the correlation function can be brought into a universal form. As a first step the thermodynamic functions are made dimensionless with the aid of the critical density ρ_c , the critical temperature T_c and the critical pressure p_c . Specifically we define

$$\Delta T^* = (T - T_c) / T_c, \quad \Delta p^* = (\rho - \rho_c) / \rho_c, \quad (3.1)$$

$$\Delta \mu^* = [\mu(\rho, T) - \mu(\rho_c, T)] \rho_c / p_c, \quad (3.2)$$

$$\chi^* = \chi \rho_c / \rho_c^2, \quad A^* = A \rho_c^2 / p_c = \xi^2 / \chi^*. \quad (3.3)$$

The quantities $\Delta \mu^*$, χ^* , ξ and, hence, A^* are those of a homogeneous system with density ρ and temperature T . Near the critical point these quantities can be represented in terms of scaling laws with universal exponents and universal scaling functions in terms of a scaling variable $u = \Delta T^* / x_0 |\Delta p^*|^{1/\beta}$, where $x_0 = B^{-1/\beta}$ is related to the amplitude of the power law $\Delta \rho_{\text{coex}}^* = \pm B |\Delta T^*|^\beta$ for the density along the coexistence curve. The scaling laws have the form¹⁶

$$\Delta \mu^* = \pm D |\Delta p^*|^\delta h(u), \quad (3.4)$$

$$\chi^{*-1} = D |\Delta p^*|^{\gamma/\beta} X(u), \quad (3.5)$$

$$A^* = \frac{\xi_0^2 |\Delta p^*|^{-\eta\nu/\beta}}{D^{\eta\nu/\gamma} \Gamma^{2\nu/\gamma}} Y(u). \quad (3.6)$$

The scaling function $X(u)$ for χ^{*-1} is related to the scaling function $h(u)$ for $\Delta \mu^*$ by $X(u) = \delta h(u) - \beta^{-1} u dh(u)/du$. The exponents β , γ , $\delta = (\beta + \gamma)/\beta$, $\nu = (2\beta + \gamma)/3$ and $\eta = (2\nu - \gamma)/\nu$ are the usual critical exponents, while x_0 , D , Γ and ξ_0 are system-dependent amplitudes. We use the universal critical exponent values $\beta = 0.325$ and $\gamma = 1.240$, from which the other exponents follow. The corresponding values of the system-dependent amplitudes x_0 , D , Γ and ξ_0 have been presented in I and II for a number of fluids^{6,7}.

To specify the universal scaling functions $h(u)$ and $Y(u)$ we need to make a distinction between the one-phase region where $u > -1$ and the two-phase region where $u < -1$. In the one-phase region we use the closed-form approximants⁵⁻⁷

$$h(u) = (1+u) \left[\frac{1+E(1+u)^{2\beta}}{1+E} \right]^{(\gamma-1)/2\beta} \quad (u > -1), \quad (3.7)$$

with $E=0.287$ and

$$Y(u) = R^2(u)X^{-\eta\nu/\gamma}(u) \quad (u > -1), \quad (3.8)$$

with $R(u)=(8+u)/(7+u)$. In the two-phase region we adopt the procedure of the Fisk-Widom theory for interpolating at densities between those of the liquid and vapour at coexistence^{4,18} as discussed in III. In our terminology this procedure yields

$$h(u) = b[1-|u|^\gamma] \quad (u < -1), \quad (3.9)$$

$$Y(u) = Y(-1)|u|^{-\eta\nu} \quad (u < -1), \quad (3.10)$$

with

$$\frac{b}{\delta-1} = \frac{X(-1)}{\gamma} \left(\frac{1}{1+E} \right)^{(\gamma-1)/2\beta} = 0.735. \quad (3.11)$$

As a next step we define

$$g^* = g/g_0, \quad H_0 = p_c/\rho_c g_0, \quad (3.12)$$

where $g_0 = 9.81 \text{ m/s}^2$ is the gravitational acceleration constant at the surface of the earth and rescale density, temperature and lengths as⁵⁻⁷

$$\Delta\rho^* = \lambda\overline{\Delta\rho}, \quad \Delta T^* = \tau\overline{\Delta T}, \quad z = \zeta\bar{z}, \quad Z = \zeta\bar{Z}, \quad \xi = \zeta\bar{\xi}. \quad (3.13)$$

such that

$$\lambda = \lambda_0 g^{*\beta\phi}, \quad \tau = \tau_0 g^{*\phi}, \quad \zeta = \zeta_0 g^{*- \nu\phi}, \quad (3.14)$$

with $\phi = 1/(\beta\delta + \nu)$. The scale factors are

$$\lambda_0 = A_0^{\beta\phi/2}, \quad \tau_0 = x_0 A_0^{\phi/2}, \quad \zeta_0 = DH_0 A_0^{\beta\delta\phi/2}, \quad (3.15)$$

with

$$A_0 = \frac{\xi_0^2 Y(0)}{D^2 H_0^2 (D\Gamma)^{2\nu/\gamma}} = \frac{\xi_0^2 R^2(0)}{D^2 H_0^2 (D\Gamma)^{2\nu/\gamma\delta\eta\nu/\gamma}}. \quad (3.16)$$

Values of the system-dependent scale factors λ_0 , τ_0 and ζ_0 have been presented in previous publications for a number of fluids^{6,17}. In addition we find it convenient to define

$$\overline{\Delta\mu} = \pm |\overline{\Delta\rho}|^\delta h(u), \quad (3.17)$$

$$\overline{\chi}^{-1} = |\overline{\Delta\rho}|^{\gamma\beta} X(u), \quad (3.18)$$

$$\bar{A}^{-1} = |\bar{\Delta\rho}|^{\eta\nu/\beta} G(u), \quad (3.19)$$

with $G(u) = Y(0)/Y(u)$.

The gravitationally induced inhomogeneities are symmetric with respect to the central level where $\rho = \rho_c$. Hence, it is sufficient to solve the differential equations (2.1) for $z > 0$ and the differential equations (2.19) and (2.20) for $Z > 0$. In terms of the rescaled quantities the differential equations become⁵⁻⁷

$$\frac{d^2}{d\bar{z}^2} |\bar{\Delta\rho}| = (\bar{\Delta\mu} - \bar{z}) \bar{A}^{-1} \quad (3.20)$$

and

$$\left[\frac{d^2}{d\bar{z}^2} - \bar{V}(\bar{z}) \right] \bar{g}(\bar{z}, \bar{Z}) = \delta(\bar{z} - \bar{Z}), \quad (3.21)$$

$$\left[\frac{d^2}{d\bar{z}^2} - \bar{V}(\bar{z}) \right] \bar{h}(\bar{z}, \bar{Z}) = -\bar{g}(\bar{z}, \bar{Z}), \quad (3.22)$$

with

$$\bar{V}(\bar{z}) = \bar{A}^{-1} \bar{\chi}^{-1} = |\bar{\Delta\rho}|^{2\nu/\beta} X(u) G(u). \quad (3.23)$$

The functions $\bar{g}(\bar{z}, \bar{Z})$ and $\bar{h}(\bar{z}, \bar{Z})$ are related to the functions $g(z, Z)$ and $h(z, Z)$ in (2.13) by

$$g(z, Z) = \zeta \bar{g}(\bar{z}, \bar{Z}), \quad h(z, Z) = \zeta^3 \bar{h}(\bar{z}, \bar{Z}). \quad (3.24)$$

We note that the functions $\bar{\Delta\mu}$, \bar{A} and \bar{V} depend on \bar{z} through the density $\bar{\Delta\rho}(\bar{z})$.

In conclusion, we first determine the function $\bar{\Delta\rho}(\bar{z})$ from (3.20) as described in I and III. We then solve the differential equations (3.21) and (3.22) for $\bar{g}(\bar{z}, \bar{Z})$ and $\bar{h}(\bar{z}, \bar{Z})$ and finally calculate the scaled correlation lengths $\bar{a} = a/\zeta$, $\bar{\xi}_l = \xi_l/\zeta$ and $\bar{\xi}_r = \xi_r/\zeta$ from

$$\bar{a}(\bar{Z}) = \int_{-\infty}^{\infty} d\bar{z} (\bar{z} - \bar{Z}) \bar{g}(\bar{z}, \bar{Z}) / \bar{Q}(\bar{Z}), \quad (3.25)$$

$$\bar{\xi}_l^2(\bar{Z}) = \frac{1}{2} \int_{-\infty}^{\infty} d\bar{z} (\bar{z} - \bar{Z})^2 \bar{g}(\bar{z}, \bar{Z}) / \bar{Q}(\bar{Z}), \quad (3.26)$$

$$\bar{\xi}_r^2(\bar{Z}) = \int_{-\infty}^{\infty} d\bar{z} \bar{h}(\bar{z}, \bar{Z}) / \bar{Q}(\bar{Z}), \quad (3.27)$$

with

$$\bar{Q}(\bar{Z}) = \int_{-\infty}^{\infty} d\bar{z} \bar{g}(\bar{z}, \bar{Z}). \quad (3.28)$$

These scaled correlation lengths are universal functions of the scaled height \bar{Z} and the scaled temperature $\bar{\Delta T}$.

4. Method of solution

In this chapter we focus our attention on the correlation lengths \bar{a} , $\bar{\xi}_l$ and $\bar{\xi}_i$ in and near the liquid-vapour interface. The density profiles $\bar{\Delta\rho}(\bar{z})$ through the interface are calculated from (3.20) as a function of $\bar{\Delta T}$ as described in III. The differential equations (3.21) and (3.22) are then solved numerically for a given \bar{Z} . The procedure is similar to the procedure adopted in II for the determination of the correlation function in the one-phase region above T_c except the boundary conditions are now treated by the presence of the δ -function in (3.21). We first solve numerically the auxiliary problem⁶

$$\left[\frac{d^2}{d\bar{z}^2} - \bar{V}(\bar{z}) \right] f_0(\bar{z}) = 0, \quad (4.1)$$

$$\left[\frac{d^2}{d\bar{z}^2} - \bar{V}(\bar{z}) \right] f_1(\bar{z}) = -f_0(\bar{z}), \quad (4.2)$$

subject to the boundary conditions

$$f_0(0) = 1, \quad \dot{f}_1(0) = 0, \quad (4.3)$$

$$\lim_{\bar{z} \rightarrow \infty} f_0(\bar{z}) = 0, \quad \lim_{\bar{z} \rightarrow \infty} f_1(\bar{z}) = 0. \quad (4.4)$$

Here we adopt the notation $\dot{f}(z) = df/dz$. The solution of (3.21) is constructed as

$$\bar{g}(\bar{z}, \bar{Z}) = \psi(\bar{Z}) f_0(\bar{z}) / f_0(\bar{Z}), \quad \text{for } \bar{z} > \bar{Z}, \quad (4.5a)$$

$$\bar{g}(\bar{z}, \bar{Z}) = \psi(\bar{Z}) f_0(-\bar{z}) / f_0(-\bar{Z}), \quad \text{for } \bar{z} < \bar{Z}, \quad (4.5b)$$

where the parameter $\psi(\bar{Z})$ is determined by the condition

$$\lim_{\bar{z} \rightarrow \bar{Z}^+} \frac{d\bar{g}(\bar{z}, \bar{Z})}{d\bar{z}} - \lim_{\bar{z} \rightarrow \bar{Z}^-} \frac{d\bar{g}(\bar{z}, \bar{Z})}{d\bar{z}} = -1, \quad (4.6)$$

which yields

$$\psi(\bar{Z}) = -\frac{1}{f_0(\bar{Z})/f_0(\bar{Z}) + f_0(-\bar{Z})/f_0(-\bar{Z})}. \quad (4.7)$$

The solution of (3.22) is subsequently constructed as

$$\bar{h}(\bar{z}, \bar{Z}) = \psi(\bar{Z}) [f_1(\bar{z}) + p(\bar{Z}) f_0(\bar{z})] / f_0(\bar{Z}), \quad \text{for } \bar{z} > \bar{Z}, \quad (4.8a)$$

$$\bar{h}(\bar{z}, \bar{Z}) = \psi(\bar{Z}) [f_1(-\bar{z}) + q(\bar{Z}) f_0(-\bar{z})] / f_0(-\bar{Z}), \quad \text{for } \bar{z} < \bar{Z}. \quad (4.8b)$$

The parameters $p(\bar{Z})$ and $q(\bar{Z})$ are chosen such that $\bar{h}(\bar{z}, \bar{Z})$ is continuous in value and slope at $\bar{z}=\bar{Z}$. Hence, they are calculated from

$$p(\bar{Z}) + f_1(\bar{Z})/f_0(\bar{Z}) = q(\bar{Z}) + f_1(-\bar{Z})/f_0(-\bar{Z}), \quad (4.9a)$$

$$[p(\bar{Z})\dot{f}_0(\bar{Z}) + \dot{f}_1(\bar{Z})]/f_0(\bar{Z}) = -[q(\bar{Z})\dot{f}_0(-\bar{Z}) + \dot{f}_1(-\bar{Z})]/f_0(-\bar{Z}). \quad (4.9b)$$

Finally, we obtain the correlation lengths $\bar{a}(\bar{Z})$, $\bar{\xi}_l(\bar{Z})$ and $\bar{\xi}_r(\bar{Z})$ from a numerical evaluation of (3.25)-(3.28).

At any given temperature $\bar{\Delta T}$ the numerical procedure for solving the differential equations becomes inaccurate for large values of $|\bar{z}|$ and $|\bar{Z}|$. However, then we can determine the solution explicitly from a small-gradient expansion like described in chapter II and III. For this purpose we expand the potential $\bar{V}(\bar{z})$ as

$$\bar{V}(\bar{z}) = \bar{V}(\bar{Z}) \sum_{n=0} X_n(\bar{Z}) s^n, \quad (4.10)$$

where

$$s = (\bar{z} - \bar{Z})/\bar{\xi}(\bar{Z}). \quad (4.11)$$

We then solve in successive approximation the differential equations

$$\left[\frac{d^2}{ds^2} - (1 + X_1 s + X_2 s^2 + \dots) \right] f_0(s) = 0, \quad (4.12)$$

$$\left[\frac{d^2}{ds^2} - (1 + X_1 s + X_2 s^2 + \dots) \right] h_1(s) = -f_0(s). \quad (4.13)$$

Explicit expressions for the expansions of $f_0(s)$ and $h_1(s)$ have been presented in II. The functions $\bar{g}(\bar{z}, \bar{Z})$ and $\bar{h}(\bar{z}, \bar{Z})$ are then obtained as

$$\bar{g}(\bar{z}, \bar{Z}) = \bar{\xi}(\bar{Z}) \psi(\bar{Z}) f_0(s), \quad (4.14)$$

$$\bar{h}(\bar{z}, \bar{Z}) = \bar{\xi}^3(\bar{Z}) \psi(\bar{Z}) h_1(s), \quad (4.15)$$

with $\psi(\bar{Z})$ again determined by the condition (4.6).

5. Asymptotic analysis for large values of $|\bar{\Delta T}|$

The small-gradient expansion mentioned in the preceding section is not suitable to determine the asymptotic behaviour of the solution of the differential equation for large $|\bar{\Delta T}|$ in and near the interface. The reason is that the potential $V(z)$ below T_c has an eigenvalue zero. In this respect the situation differs fundamentally from the situation in the one-phase region above T_c considered previously⁶.

Large values of $|\bar{\Delta T}|$ correspond to small g^* and we determine the asymptotic behaviour of the solution of the differential equations for large $|\bar{\Delta T}|$ by developing

a perturbation expansion for small g^* . The procedure is similar to the procedure adopted for the asymptotic analysis of the interface thickness in III. For this purpose it is convenient to use the revised variables⁷

$$\bar{\Delta p} = \frac{\Delta p^*}{B |\Delta T^*|^\beta} = \frac{\bar{\Delta p}}{|\bar{\Delta T}|^\beta}, \quad (5.1)$$

$$\bar{z} = \frac{z}{\xi_{cxc}} = \frac{\bar{z}}{\xi_{cxc}}, \quad \bar{Z} = \frac{Z}{\xi_{cxc}} = \frac{\bar{Z}}{\xi_{cxc}}, \quad (5.2)$$

where $\xi_{cxc} = \xi \bar{\xi}_{cxc}$ is the bulk correlation length of the homogeneous liquid and vapour phases at coexistence. This bulk correlation length $\xi_{cxc} = \xi(\Delta p_{cxc})$ is given by

$$\bar{\xi}_{cxc} = \bar{A}(-1)\bar{\chi}(-1) = \bar{\xi}_0^2 |\bar{\Delta T}|^{-2\nu}, \quad (5.3)$$

with $\bar{\xi}_0 = [X(-1)G(-1)]^{-1/2} = 0.613$. The differential equation (3.20) for the density profile becomes

$$\frac{d^2}{d\bar{z}^2} |\bar{\Delta p}| = \left[\frac{|\bar{\Delta p}|^b h(u)}{b(8-1)} - \bar{g}\bar{z} \right] |\bar{\Delta p}|^{\eta w/\beta} \frac{G(u)}{G(-1)}, \quad (5.4)$$

where b is defined by (3.11) and where

$$\bar{g} = \bar{\xi}_0^{-3} G(-1) |\bar{\Delta T}|^{-1/\phi}. \quad (5.5)$$

The variables $\bar{\Delta p}$, \bar{z} and \bar{g} are chosen such that in the two-phase region, i.e. for $|\bar{\Delta p}| \leq 1$, the differential equations for the density $\bar{\Delta p}(\bar{z})$ and the density gradient $\bar{\Phi}(\bar{z}) \equiv d\bar{\Delta p}/d\bar{z}$ become

$$\frac{d^2}{d\bar{z}^2} |\bar{\Delta p}| = \frac{1}{8-1} [|\bar{\Delta p}|^8 - |\bar{\Delta p}|] - \bar{g}\bar{z}, \quad (5.6)$$

$$\left[\frac{d^2}{d\bar{z}^2} - \bar{V}(\bar{z}) \right] \bar{\Phi}(\bar{z}) = \bar{g}, \quad (5.7)$$

with

$$\bar{V}(\bar{z}) = \frac{1}{8-1} [\delta |\bar{\Delta p}|^{8-1} - 1]. \quad (5.8)$$

The scaled correlation lengths $\bar{a} = a/\xi_{cxc}$, $\bar{\xi}_l = \xi_l/\xi_{cxc}$ and $\bar{\xi}_v = \xi_v/\xi_{cxc}$ are now related to the functions $\bar{g}(\bar{z}, \bar{Z}) = g(z, Z)/\xi_{cxc}$ and $\bar{h}(\bar{z}, \bar{Z}) = h(z, Z)/\xi_{cxc}^3$ to be determined from

$$\left[\frac{d^2}{d\bar{z}^2} - \bar{V}(\bar{z}) \right] \bar{g}(\bar{z}, \bar{Z}) = \delta(\bar{z} - \bar{Z}), \quad (5.9)$$

$$\left[\frac{d^2}{d\bar{z}^2} - \bar{V}(\bar{z}) \right] \bar{h}(\bar{z}, \bar{Z}) = -\bar{g}(\bar{z}, \bar{Z}). \quad (5.10)$$

From (3.13), (3.14) and (5.5) we note that \bar{g} is proportional to g^* . If we take $\bar{g}=0$, we obtain from (5.6) the intrinsic density profile $\bar{\Delta p}_0(\bar{z})$ of the Fisk-Widom theory. We now develop a perturbation expansion for small \bar{g} and write

$$\bar{\Delta p}(\bar{z}) = \bar{\Delta p}_0(\bar{z}) + \bar{\Delta p}_1(\bar{z}) + \dots, \quad (5.11)$$

$$\bar{\Phi}(\bar{z}) = \bar{\Phi}_0(\bar{z}) + \bar{\Phi}_1(\bar{z}) + \dots, \quad (5.12)$$

$$\bar{V}(\bar{z}) = \bar{V}_0(\bar{z}) + \bar{V}_1(\bar{z}) + \dots, \quad (5.13)$$

where $\bar{\Phi}_0(\bar{z}) \equiv d\bar{\Delta p}_0/d\bar{z}$ and where $\bar{V}_0(\bar{z})$ is obtained from (5.8) by substitution of $\bar{\Delta p}_0(\bar{z})$. Our notation is such that $\bar{\Delta p}_i(\bar{z})$, $\bar{\Phi}_i(\bar{z})$ and $\bar{V}_i(\bar{z})$ are of order \bar{g}^i . We note that $\bar{\Delta p}_0(\pm\infty) = \mp 1$, so that $\bar{V}_0(\pm\infty) = 1$ and

$$m^{(0)} = \int_{-\infty}^{+\infty} d\bar{z} \bar{\Phi}_0(\bar{z}) = -2. \quad (5.14)$$

For the equation-of-state parameters adopted by us $\bar{\Delta p}_0(\bar{z})$ was determined in III. For the second moment of $\bar{\Phi}_0(\bar{z})$ we find

$$m^{(2)} = \int_{-\infty}^{+\infty} d\bar{z} \bar{z}^2 \bar{\Phi}_0(\bar{z}) = -2.053. \quad (5.15)$$

We first consider the expansion for the function $\bar{g}(\bar{z}, \bar{Z})$

$$\bar{g}(\bar{z}, \bar{Z}) = g_{-1}(\bar{z}, \bar{Z}) + g_0(\bar{z}, \bar{Z}) + \dots, \quad (5.16)$$

where g_{-1} and g_0 satisfy the differential equations

$$\left[\frac{d^2}{d\bar{z}^2} - \bar{V}_0(\bar{z}) \right] g_{-1}(\bar{z}, \bar{Z}) = 0, \quad (5.17)$$

$$\left[\frac{d^2}{d\bar{z}^2} - \bar{V}_0(\bar{z}) \right] g_0(\bar{z}, \bar{Z}) = \bar{V}_1(\bar{z}) g_{-1}(\bar{z}, \bar{Z}) + \delta(\bar{z} - \bar{Z}). \quad (5.18)$$

The solution of (5.17) is of the form

$$g_{-1}(\bar{z}, \bar{Z}) = c_{-1} \bar{\Phi}_0(\bar{z}) \bar{\Phi}_0(\bar{Z}), \quad (5.19)$$

with the coefficient c_{-1} arbitrary. As the differential operator on the left-hand side of (5.18) has an eigenvalue zero with the eigenfunction $\bar{\Phi}_0(\bar{z})$, the right-hand side of (5.18) must be orthogonal to $\bar{\Phi}_0(\bar{z})$. The same holds for the gradient $\bar{\Phi}_1(\bar{z}) \equiv d\bar{\Delta p}_1/d\bar{z}$ which satisfies the equation

$$\left[\frac{d^2}{d\bar{z}^2} - \bar{V}_0(\bar{z}) \right] \bar{\Phi}_1(\bar{z}) = \bar{V}_1(\bar{z}) \bar{\Phi}_0(\bar{z}) + \bar{g}. \quad (5.20)$$

if we multiply (5.18) and (5.20) with $\tilde{\Phi}_0(\tilde{z})$ and integrate over all \tilde{z} , we obtain

$$c_{-1} \int_{-\infty}^{+\infty} d\tilde{z} \tilde{\Phi}_0(\tilde{z}) \tilde{V}_1(\tilde{z}) \tilde{\Phi}_0(\tilde{z}) + 1 = 0. \quad (5.21)$$

$$\int_{-\infty}^{+\infty} d\tilde{z} \tilde{\Phi}_0(\tilde{z}) \tilde{V}_1(\tilde{z}) \tilde{\Phi}_0(\tilde{z}) + m^{(0)} \tilde{g} = 0, \quad (5.22)$$

and we conclude

$$c_{-1} = \frac{1}{m^{(0)} \tilde{g}} = -\frac{1}{2\tilde{g}}. \quad (5.23)$$

To evaluate the correlation lengths $\tilde{a}(\tilde{Z})$ and $\tilde{\xi}_i(\tilde{Z})$ we consider the moments

$$\tilde{M}_i^{(n)} = \int_{-\infty}^{+\infty} d\tilde{z} \tilde{z}^n g_i(\tilde{z}, \tilde{Z}), \quad (5.24)$$

so that (cf. (3.25), (3.26), (3.28))

$$\tilde{a}(\tilde{Z}) = \sum_{i=-1}^0 [M_i^{(1)}(\tilde{Z}) - \tilde{Z} M_i^{(0)}(\tilde{Z})] / \tilde{Q}(\tilde{Z}), \quad (5.25)$$

$$\tilde{\xi}_i^2(\tilde{Z}) = \frac{1}{2} \sum_{i=-1}^0 [M_i^{(2)}(\tilde{Z}) - 2\tilde{Z} M_i^{(1)}(\tilde{Z}) + \tilde{Z}^2 M_i^{(0)}(\tilde{Z})] / \tilde{Q}(\tilde{Z}), \quad (5.26)$$

with

$$\tilde{Q}(\tilde{Z}) = M_{-1}^{(0)}(\tilde{Z}) + M_0^{(0)}(\tilde{Z}), \quad (5.27)$$

if we terminate the expansion (5.16) at $i=0$. From (5.19) and (5.23) we obtain

$$\begin{aligned} M_{-1}^{(0)} &= \tilde{g}^{-1} \tilde{\Phi}_0(\tilde{z}), \quad M_{-1}^{(1)}(\tilde{Z}) = 0, \\ M_{-1}^{(2)}(\tilde{Z}) &= \tilde{g}^{-1} (m^{(2)}/m^{(0)}) \tilde{\Phi}_0(\tilde{Z}). \end{aligned} \quad (5.28)$$

Because of the symmetry of $g_0(\tilde{z}, \tilde{Z})$ the moments $M_0^{(n)}(\tilde{z})$ satisfy the differential equation

$$\left[\frac{d^2}{d\tilde{z}^2} - \tilde{V}_0(\tilde{z}) \right] M_0^{(n)} = \tilde{V}_1(\tilde{z}) c_{-1} m^{(n)} \tilde{\Phi}_0(\tilde{z}) + \tilde{z}^n. \quad (5.29)$$

For large values of \tilde{z} the gradient $\tilde{\Phi}_0(\tilde{z})$ decays exponentially⁷, while $\tilde{V}_0(\tilde{z})$ approaches unity. Hence, for large values of \tilde{z} the moments $M_0^{(n)}(\tilde{z})$ approach the values

$$M_0^{(0)}(\tilde{z}) \approx -1, \quad M_0^{(1)}(\tilde{z}) \approx -\tilde{z}, \quad M_0^{(2)}(\tilde{z}) \approx -(\tilde{z}^2 + 2). \quad (5.30)$$

The moments $M_{-1}^{(0)}(\tilde{Z})$ and $M_{-1}^{(2)}(\tilde{Z})$ in (5.25) and (5.26) dominate for small \tilde{Z}

where $\tilde{\Phi}_0(\tilde{Z})$ is very large, while the moments $M_0^{(n)}(\tilde{Z})$ take over for large \tilde{Z} where $\tilde{\Phi}_0(\tilde{Z})$ vanishes. Then, however, the asymptotic forms (5.30) apply and we obtain for all practical purposes

$$\bar{a}(\tilde{Z}) = -\frac{\tilde{Z}\tilde{\Phi}_0(\tilde{Z})}{\tilde{\Phi}_0(\tilde{Z}) - \bar{g}} \quad (5.31)$$

$$\bar{\xi}_l^2(\tilde{Z}) = \frac{1}{2} \frac{(\tilde{Z}^2 + m^{(2)}/m^{(0)})\tilde{\Phi}_0(\tilde{Z}) - 2\bar{g}}{\tilde{\Phi}_0(\tilde{Z}) - \bar{g}} \quad (5.32)$$

We next consider the expansion for the function $\tilde{h}(\tilde{z}, \tilde{Z})$,

$$\tilde{h}(\tilde{z}, \tilde{Z}) = h_{-2}(\tilde{z}, \tilde{Z}) + h_{-1}(\tilde{z}, \tilde{Z}) + h_0(\tilde{z}, \tilde{Z}) + \dots, \quad (5.33)$$

where h_{-2} , h_{-1} and h_0 satisfy the differential equations

$$\left[\frac{d^2}{d\tilde{z}^2} - \tilde{V}_0(\tilde{z}) \right] h_{-2}(\tilde{z}, \tilde{Z}) = 0, \quad (5.34)$$

$$\left[\frac{d^2}{d\tilde{z}^2} - \tilde{V}_0(\tilde{z}) \right] h_{-1}(\tilde{z}, \tilde{Z}) = \tilde{V}_1(\tilde{z})h_{-2}(\tilde{z}, \tilde{Z}) - g_{-1}(\tilde{z}, \tilde{Z}), \quad (5.35)$$

$$\left[\frac{d^2}{d\tilde{z}^2} - \tilde{V}_0(\tilde{z}) \right] h_0(\tilde{z}, \tilde{Z}) = \tilde{V}_1(\tilde{z})h_{-1}(\tilde{z}, \tilde{Z}) + \tilde{V}_2(\tilde{z})h_{-2}(\tilde{z}, \tilde{Z}) - g_0(\tilde{z}, \tilde{Z}). \quad (5.36)$$

Again we need the freedom in the solution of (5.34),

$$h_{-2}(\tilde{z}, \tilde{Z}) = c_{-2}\tilde{\Phi}_0(\tilde{z})\tilde{\Phi}_0(\tilde{Z}), \quad (5.37)$$

to make (5.35) soluble. If we multiply (5.35) with $\tilde{\Phi}_0(\tilde{z})$ and integrate over all \tilde{z} , we obtain with (5.19) and (5.21)

$$c_{-2} = -c_{-1}^2 \int_{-\infty}^{+\infty} d\tilde{z} \tilde{\Phi}_0(\tilde{z})^2 = -4c_{-1}^2 K, \quad (5.38)$$

where⁷

$$K = \frac{1}{\sqrt{2(8^2-1)}} \int_0^1 dy \left(y^{8+1} - \frac{8+1}{2}y^2 + \frac{8-1}{2} \right)^{1/2} = 0.144. \quad (5.39)$$

To evaluate the transverse correlation length $\tilde{\xi}_t(\tilde{Z})$ we need the zeroth moments

$$N_i(\tilde{Z}) = \int_{-\infty}^{+\infty} d\tilde{z} h_i(\tilde{z}, \tilde{Z}), \quad (5.40)$$

so that (cf. (3.27))

$$\bar{\xi}_i^2(\bar{Z}) = \sum_{i=-2}^0 N_i(\bar{Z})/\bar{Q}(\bar{Z}) . \quad (5.41)$$

For the moment $N_{-2}(\bar{Z})$ we obtain

$$N_{-2}(\bar{Z}) = c_{-2} m^{(0)} \bar{\Phi}_0(\bar{Z}) = 2K\bar{g}^{-2} \bar{\Phi}_0(\bar{Z}) . \quad (5.42)$$

The moment $N_{-1}(\bar{Z})$ is not interesting, since it is restricted to small \bar{Z} as one finds from (5.35); there, however, $N_{-2}(\bar{Z})$ dominates. Because of the symmetry of $h_0(\bar{z}, \bar{Z})$, the moment $N_0(\bar{z})$ satisfies the differential equation

$$\left[\frac{d^2}{d\bar{z}^2} - \bar{V}_0(\bar{z}) \right] N_0(\bar{z}) = \bar{V}_1(\bar{z}) N_{-1}(\bar{z}) + \bar{V}_2(\bar{z}) N_{-2}(\bar{z}) - M_0^{(0)}(\bar{z}) , \quad (5.43)$$

from which we conclude that asymptotically for large \bar{z}

$$N_0(\bar{z}) \approx M_0^{(0)}(\bar{z}) \approx -1 . \quad (5.44)$$

We thus obtain from (5.41)

$$\bar{\xi}_i^2(\bar{Z}) = \frac{-2K\bar{\Phi}_0(\bar{Z}) + \bar{g}^2}{-\bar{g}\bar{\Phi}_0(\bar{Z}) + \bar{g}^2} . \quad (5.45)$$

The asymptotic expressions (5.31), (5.32) and (5.45) for the correlation lengths supplement the numerical data in the regime of small \bar{g} and, hence, large $|\Delta T|_1$, where the numerical procedure is in practice restricted to very small values of Z only.

It is of interest to consider the value of the transverse correlation length at the central layer $\bar{Z}=0$. For small values of \bar{g} we obtain from (5.45)

$$\bar{\xi}_i^2(0) = 2K/\bar{g} , \quad (5.46)$$

or, using (5.2) and (5.5),

$$\bar{\xi}_i^2(0) = \frac{1}{2} \bar{\sigma}_0 |\Delta T|^{2\nu-\beta} , \quad (5.47)$$

with $\bar{\sigma}_0 = 4K[X(-1)/G(-1)]^{1/2} = 0.99$. As discussed in III, $\bar{\sigma} = \bar{\sigma}_0 |\Delta T|^{2\nu}$ is the scaled surface tension in the Fisk-Widom limit $\bar{g} \rightarrow 0$. The capillary length $L_\sigma = \zeta L_\sigma$ is defined by $L_\sigma^2 = \sigma/2g |\Delta \rho_{exc}|$ so that

$$\bar{L}_\sigma^2 = \frac{\bar{\sigma}}{2|\Delta T|^\beta} = \frac{1}{2} \bar{\sigma}_0 |\Delta T|^{2\nu-\beta} . \quad (5.48)$$

On comparing (5.47) with (5.48) we conclude that the transverse correlation length $\bar{\xi}_i(0)$ approaches the capillary length L_σ at temperatures well below the critical temperature^{19,20}.

6. Results

Using the method described in section 4, we have determined the correlation length profiles $\bar{a}(Z)$, $\xi_l(Z)$ and $\xi_v(Z)$ for a large number of temperatures. In figs. 1-3 we show the correlation length profiles obtained at a number of selected temperatures below the critical temperature. Values of some characteristic quantities associated with these correlation length profiles are given in table I. Of special interest are the levels $Z = \pm Z_{cx}$, where the local density $\Delta\rho$ equals the density $\Delta\rho_{cx} = \pm |\Delta T|^\beta$ of the homogeneous liquid and vapour phases at coexistence. These heights are also indicated in figs. 1-3. At temperatures above the critical temperature we recover the results reported in II. For comparison we show in figs. 4-6 the same correlation length profiles at a few temperatures above and below the critical temperature.

We first consider the profiles $\bar{a}(Z)$ shown in figs. 1 and 4. As discussed in II \bar{a} is the difference between the two unidirectional correlation lengths in the positive and the negative z directions and is, therefore, a measure of the lack of symmetry of the correlation function in the directions parallel and opposite to the gravitational field. The structure of the profiles $\bar{a}(Z)$ as a function of height below the critical temperature is similar to the structure found in II for $\bar{a}(Z)$ in the one-phase

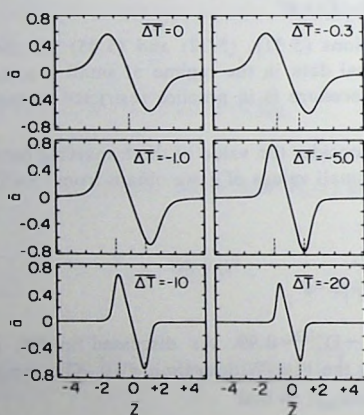


Fig. 1. Scaled asymmetry correlation length \bar{a} as a function of Z for various values of $\Delta T \leq 0$. The dashed marks on the Z -axis indicate the positions $Z = \pm Z_{cx}$, where $\Delta\rho = \pm |\Delta\rho_{cx}|$.

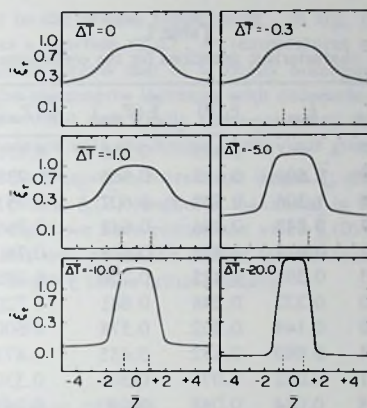


Fig. 2. Scaled transverse correlation length $\bar{\xi}_t$ as a function of \bar{Z} for various values of $\Delta T \leq 0$. The dashed marks on the \bar{Z} -axis indicate the positions $\bar{Z} = \pm \bar{Z}_{cxc}$ where $\Delta \rho = \pm |\Delta \rho_{cxc}|$.

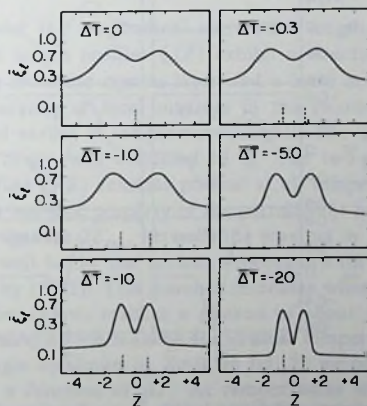


Fig. 3. Scaled longitudinal correlation length $\bar{\xi}_l$ as a function of \bar{Z} for various values of $\Delta T \leq 0$. The dashed marks on the \bar{Z} -axis indicate the positions $\bar{Z} = \pm \bar{Z}_{cxc}$ where $\Delta \rho = \pm |\Delta \rho_{cxc}|$.

Table I
Values of some characteristic quantities for the correlation length profiles.

ΔT	\bar{Z}_{exc}	\bar{Z}_{max}	$\bar{\xi}_{exc}$	$\bar{\xi}_l(0)$	$\bar{\xi}_l(\bar{Z}_{exc})$	$\bar{\xi}_l(\bar{Z}_{max})$	$\bar{\xi}_l(0)$	$\bar{\xi}_l(\bar{Z}_{exc})$
0.0	0	1.57	∞	0.515	0.515	0.731	0.889	0.889
-0.1	0.51	1.57	2.601	0.513	0.563	0.738	0.903	0.888
-0.3	0.72	1.57	1.305	0.508	0.607	0.751	0.927	0.897
-0.6	0.87	1.55	0.843	0.496	0.648	0.766	0.963	0.916
-1.0	0.98	1.52	0.612	0.478	0.686	0.780	1.014	0.948
-2.0	1.07	1.43	0.395	0.425	0.726	0.788	1.143	1.051
-5.0	0.99	1.20	0.222	0.298	0.681	0.720	1.547	1.416
-10.0	0.84	0.95	0.144	0.202	0.578	0.600	2.083	1.923
-20.0	0.67	0.74	0.093	0.132	0.455	0.473	2.86	2.66
-50.0	0.47	0.51	0.052	0.075	0.306	0.330	4.38	4.18
-100.0	0.35	0.38	0.034	0.048	0.240	0.245	6.06	5.78

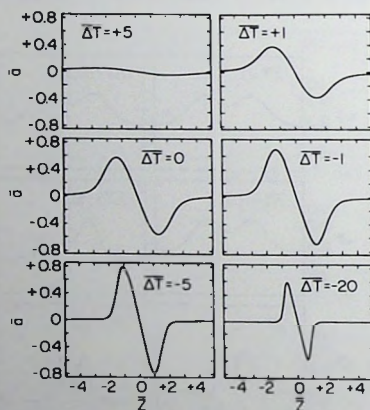


Fig. 4. Scaled asymmetry correlation length \bar{a} as a function of \bar{Z} for selected values of ΔT .

region above but close to the critical temperature. In fig. 7 we have plotted the maximum value \bar{a}_{\max} as a function of ΔT . At temperatures sufficiently well above T_c the correlation function equals that of a locally homogeneous system without any asymmetry, then the asymmetry increases with decreasing temperatures reaching a maximum at $\Delta T \approx -3.9$ and finally the asymmetry decreases upon further decrease of ΔT in accordance with the limiting behaviour given by (5.31).

Next we consider the transverse correlation length $\bar{\xi}_t$ shown in figs. 2 and 5. The correlation length profile $\bar{\xi}_t(\bar{Z})$ reaches a maximum in the central layer $\bar{Z}=0$ at all temperatures. In fig. 8 we have plotted the value $\bar{\xi}_t(0)$ as a function of temperature. At temperatures well above the critical temperature $\bar{\xi}_t(0)$ becomes equal to the bulk correlation length $\bar{\xi}$ at the critical density

$$\bar{\xi}(0) = \bar{\xi}_0 |\Delta T|^{-\nu}, \quad (6.1)$$

with

$$\bar{\xi}_0 = \lim_{u \rightarrow \infty} \frac{u^\nu}{\sqrt{X(u)G(u)}} = 1.174. \quad (6.2)$$

The transverse correlation length $\bar{\xi}_t(0)$ increases monotonically with decreasing temperatures crossing over smoothly from the bulk correlation length (6.1) well above the critical temperature to the capillary length (5.48) well below the critical temperature.

Finally, we consider the longitudinal correlation length $\bar{\xi}_l$ shown in figs. 3 and 6. The correlation length profiles $\bar{\xi}_l(\bar{Z})$ exhibit a structure with two peaks at levels $\bar{Z} = \pm \bar{Z}_{\max}$ away from the central layer and a local minimum at the central level $\bar{Z}=0$. The appearance of local maxima in the second-moment correlation length was also noticed earlier at temperatures slightly above the critical temperature and its physical origin was discussed in II. The two-peak structure in the correlation length profiles $\bar{\xi}_l(\bar{Z})$ remains present at all temperatures below T_c and hence appears to be an intrinsic property of the correlations in the interface. In fig. 9 we have plotted the distance $2\bar{Z}_{\max}$ between the maxima in $\bar{\xi}_l(\bar{Z})$ as a function of ΔT . At temperatures well below the critical temperature this distance approaches the behaviour implied by (5.32). This distance increases when the critical temperature is approached from below, reaches a plateau of about 3.14 near $\Delta T=0$ and vanishes at a temperature $\Delta T=3.8$ above the critical temperature, where the two peaks merge into a single maximum at $\bar{Z}=0$. In fig. 10 we have plotted the values $\bar{\xi}_l(\bar{Z}_{\max})$ and $\bar{\xi}_l(0)$ as a function of ΔT . At temperatures well above the critical temperature, the correlation length $\bar{\xi}_l(0)$ approaches the bulk correlation length (6.1). When the temperature decreases $\bar{\xi}_l(0)$ approaches passes through a maximum value $\bar{\xi}_l(0)=0.52$ at a temperature slightly above the critical temperature and $\bar{\xi}_l(\bar{Z}_{\max})$ through a maximum value $\bar{\xi}_l(\bar{Z}_{\max})=0.79$ at a temperature slightly

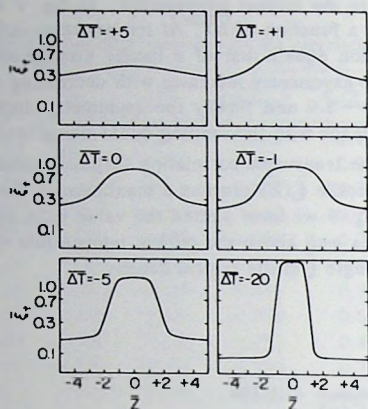


Fig. 5. Scaled transverse correlation length $\bar{\xi}_t$ as a function of \bar{Z} for various values of ΔT .

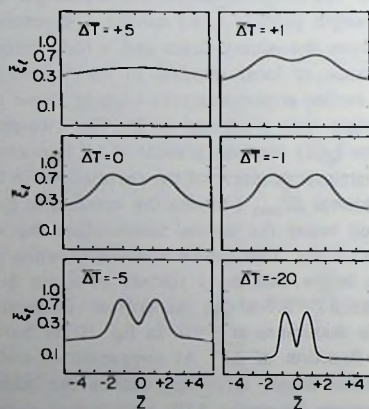


Fig. 6. Scaled longitudinal correlation length $\bar{\xi}_l$ as a function of \bar{Z} for selected values of ΔT .

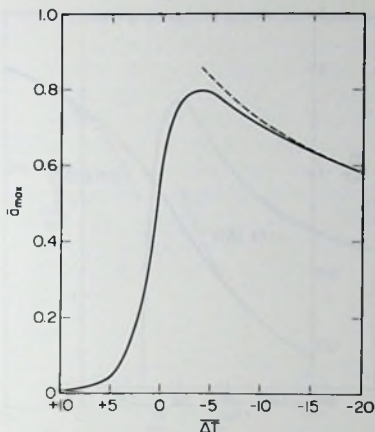


Fig. 7. Maximum value \bar{a}_{\max} of the asymmetry correlation length as a function of ΔT . The dashed curve represents the asymptotic behaviour implied by (5.31).

below the critical temperature $\bar{\xi}_l(0)$ and $\bar{\xi}_l(\bar{Z}_{\max})$ decrease with decreasing temperatures in accordance with the asymptotic behaviour implied by (5.32)

The interface thickness $L = \zeta \bar{L}$ was defined in III as the distance over which the density varies from that of the bulk liquid and vapour at coexistence

$$\bar{L} = 2\bar{Z}_{cxc} \quad (6.3)$$

Some values of the height \bar{Z}_{cxc} are given in table I. The positions $\bar{Z} = \pm \bar{Z}_{cxc}$ where the density becomes equal to that of the homogeneous liquid and vapour at the phase boundary are also indicated in figs. 1-3. In table I we have also included the corresponding values $\bar{\xi}_l(\bar{Z}_{cxc})$ and $\bar{\xi}_r(\bar{Z}_{cxc})$ of the correlation se levels $\bar{\xi}_l$ and $\bar{\xi}_r$ still differ significantly from the bulk correlation length $\bar{\xi}_{cxc} = \bar{\xi}(\Delta p_{cxc})$.

The definition (6.3) of the interface thickness based on the density profiles implies that L goes to zero at the critical temperature. From the information provided in figs. 1-3 and in table I, we see that the actual correlation lengths $\bar{\xi}_l$ and $\bar{\xi}_r$ differ from the bulk correlation length of the coexisting liquid and vapour phases over a distance appreciably larger than \bar{L} . In fact we note from table I that the peaks in $\bar{\xi}_l(\bar{Z})$ are located at a distance \bar{Z}_{\max} which is larger than \bar{Z}_{cxc} . Let $\bar{Z} = \pm \bar{Z}'$ be the levels where the actual correlation lengths reach values close to the correlation length $\bar{\xi}(\Delta p)$ of the locally homogeneous liquid and vapour phases. From figs. 2 and 3 we note that the levels $\bar{Z} = \pm \bar{Z}'$ can be identified reasonably well at lower

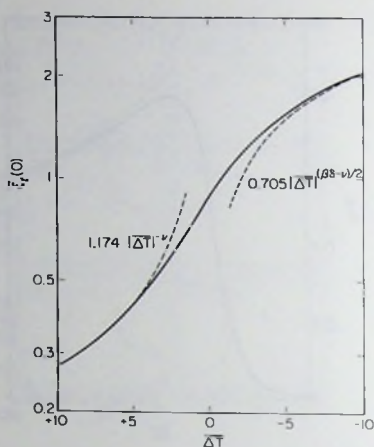


Fig. 8. The transverse correlation length $\bar{\xi}_t(0)$ at $\bar{Z}=0$ as a function of $\bar{\Delta T}$. The dashed curve for $\bar{\Delta T} > 0$ indicates the power law (6.1) for the bulk correlation length $\bar{\xi}(0)$. The dashed curve for $\bar{\Delta T} < 0$ indicates the power law (5.48) for the capillary length \bar{L}_c .

temperatures. Hence, we can consider an alternate interface thickness \bar{L} based on the density profiles. Closer to the critical temperature the interface thickness \bar{L}' based on the correlations can be defined less precisely, but it is certainly larger than the distance $2\bar{Z}_{\max}$ between the two peaks in the profiles of the longitudinal correlation length. Thus an interface thickness based on measurements of the structure factor of the interface does not vanish at the critical temperature, but at a temperature somewhat above T_c .

7. Discussion

The range of the correlation function of a fluid close to the critical point in the presence of a gravitational field can be characterized by three correlation length a , ξ_t , and ξ_l . The quantity a is a measure of the asymmetry of the correlations in the directions parallel and opposite to the gravitational field, ξ_t the transverse correlation length, i.e. the correlation length in the direction perpendicular to the gravitational field, and ξ_l the longitudinal correlation length, i.e. the correlation length in the direction along the gravitational field. These correlation lengths depend on the height Z , the temperature ΔT^* and the strength of the

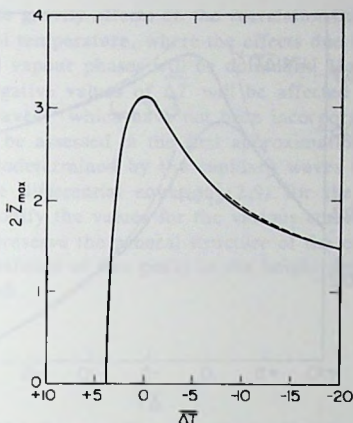


Fig. 9. The distance $2\bar{Z}_{\max}$ between the location of the maxima in $\bar{\xi}_l(\bar{Z})$ as a function of ΔT . The dashed curve indicates the asymptotic behaviour implied by (5.32).

gravitational field g^* . They satisfy scaling laws of the form

$$a(Z, \Delta T^*, g^*) = \zeta_0 g^{*-v\phi} \bar{a}\left(\frac{Z}{\zeta_0 g^{*-v\phi}}, \frac{\Delta T^*}{\tau_0 g^{*\phi}}\right), \quad (7.1)$$

$$\xi_r(Z, \Delta T^*, g^*) = \zeta_0 g^{*-v\phi} \bar{\xi}_r\left(\frac{Z}{\zeta_0 g^{*-v\phi}}, \frac{\Delta T^*}{\tau_0 g^{*\phi}}\right), \quad (7.2)$$

$$\xi_l(Z, \Delta T^*, g^*) = \zeta_0 g^{*-v\phi} \bar{\xi}_l\left(\frac{Z}{\zeta_0 g^{*-v\phi}}, \frac{\Delta T^*}{\tau_0 g^{*\phi}}\right), \quad (7.3)$$

where $\bar{a}(\bar{Z}, \bar{\Delta T})$, $\bar{\xi}_r(\bar{Z}, \bar{\Delta T})$ and $\bar{\xi}_l(\bar{Z}, \bar{\Delta T})$ are universal scaling functions. In this chapter we have determined these scaling functions for the correlation lengths as a function of \bar{Z} and $\bar{\Delta T}$. The correlation length profiles in the two-phase region below T_c are smoothly connected with the correlation length profiles in the one-phase region above T_c . When the temperature is decreased the transverse correlation length ξ_r increases monotonically from the bulk correlation length ξ at temperatures well above T_c to the capillary length L_σ at temperatures well below T_c with a finite value at the critical temperature itself. The longitudinal correlation length ξ_l exhibits a two-peak structure at all temperatures below T_c . This two-peak

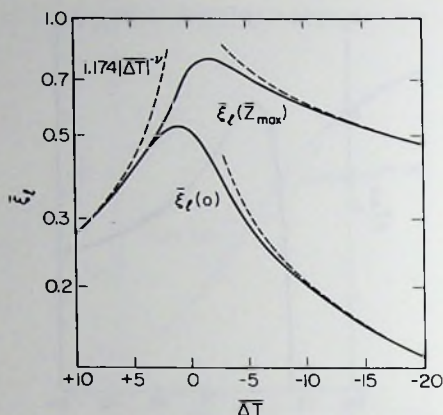


Fig. 10. The values $\bar{\xi}_l(\bar{Z}_{max})$ and $\bar{\xi}_l(0)$ of the longitudinal correlation length $\bar{\xi}_l$. The dashed curve for $\Delta T > 0$ indicates the power law (6.1) for the bulk correlation length. The dashed curves for $\Delta T < 0$ indicate the asymptotic behaviour for $\bar{\xi}_l(\bar{Z}_{max})$ and $\bar{\xi}_l(0)$ implied by (5.32).

structure persists at the critical temperature and disappears at a temperature above T_c .

Below the critical temperature the scaling laws (7.1)-(7.3) can be written in the alternate form

$$a(Z, \Delta T^*, g^*) = \xi_{cxc} \bar{a} \left(\frac{Z}{\xi_{cxc}}, \frac{L_\sigma}{\xi_{cxc}} \right), \quad (7.4)$$

$$\xi_t(Z, \Delta T^*, g^*) = \xi_{cxc} \bar{\xi}_t \left(\frac{Z}{\xi_{cxc}}, \frac{L_\sigma}{\xi_{cxc}} \right), \quad (7.5)$$

$$\xi_l(Z, \Delta T^*, g^*) = \xi_{cxc} \bar{\xi}_l \left(\frac{Z}{\xi_{cxc}}, \frac{L_\sigma}{\xi_{cxc}} \right), \quad (7.6)$$

where $\bar{L}_\sigma = L_\sigma / \xi_{cxc}$ is inversely proportional to \sqrt{g} in accordance with (5.46). This alternate form shows explicitly that gravity enters via the capillary length L_σ .

Our analysis of the gravity effects on the correlations applies to temperatures very close to the critical temperature, where the effects due to the large compressibility of the liquid and vapour phases will be dominant. However, the asymptotic behaviour for large negative values of ΔT will be affected by effects due to the presence of capillary waves¹¹ which have not been incorporated here. The effects of capillary waves can be assessed in the first approximation by adopting the full density profile $\Delta\rho(z)$ codetermined by the capillary waves and then solving with this density profile the differential equation (2.9) for the correlation function. This procedure may modify the values for the various correlation lengths at large negative ΔT , but will preserve the general structure of the correlation lengths profiles including the appearance of two peaks in the height dependence of the longitudinal correlation length.

References

- 1) P.C. Hohenberg and M. Barmatz, Phys. Rev. A **6** (1972) 289.
- 2) J.M.H. Levelt Sengers, in *Experimental Thermodynamics II*, B. Le Neindre and B. Vodar, eds. (Butterworths, London, 1975), p.657.
- 3) M.R. Moldover, J.V. Sengers, R.W. Gammon and R.J. Hocken, Rev. Mod. Phys. **51** (1979) 79.
- 4) J.S. Rowlinson and B. Widom, *Molecular Theory of Capillarity* (Clarendon, Oxford, 1982).
- 5) J.V. Sengers and J.M.J. van Leeuwen, Physica **116A** (1982) 345, to be referred to as I.
- 6) J.M.J. van Leeuwen and J.V. Sengers, Physica **128A** (1984) 99, to be referred to as II.
- 7) J.M.J. van Leeuwen and J.V. Sengers, Physica **132A** (1985) 207, to be referred to as III.
- 8) D.J. Klinger, M.E. Fisher and S. Fishman, J.Chem. Phys. **80** (1984) 3392.
- 9) J.D. Weeks, J. Chem. Phys. **67** (1977) 3106.
- 10) B. Widom, Faraday Symp. Chem. Soc. **16** (1981) 7.
- 11) D. Jasnow, Rep. Progr. Phys. **47** (1984) 1059.
- 12) D. Bedeaux, in *Fundamental Problems in Statistical Mechanics VI*, E.G.D. Cohen, ed. (North-Holland, Amsterdam, 1985), p.125.

- 13) D.A. Huse, W. van Saarloos and J.D. Weeks, *Phys. Rev. B* **32** (1985) 233.
- 14) J.V. Sengers and J.M.J. van Leeuwen, *J. Phys. Chem.* **88** (1984) 6479.
- 15) M.E. Fisher, *J. Math. Phys.* **5** (1964) 944.
- 16) J.V. Sengers and J.M.H. Levelt Sengers, in *Progress in Liquid Physics*, C.A. Croxton, ed. (Wiley, New York, 1978), p. 103.
- 17) J.V. Sengers and J.M.J. van Leeuwen, *Intern. J. Thermophys.* **6** (1985) 545.
- 18) S. Fisk and B. Widom, *J. Chem. Phys.* **50** (1969) 3219.
- 19) R. Evans, *Adv. Phys.* **28** (1979) 143.
- 20) R. Evans, *Mol. Phys.* **42** (1981) 1169.

CHAPTER V

**A MOLECULAR-DYNAMICS SIMULATION OF
A LIQUID-VAPOUR INTERFACE IN TWO DIMENSIONS**

ABSTRACT

We present a simulation of a two-dimensional system of Lennard-Jones particles, carried out on a special purpose molecular-dynamics hardware processor. We study the behaviour of the liquid-vapour interface in *two* dimensions. The interface width is observed to diverge as a function of the interface length in accordance with capillary wave theory. Also the transverse structure function is seen to diverge for small wavenumbers, which indicates the development of long wavelength correlations along the interface.

1. Introduction

In the last ten years several computer simulations of liquid-vapour coexistence have been carried out, most of them in three dimensions¹⁻⁴ for small particle numbers and system sizes. A simulation of two-dimensional liquid-vapour coexistence has been carried out by Abraham⁵. This author simulated a 256 particle system by Monte Carlo methods, proving the existence of an equilibrium liquid-vapour interface in two dimensions. Because of the small interface tension in two dimensions the interface strongly fluctuates and is irregularly structured.

A theory describing interface fluctuations is due to Buff, Lovett and Stillinger⁶, who argue that the actual interface is build up by thermally excited interface modes, called capillary waves, superimposed on an intrinsic interface. These capillary waves cause the interface width w to diverge as a function of the interface length L . In three dimensions this leads to the divergence $w^2 \sim \ln(L/a_0)$, a_0 being a microscopic length. This divergence is too weak to be observed in experiments or simulations. In two dimensions, however, the divergence goes as $w^2 \sim (L - a_0)$, which should be observable for system sizes large enough.

Here we present a molecular-dynamics simulation of a two dimensional liquid in coexistence with its vapour in which the divergence mentioned above can be observed. The molecular-dynamics simulation been carried out with the aid of the special purpose computer constructed by Bakker⁷⁻⁹. This molecular-dynamics processor has been used before by Bakker, Bruin and Hilhorst¹⁰ to study two dimensional melting, and by Bruin, Bakker and Bishop¹¹ to study the two dimensional phase diagram of Lennard-Jones particles. The special purpose computer uses the leap-frog scheme for numerical integration of the equations of motion of up to 16383 particles. One time-step for a 16000 particle system takes about three seconds of computation time. The hardware of the molecular-dynamics processor confines the particles to a square $L \times L$ box on which periodic boundary conditions are imposed.

In the simulation described here, the liquid phase was located in a strip parallel to the x -axis of the periodic box, the vapour filling the remaining space. We have simulated system sizes ranging from $L=38\sigma$ to $L=236\sigma$ (σ being the effective diameter) during very long simulation times, using from 5432 to 16000 particles. The interface width has been determined for different interface lengths.

2. The two-dimensional simulation

In our simulation the particles interact via a truncated Lennard-Jones pair potential given by

$$V(r) = \begin{cases} 4\epsilon[(\sigma/r)^{12} - (\sigma/r)^6] & , r \leq r_c \\ 0 & , r > r_c \end{cases} \quad (2.1)$$

The value of r_c is taken to be 2.5σ . For convenience we define a reduced temperature T^* , density ρ^* , and time t^* by

$$T^* = k_B T / \epsilon, \rho^* = \rho \sigma^3, t^* = t / (\sigma \sqrt{m / \epsilon}), \quad (2.2)$$

with m the particle mass, and k_B Boltzmann's constant.

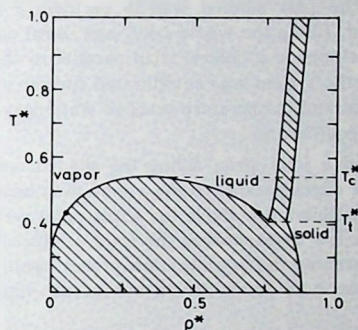


Fig. 1. Phase diagram of a two dimensional system of Lennard-Jones particles. The triple and the critical temperatures are $T_t^* = 0.415$ and $T_c^* = 0.533$, respectively¹².

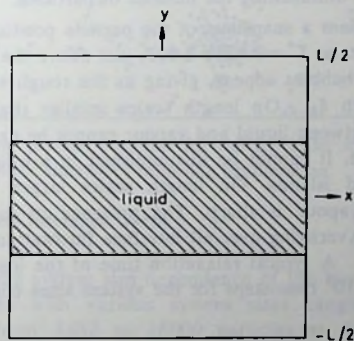


Fig. 2. Schematic drawing of the liquid (shaded area) and vapour regions of the system.

We have simulated a two-dimensional film coexisting with its vapour. The phase diagram of fig. 1 for a two-dimensional Lennard-Jones system shows that the region where an equilibrium interface can exist is rather narrow, since there is a triple temperature of $T_t^* = 0.415^{12}$ and a critical temperature of $T_c^* = 0.533^{12}$. The temperature in our simulation was chosen just above T_t^* .

In the first few runs the initial liquid-vapour configurations were constructed in two different ways. The first method was to perform a molecular-dynamics simulation of a bulk liquid, filling the whole $L \times L$ box, until equilibrium was established. Then all particles outside a central strip parallel to the x -axis were eliminated (see fig. 2). Next, the system was equilibrated further until via evaporation liquid and vapour densities and temperature reached stationary values and the two free interfaces relaxed to equilibrium.

In the second method a solid strip, filling the shaded area in fig. 2, at low temperature and with free edges parallel to the x -axis, was heated very slowly and melted until a stationary temperature above the triple point was reached and there equilibrated further. In a few cases melting the solid produced a large hole in the bulk liquid. We then continued the equilibration process until the large interface fluctuations, caused by the hole being driven out of the liquid, had relaxed to equilibrium.

Both methods took almost 10^5 time-steps, with $\Delta t^* = 0.005$, to produce an equilibrium interface. Both methods also led to interfaces with the same gross features, which is additional evidence that true equilibrium had been reached. In all later runs the second method was chosen, because that method produces initial configurations without diminishing the number of particles.

In figs. 3 we present a snapshots of the particle positions of an $L = 113\sigma$ system with 5432 particles at $T^* = 0.427 \pm 0.003$, just above the triple temperature. In the bulk liquid many bubbles appear, giving us the rough estimate $\xi_B \approx 4\sigma$ for the bulk correlation length ξ_B . On length scales smaller than the bulk correlation length the interface between liquid and vapour cannot be expected to behave like a single-valued interface. It cannot be distinguished in a unique way from the surrounding bubbles and islands. On length scales larger than ξ_B the interface between liquid and vapour is sharp. The presence of interface waves is quite apparent in figs. 3. Averaging over all interface fluctuations results in a value for the interface width w . A typical relaxation time of the long wavelength interface fluctuations is of 10^4 - 10^5 time-steps for the system sizes considered in our simulation.

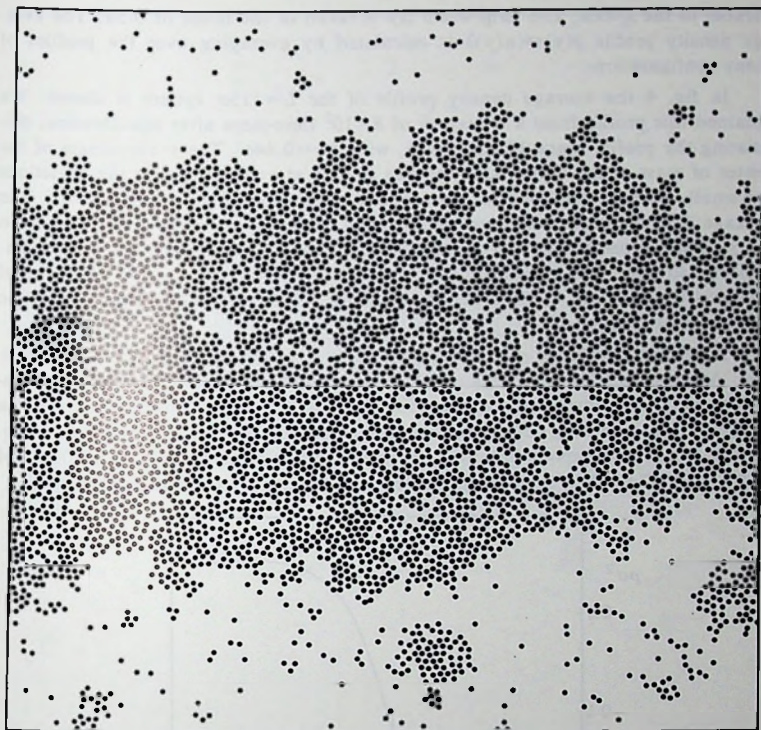


Fig. 3. Snapshot of the particle positions for the $L=113\sigma$ system at $T^*=0.427$ after a trajectory of 7×10^5 time-steps following equilibration.

3. Interfacial profile and interface width

In order to study the system size dependence of the interface width, we have carried out calculations with various system sizes ranging from $L=38\sigma$ to $L=236\sigma$, and using from 5432 to 16000 particles at the same temperature $T^*=0.427 \pm 0.003$.

The density profile $n(y)$ of an individual configuration is defined such that $n(y)L\Delta y$ is the number of particles in a strip of width Δy centered at y and

parallel to the x -axis. The strip-width Δy is taken of the order of 0.5σ . The average density profile $\rho(y)=\langle n(y) \rangle$ is calculated by averaging over the profiles of many configurations.

In fig. 4 the average density profile of the $L=113\sigma$ system is shown. We obtained this profile from a trajectory of 8×10^5 time-steps after equilibration, calculating the profile every 10 time-steps, with $\Delta y=0.44\sigma$. The y coordinate of the center of mass of the liquid does not stay exactly at $y=0$. Although the deviations are small, we have corrected for them in our calculation of the density profile. The average density profile has been symmetrized with respect to $y=0$. The noise on the profile flattens out as one averages over longer system trajectories and is considered to be of statistical origin. We observed a vapour density of $\rho_v^*=0.040 \pm 0.003$ and a liquid density of $\rho_l^*=0.709 \pm 0.004$, which agrees with the known phase diagram¹².

A second simulation was carried out for a $L=236\sigma$ system with 16000 particles. After an equilibration time of 10^5 , we averaged the density profile over a trajectory of 5×10^5 time-steps. A snapshot of a 16000 particle configuration is given in fig. 5. The resulting density profile, calculated with $\Delta y=0.45\sigma$, is shown in fig. 6. The liquid and vapour densities observed for this system are $\rho_l^*=0.710 \pm 0.004$ and $\rho_v^*=0.037 \pm 0.003$, in good agreement with the densities of the smaller system.

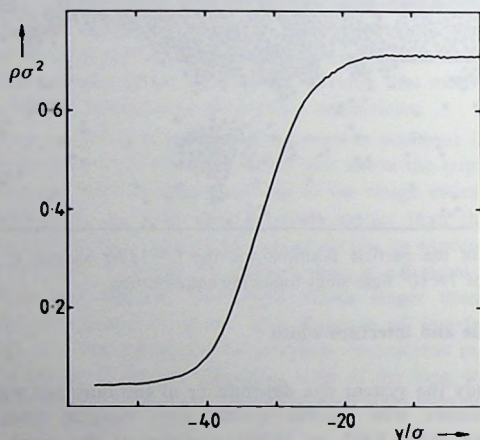


Fig. 4. The symmetrized average density profile $\rho(y)$ for the $L=113\sigma$ system, obtained from a trajectory of 8×10^5 time-steps after equilibration. The observed liquid and vapour densities are $\rho_l^*=0.709 \pm 0.004$ and $\rho_v^*=0.040 \pm 0.003$.

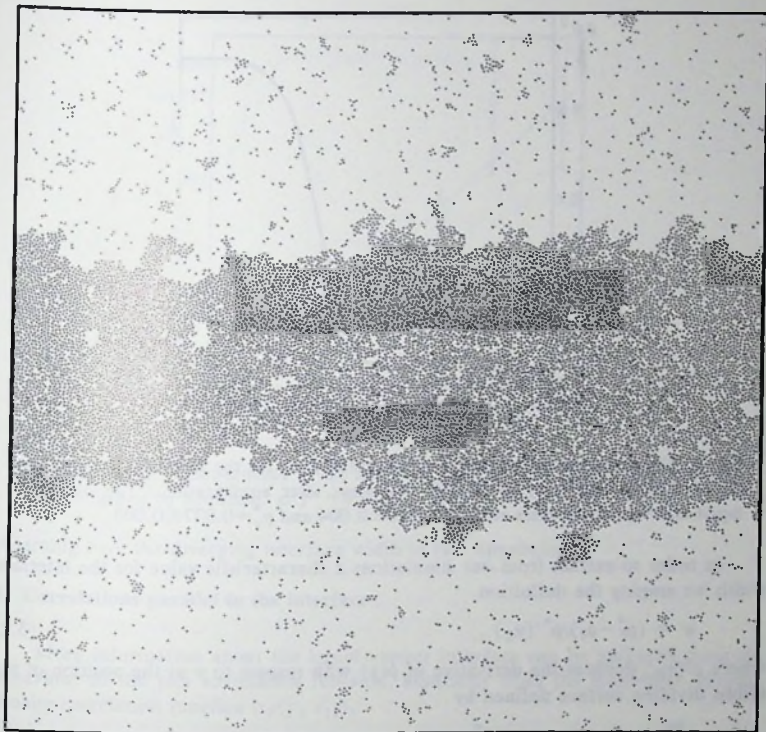


Fig. 5. Snapshot of the particle positions for the $L=236\sigma$ system after a trajectory of 5×10^5 time-steps following equilibration.

Comparing figs. 4 and 6 we see a large system-size effect on the width of the profile. According to capillary wave theory the interface width is mainly due to thermally excited interface waves⁶. In two dimensions these interface modes cause the interface width w to diverge as the square root of the box-length L .

$$w \approx \left[\frac{k_B T}{\gamma_b} (L - a_0) \right]^{1/2} \quad (L \rightarrow \infty), \quad (3.1)$$

where γ_b is the bare interface tension and a_0 is a characteristic length of the bulk liquid.

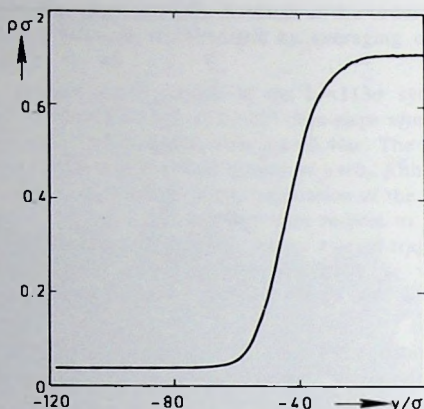


Fig. 6. The symmetrized average density profile $p(y)$ for the $L=236\sigma$ system, obtained from a trajectory of 5×10^5 time-steps after equilibration. The observed liquid and vapour densities are $\rho_l^* = 0.710 \pm 0.004$ and $\rho_v^* = 0.037 \pm 0.003$.

In order to extract from our simulations a characteristic value for the interface width we employ the definition

$$w = (\rho_l^* - \rho_v^*) / \rho^{*'}(y_G), \quad (3.2)$$

where $\rho'(y_G)$ denotes the derivative of $p(y)$ with respect to y at the position of the Gibbs dividing surface defined by

$$\int_{-L/2}^{y_G} dy [\rho^*(y) - \rho_v^*] = \int_{y_G}^0 dy [\rho_l^* - \rho^*(y)]. \quad (3.3)$$

Fig. 7 shows the observed box-length dependence of the interface width. Included are also the results of simulations of systems with $L=38\sigma$, 64σ , 153σ and 189σ , obtained from 1×10^5 , 1.4×10^5 , 4×10^5 , and 3×10^5 time-steps, respectively. A point computed by Abraham⁵ at a slightly different temperature $T^*=0.445$ has also been represented. The error bars in fig. 7 are based on the values of w obtained from partial results (see fig. 8), which are averages over blocks of 5×10^4 consecutive time-steps.

Within the statistical uncertainty, the interface width is seen to follow the square root behaviour (3.1) predicted by the capillary wave theory. Hence we are

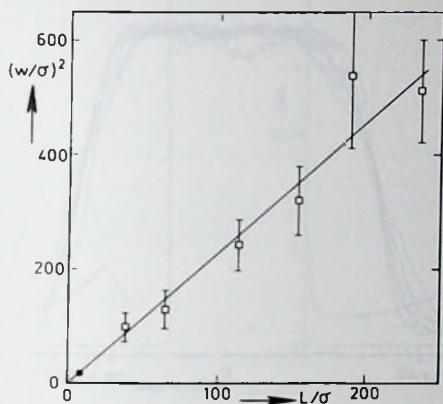


Fig 7. Boxlength L dependence of the interface width w . The filled circle denotes a point computed by Abraham⁵ at $T^*=0.445$.

observing here the diverging interface width in two dimensions.

4. Correlations parallel to the interface

More information about the liquid-vapour interface can be gathered from the behaviour of the pair correlation function, especially from the transverse density-density correlation function $\sigma_T(y, x_{12})$.

$$\sigma_T(y, x_{12}) = \rho_T(y, x_{12}) - \rho(y)^2, \quad (4.1)$$

where $\rho_T(y, x_{12})$ is the distribution function of pairs at distance x_{12} with given y . The Fourier transform of σ_T with respect to the x coordinate, called the transverse structure factor, is

$$\hat{\sigma}_T(y, k) = \frac{1}{\rho(y)} \int \sigma_T(y, x) \exp(ikx) dx. \quad (4.2)$$

Wertheim¹³ showed by theoretical arguments that in the interfacial region $\hat{\sigma}_T(y, k)$ exhibits a divergence for $k \rightarrow 0$, which demonstrates the existence of long-range correlation parallel to the interface. In a molecular-dynamics study of a three-dimensional system this divergence was observed by Kalos, Percus and Rao¹⁴, who identified the origin of these long range correlations as capillary

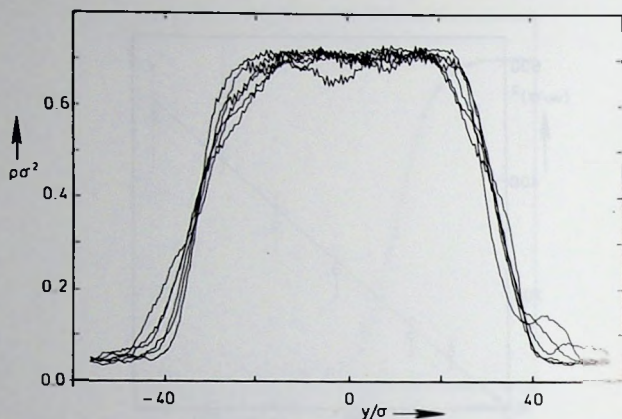


Fig. 8. Some partial results for the density profile of the $L=113\sigma$ system averaged over blocks of 5×10^4 consecutive time-steps.

waves. Following Kalos et al.¹⁴ we computed in our two-dimensional simulation the function

$$\hat{S}_T(y, k) = \langle \sum_{i,j=1}^{N(\Delta y)} \exp[-ik(x_i - x_j)] \rangle / \langle N(\Delta y) \rangle, \quad (4.3)$$

where $k=2\pi\kappa/L$; $\kappa=1,2,\dots$. The summation over i and j runs over all $N(\Delta y)$ particles in a strip of width Δy centered at y and parallel to the x -axis. For small strip width Δy the function $\hat{S}_T(y, k)$ is connected to the transverse structure factor $\hat{\sigma}_T(y, k)$ by¹⁴

$$\hat{S}_T(y, k) = 1 + \hat{\sigma}_T(y, k)\Delta y. \quad (4.4)$$

The summation over terms with $i=j$ in (4.3) gives rise to the first term on the right-hand side of (4.4).

In fig. 9 we show $\hat{S}_T(y, k)$ calculated for the system with $L=236\sigma$ and 16000 particles by averaging over a trajectory of 3.25×10^5 time-steps. The full line has been computed at $y=\pm 44.1\sigma$, i.e. in the center of the interfacial regions on both sides of the film. The dots come from the bulk liquid. We chose $\Delta y=0.46\sigma$, small enough not to influence the results very much and large enough to obtain sufficient statistics. The $k \rightarrow 0$ divergence of $\hat{S}_T(y, k)$ in the interfacial region is clear, indicating the presence of long wavelength correlations up to the size of the box. The

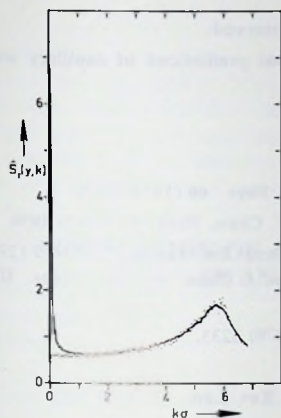


fig. 9

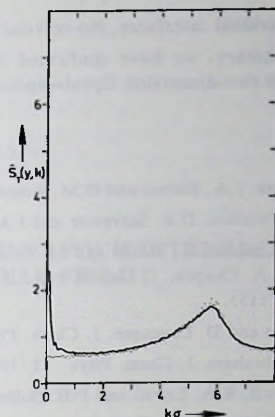


fig. 10

Fig. 9. The transverse structure factor $\hat{S}_T(y, k)$ for $L=236\sigma$. The full line has been computed in the center of the interface over a trajectory of 3.25×10^5 time-steps. The dots come from the bulk liquid.

Fig. 10. The transverse structure factor $\hat{S}_T(y, k)$ for $L=113\sigma$, averaged over a trajectory of 2.5×10^5 time-steps. The full line has been computed in the center of the interface. The dots come from the bulk liquid.

result of $\hat{S}_T(y, k)$ for smaller system ($L=113\sigma$, $\Delta y=0.44\sigma$) is given in fig. 10. It shows a reasonable agreement with the larger system up to the smallest possible wavenumber k , which we take as evidence for the reliability of our results.

5. Concluding remarks

The interface in two dimensions turns out to be very rough and foamy. This is due to the very small two-dimensional interface tension. The averaging over the large interface fluctuations leads to the interface width, which diverges as a function of the box-length L . A typical relaxation time of the long wavelength interface fluctuations for the system sizes considered here is 10^4 to 10^5 time-steps.

A feature due to the square-box geometry is that our liquid film has a relatively small width-to-length ratio as compared to other simulations. We have looked for correlations between the shapes of the two interfaces by comparing subaverages of $\hat{S}_T(y, k)$ (on blocks of 2.5×10^4 time-steps), calculated separately

for the individual interfaces. No correlation was observed.

In summary, we have confirmed the principal predictions of capillary wave theory for a two-dimension liquid-vapour interface.

References

- 1) J.K. Lee, J.A. Barker and G.M. Pound, *J. Chem. Phys.* **60** (1974) 1976.
- 2) F.F. Abraham, D.E. Schreiber and J.A. Barker, *J. Chem. Phys.* **62** (1975) 1958.
- 3) G.A. Chapela, G. Saville and J.S. Rowlinson, *Chem. Soc. Faraday Disc.* **59** (1975) 22. G.A. Chapela, G. Saville and J.S. Rowlinson, *J. Chem. Soc. Far. Trans. II* **73** (1977) 1133.
- 4) M. Rao and D. Levesque, *J. Chem. Phys.* **65** (1976) 3233.
- 5) F.F. Abraham, *J. Chem. Phys.* **72** (1980) 1412.
- 6) F.P. Buff, R.A. Lovett and F.H. Stillinger, *Phys. Rev. Lett.* **15** (1965) 621.
- 7) A.F. Bakker, thesis, Delft University of Technology (1983).
- 8) H.J. Hilhorst, A.F. Bakker, C. Bruin, A. Compagner and A. Hoogland, *J. Stat. Phys.* **34** (1984) 987.
- 9) A.F. Bakker, C. Bruin, F. van Dieren and H.J. Hilhorst, *Phys. Lett.* **93A** (1982) 67.
- 10) A.F. Bakker, C. Bruin and H.J. Hilhorst, *Phys. Rev. Lett.* **52** (1984) 449.
- 11) C. Bruin, A.F. Bakker and M. Bishop, *J. Chem. Phys.* **80** (1984) 5859.
- 12) J.A. Barker, D. Henderson and F.F. Abraham, *Physica* **106A** (1981) 226.
- 13) M.S. Wertheim, *J. Chem. Phys.* **65** (1976) 2377.
- 14) M.H. Kalos, J.K. Percus and M. Rao, *J. Stat. Phys.* **17** (1977) 111.

CHAPTER VI

**SIMULATION OF A LIQUID-VAPOUR INTERFACE
IN AN EXTERNAL FIELD**

ABSTRACT

The influence of gravity on the suppression of the capillary fluctuations of a liquid-vapour interface is studied by simulating a Lennard-Jones system in two dimensions in a gravity-like field. The results are compared to the capillary wave theory. A lower length cut-off is found for the capillary wave lengths which is an order of magnitude larger than the estimated width of the intrinsic interface.

1. Introduction

It is well known that the interface between coexisting liquid and vapour is not properly defined without an external field. The reason is that thermal or capillary waves of the interface tend to diverge and therefore smear out the interface unless a field, like the gravitational field, suppresses these waves¹. So the structure of the interfacial profile, as it is observed in the laboratory, is to a certain extent influenced by the gravitational field.

In a three-dimension system the effects of the capillary waves are relatively small, but in lower dimensions the effects are large. Therefore we have made a molecular-dynamics simulation of a two-dimensional liquid-vapour interface in order to analyse the field effects on the interface and see whether it is possible to make a distinction between the "intrinsic" and the "external" part of the interfacial profile.

In the limit of small field, i.e. small gravitational acceleration g , the field effects on the interface are well described by the capillary wave theory. This theory assumes the existence of an intrinsic or bare interface with a surface tension γ_b and a width w_b , and calculates the spectrum of the thermal waves of such an interface^{2,3}. The only ambiguity in the theory is the lower wavelength cut-off a_0 on the capillary waves. In a three-dimensional system this cut-off has to be imposed to avoid small wavelength divergences. In two-dimensional systems a_0 is not necessary to reach a formal consistent theory, but it is clear that the notion of capillary waves is not well defined on scales smaller than the intrinsic width. It is therefore reasonable to take a_0 near w_b the width of the bare interface, which is of the order of the bulk correlation length ξ_B . Shifts in a_0 are conceptually a matter of whether the small wavelength capillary waves are seen as excitations contributing to the shape of the intrinsic interface or as waves of the intrinsic interface.

The appropriate value of the cut-off a_0 has been a dispute for some time. In a recent paper Kayser⁴ calculates a_0 near the triple point and arrives at values 10 times the correlation length ξ_B (which equals the interparticle distance at the triple point). Near the critical point a_0 may increase to values of 20 ξ_B . These estimates are based on the influences of a finite geometry.

In chapter V⁵, we have simulated a two-dimensional (12-6) Lennard-Jones system near its triple point without a field and observed the effects of a finite geometry on the interfacial width. The dependence of the width on the size of the system was found to be in good agreement with the theory. In this chapter we add a gravity field and study the effects of varying g on the interface width w . We note that realistic values of g , i.e. those corresponding to the earthly gravitational effects on noble gases are hard to simulate because of the extreme weakness of the earthly gravitational force as compared to the intermolecular forces. In the

simulation we have to use much stronger values of g in order to have any effect on the significant bits of the position variables of the particles. By varying g we can easily interpolate between the strong field and the zero field case simulated earlier in order to predict the effect for realistic values of g .

The simulations have been carried out using the *Delft Molecular Dynamics Processor*⁶. This required certain special arrangements for the representation of the gravitational field. As we have to use strict periodic boundary conditions we have to split the square box into two halves. In the upper part the particles feel a linearly varying potential with gradient $-g$ and in the lower half the particles feel a gradient $+g$. So all particles are gently driven to the middle layer of the box. The result is a liquid layer in the middle of the system flanked by a top and bottom layer of vapour. Thus we simulate two liquid-vapour interfaces simultaneously.

This chapter is organized as follows. In section 2 we give a brief outline of capillary wave theory. In section 3 some simulation details are given and in section 4 we present the results. The chapter closes with a discussion of the results.

2. Capillary wave theory

In capillary wave theory the interfacial profile $\rho(y)$ which interpolates smoothly between the densities of liquid and vapour phases, is formed by averaging over the ensemble of thermal fluctuations $\zeta(\mathbf{r})$ around an intrinsic interface $\rho_b(y)$, which is located at $y=0$. The thermal excitations of the interface are called capillary waves. The gravitational potential gy is taken to increase as function of y .

The probability that a fluctuation $\zeta(\mathbf{r})$ develops is given by $\exp(-A/k_B T)$, where the Helmholtz free energy A exists of an intrinsic free energy, associated with the intrinsic interface, and a free energy W which represents the work required to create $\zeta(\mathbf{r})$. In the capillary wave approximation we confine ourselves to smooth and single-valued $\zeta(\mathbf{r})=\zeta(x)$. The resulting density profile is found as

$$\rho(y) = \langle \rho_b(y - \zeta(x)) \rangle \quad (2.1)$$

where the brackets denote a statistical average over all possible fluctuations of the interface. The displaced interface $\rho_b(y - \zeta(x))$ can be written as

$$\begin{aligned} \rho_b(y - \zeta(x)) &= \int_{-\infty}^{+\infty} dy' \delta(y' - \zeta(x)) \rho_b(y - y') \\ &= \frac{1}{\sqrt{2\pi}} \int_{-\infty}^{+\infty} dy' \int_{-\infty}^{+\infty} dq e^{-iq(y' - \zeta(x))} \rho_b(y - y') \end{aligned} \quad (2.2)$$

so that the average profile is

$$\rho(y) = \frac{1}{\sqrt{2\pi}} \int_{-\infty}^{+\infty} dq \int_{-\infty}^{+\infty} dy' \rho_b(y-y') e^{-iqy'} \langle e^{iq\zeta} \rangle \quad (2.3)$$

The work needed to create $\zeta(x)$ exists of a gravitational term and a term which accounts for the increase of interfacial area compared to the area of a flat interface

$$W = (\rho_l - \rho_v) \int_L \left[\int_0^{\zeta(x)} gy \, dy \right] dx + \gamma_b \int_L \left[1 + \left(\frac{d\zeta(x)}{dx} \right)^2 \right]^{\frac{1}{2}} dx, \quad (2.4)$$

where ρ_l and ρ_v , respectively, are the liquid and the vapour densities of the bulk coexistent phases, and γ_b is the surface tension of the intrinsic interface.

In the case of small interface oscillations the square root in (2.4) can be linearized. Then the different surface modes in a fluctuation $\zeta(x)$ are decoupled, which becomes clear when we express $\zeta(x)$ in its Fourier series

$$\zeta(x) = \sum_k A(k) \exp(ikx). \quad (2.5)$$

Because of the periodicity of the system in the simulations the allowed wave vectors are

$$k = \frac{2\pi n}{L}, \quad n = 1, 2, \dots \quad (2.6)$$

where L is the length of the system. Substitution of (2.5) into (2.4) results in

$$W = \sum_k |A(k)|^2 \left[\frac{1}{2}(\rho_l - \rho_v)g + \frac{1}{2}\gamma_b k^2 \right] L. \quad (2.7)$$

Using (2.7) we can easily calculate $\langle e^{iq\zeta} \rangle$ to be

$$\langle e^{iq\zeta} \rangle = \exp \left(-\frac{q^2 w_{cap}^2}{2} \right), \quad (2.8)$$

where w_{cap}^2 is the mean square fluctuation $\zeta(x)$

$$w_{cap}^2 = \langle \bar{\zeta}^2 - \langle \bar{\zeta} \rangle^2 \rangle = \sum_{k>0} \left\{ \frac{L}{k_B T} \left[\frac{1}{2}(\rho_l - \rho_v)g + \frac{1}{2}\gamma_b k^2 \right] \right\}^{-1}. \quad (2.9)$$

In a large system the summation over k in (2.9) may be replaced by an integral, giving

$$w_{cap}^2 = \frac{1}{\sqrt{2\pi}} \frac{k_B T L_{cap}}{\gamma_b} \left[\arctan \left(\frac{\sqrt{2\pi} L_{cap}}{a_0} \right) - \arctan \left(\frac{\sqrt{2\pi} L_{cap}}{L} \right) \right], \quad (2.10)$$

where $L_{cap} = [2\gamma_b/g(\rho_l - \rho_v)]^{1/2}$ is the capillary length and a_0 is the lower wavelength, where we cut off the capillary fluctuations. On the large wavelength side a cut-off is provided naturally by the system size L of the periodic system. With (2.8) and (2.9) we can now carry out the Fourier transform in (2.3) resulting in

$$\rho(y) = \frac{\sqrt{2}}{w_{cap}} \int_{-\infty}^{+\infty} dy' \rho_b(y-y') \exp\left(-\frac{y'^2}{2w_{cap}^2}\right). \quad (2.11)$$

We conclude that the average density profile is the convolution of the bare profile and a Gaussian term of width w_{cap} due to the capillary waves. Not much is known⁷ about $\rho_b(y)$, but we expect it to be a monotonic function of y , which smoothly connects liquid and vapour phases. When the derivative of $\rho_b(y)$ with respect to y is a Gaussian, with width w_b , the derivative of the convoluted profile will also be a Gaussian of width w , where

$$w^2 = w_b^2 + w_{cap}^2. \quad (2.12)$$

In the capillary approximation the influence of the gravity field on the intrinsic interface is supposed to be small compared to the effect of the field on the capillary fluctuations. Far from criticality this approximation is expected to be reasonable. Very close to the critical point however gravity is known to have large effects on both form and width of the intrinsic profile, due to the large compressibility of the coexisting phases near the critical point⁷. Because our simulations are performed just above the triple point we expect all dependence of w on the gravity field to be in the capillary length L_{cap} or in w_{cap} , whereas w_b is more or less a constant and small compared to w .

3. Some simulation details

We have simulated a two-dimensional liquid-vapour system by the molecular-dynamics method. The molecules interact via a truncated Lennard-Jones (12-6) pair potential.

$$V(r) = \begin{cases} 4\epsilon[(\sigma/r)^{12} - (\sigma/r)^6] & , r \leq r_c \\ 0 & , r > r_c \end{cases} \quad (3.1)$$

The distance r_c , where we cut off the potential, is chosen to be 2.5σ , which is the value commonly used in molecular-dynamics simulations. The differential equations describing the trajectories of the atoms are solved in the *Delft Molecular Dynamics Processor*. All quantities of a Lennard-Jones system can be expressed in units which refer to the potential (3.1). These reduced units are denoted by a superscript *. For example we define a reduced temperature T^* , density ρ^* and

time t^* by

$$T^* = k_B T / \epsilon, \quad \rho^* = \rho \sigma^2, \quad t^* = t / (\sigma \sqrt{m / \epsilon}) \quad (3.2)$$

and a reduced gravitational constant by

$$g^* = g (m \sigma / \epsilon). \quad (3.3)$$

The conditions of our simulations are identical to those of the previous chapter where no external field was present. We have taken systems containing 5432 molecules in a square periodic box of linear size $L = 113\sigma$. The temperature, as in chapter V, is just above the triple temperature, namely $T^* = 0.427$, while $T_{triple}^* = 0.415$.

The atoms undergo each simulation time-step Δt ($\Delta t^* = 0.005$) a constant acceleration due to the gravitational force towards $y=0$. Initial configurations for each g^* have been constructed from a configuration with a nearby field constant g^* . The $g^*=0$ configuration has been taken from the system simulated earlier⁵. For every new field strength g^* the configurations are equilibrated until the densities of liquid and vapour phases have become stable, although spatially dependent on y , and the interfaces on both sides, have relaxed to equilibrium. The whole procedure of equilibrating takes about 10^5 time-steps for each new configuration.

4. Results

The dependence of the interfacial width on an external potential is studied by simulating a liquid-vapour coexisting system in two dimensions under influence of a gravity field. The parameter g^* which governs this field has been chosen in the range from $g^*=0$ to $g^*=0.54 \times 10^{-2}$.

We define the density profile $n(y)$ of a configuration generated during the simulation such that $n(y)L\Delta y$ is the number of particles in a strip centered at y and of width Δy and transverse to the direction of the external field. The strip width Δy is determined by $\Delta y = L/256$. The quantity which can be compared to the capillary wave theory is the average density profile

$$\rho(y) = \langle n(y) \rangle, \quad (4.1)$$

which is calculated as a trajectory average of the profile $n(y)$.

In fig. 1 we show the density profile $\rho(y)$ of a system in a small external field ($g^* = 0.15 \times 10^{-2}$), while fig. 2 shows the average profile of the system in the largest field we have simulated ($g^* = 0.54 \times 10^{-2}$). Both profiles are obtained from a trajectory of 2×10^5 time-steps following equilibration, where the density profile $n(y)$ is calculated each 20 time-steps. For reference the coexisting densities of liquid and vapour phases in a field-free system ($\rho_l^* = 0.709$ and $\rho_v^* = 0.0037$)⁵ are

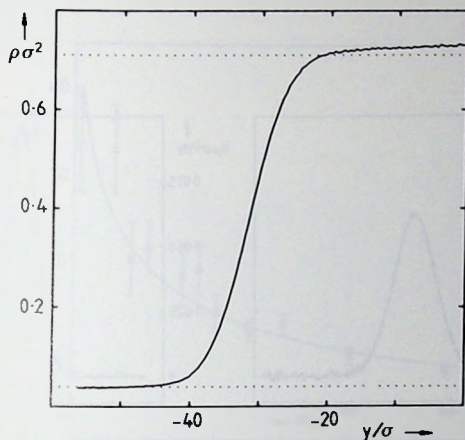


Fig. 1. Symmetrized density profile $\rho(y)$ for a system with $g^* = 0.15 \times 10^{-2}$, obtained from a trajectory of 2×10^5 time-steps following equilibration. The dotted lines denote the coexisting densities of the liquid and vapour phases as obtained in chapter V.

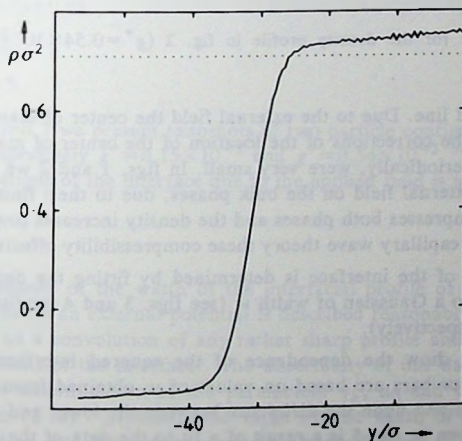


Fig. 2. Symmetrized density profile $\rho(y)$ for a system with $g^* = 0.54 \times 10^{-2}$, obtained from a trajectory of 2×10^5 time-steps following equilibration.

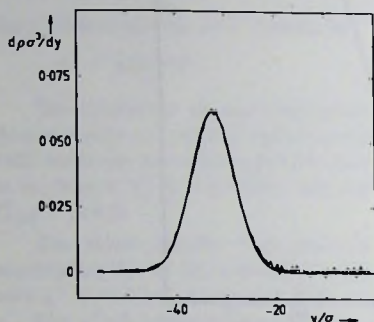


fig. 3

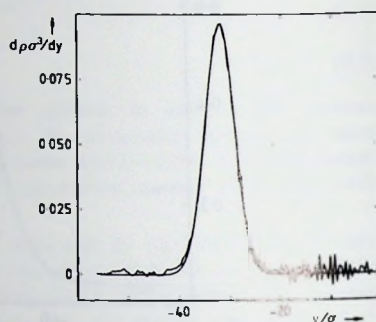


fig. 4

Fig. 3. $dp(y)/dy$ for the density profile in fig. 1 ($g^* = 0.15 \times 10^{-2}$) fitted by a Gaussian.

Fig. 4. $dp(y)/dy$ for the density profile in fig. 2 ($g^* = 0.54 \times 10^{-2}$) fitted by a Gaussian.

given by the dotted line. Due to the external field the center of mass of the system is fixed at $y=0$. The corrections of the location of the center of mass, which have been carried out periodically, were very small. In figs. 1 and 2 we can clearly see the effect of the external field on the bulk phases, due to their finite compressibility: the gravity compresses both phases and the density increases towards $y=0$, like an atmosphere. In capillary wave theory these compressibility effects are neglected.

The width w of the interface is determined by fitting the derivative of $p(y)$ with respect to y to a Gaussian of width w (see figs. 3 and 4 for fits to the profiles of figs. 1 and 2 respectively).

In fig. 5 we show the dependence of the squared interface width on the parameter g^* . Error bars are based on values of w obtained from subaverages of the density profiles and upon the difference between the lower and the upper interface. The line drawn in fig. 5 is a result of a fit to the data of the free parameters a_0 , w_b and γ_b in the capillary wave formula (2.12). The behaviour predicted by the capillary wave theory is obeyed reasonably by the simulation data, within the accuracy of the simulation. The result for the free parameters is

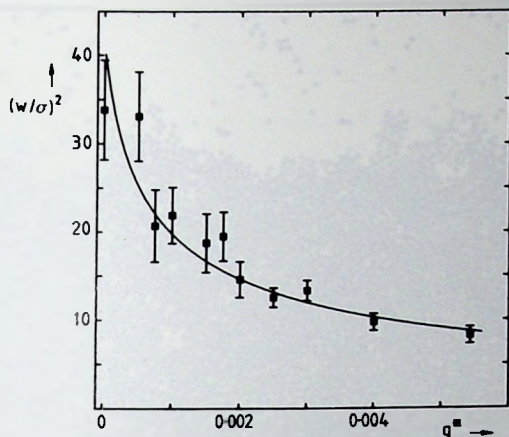


Fig. 5. Dependence of w^2 on the gravity field g^* . The fitted curve corresponds to the parameters $\gamma_b^* = 0.05$, $a_0^* = 12$ and $w_b^* = 1$.

$$\gamma_b^* = 0.05 \pm 0.01,$$

$$a_0^* = 12 \pm 5,$$

$$w_b^* \lesssim 1.5. \quad (4.2)$$

In figs. 6 and 7 we present snapshots of two particle configurations influenced by fields of respectively $g^* = 0.15 \times 10^{-2}$ and $g^* = 0.54 \times 10^{-2}$. The suppression of capillary fluctuations of the interface due to the applied field is apparent.

5. Discussion

The dependence of the width of the interfacial profile of a two-dimensional coexisting system on an external potential is described reasonably well by considering the profile as a convolution of any rather sharp profile and a part due to the capillary excitations of the interface. The uncertainty of our data does not permit a very accurate determination of the parameters γ_b , a_0 and w_b in the capillary wave expression (2.10). Especially the value for the width of the intrinsic interface w_b is hard to get. We obtain however an upper bound, $w_b \leq 1.5\sigma$. For larger values of w_b it is not possible to fit (2.10) to the large g^* data, which are most accurate because of the almost complete suppression of the capillary waves. The

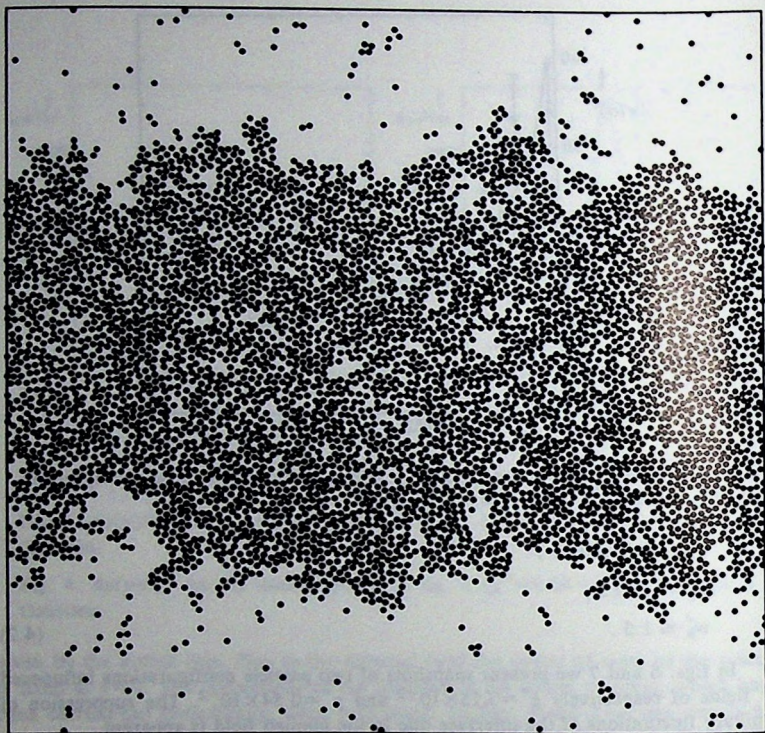


Fig. 6. Snapshot of a particle configuration influenced by a gravity field of $g^* = 0.15 \times 10^{-2}$.

intrinsic interface width of $w_b \leq 1.5\sigma$ does not disagree significantly with the value $w_b \approx 1.7\sigma$ found by Heath and Percus⁸ in a Monte Carlo simulation of a three-dimensional system.

The lower wavelength cut-off a_0 , below which the fluctuations of the interface are thought to contribute to the intrinsic interface width, is found to be $a_0 \approx 12\sigma$. Normally a_0 is estimated to be of the order of the bulk correlation length ξ_B or the width of the intrinsic interface⁹⁻¹⁴. In our field-free system we have a bulk correlation length of $\xi_B = 4\sigma$, which length has been determined from the average size of the vapour bubbles in the liquid bulk phase⁵. Our estimate of a_0 is therefore larger

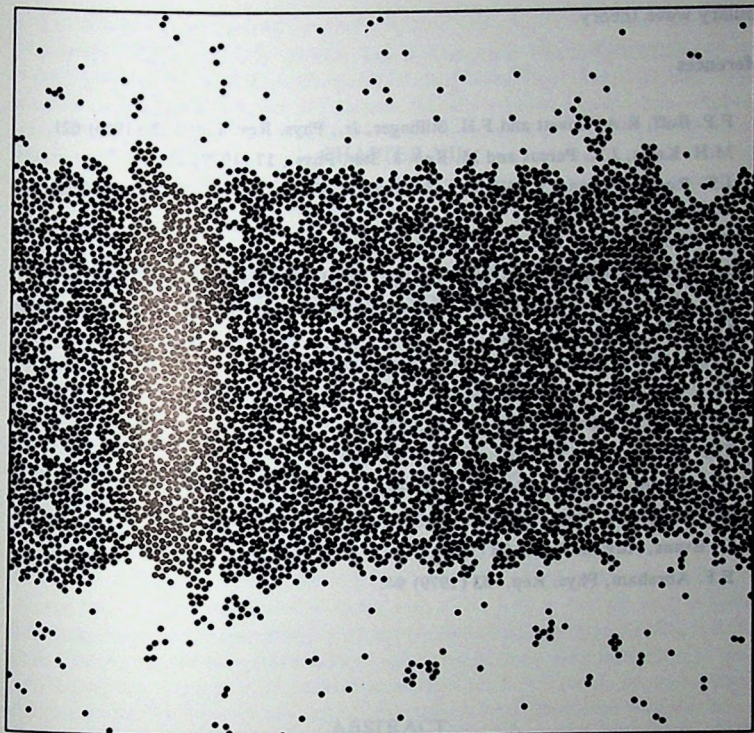


Fig. 7. Snapshot of a particle configuration influenced by a gravity field of $g^* = 0.54 \times 10^{-2}$.

then usually expected. The value however agrees with the value $a_0 \approx 10\sigma$ suggested by Kayser⁴ for an interface at temperatures near the triple point.

In the previous chapter⁵ we concluded that the interface width of a two-dimensional system in zero field diverges as the square root of the system size L , as the limit of (2.10) for small g^* predicts,

$$w_{cap}^2 = \frac{k_B T}{2\pi^2} \frac{(L - a_0)}{\gamma_b}, \quad g \rightarrow 0. \quad (5.1)$$

Together with the results of this chapter we have confirmed the predictions of

capillary wave theory.

References

- 1) F.P. Buff, R.A. Lovett and F.H. Stillinger, Jr., *Phys. Rev. Lett.* **15** (1965) 621.
- 2) M.H. Kalos, J.K. Percus and M. Rao, *J. Stat. Phys.*, **17** (1977) 111.
- 3) J.S. Rowlinson and B. Widom, *Molecular Theory of Capillarity*, (Clarendon Press, Oxford, 1982).
- 4) R.F. Kayser, *Phys. Rev. A* **33** (1986) 1948.
- 5) J.H. Sikkenk, H.J. Hilhorst and A.F. Bakker, *Physica* **131A** (1985) 587.
- 6) H.J. Hilhorst, A.F. Bakker, C. Bruin, A. Compagner and A. Honglad, *J. Stat. Phys.* **34** (1984) 987.
- 7) J.M.J. van Leeuwen, J.V. Sengers, *Physica* **138A** (1986) 1.
- 8) D.L. Heath, J.K. Percus, preprint
- 9) J.D. Weeks, *J. Chem. Phys.* **67** (1977) 3106.
- 10) F.H. Stillinger, *J. Chem. Phys.* **76** (1982) 1087.
- 11) D.A. Huse, W. van Saarloos, J.D. Weeks, preprint.
- 12) R. Evans, *Mol. Phys.* **42** (1981) 1169.
- 13) R. Evans, *Adv. in Phys.* **28** (1979) 143.
- 14) F.F. Abraham, *Phys. Rep.* **53** (1979) 94.

CHAPTER VII

**SIMULATION OF WETTING AND DRYING AT
SOLID-FLUID INTERFACES**

ABSTRACT

The adsorption is studied of a fluid at a structured solid substrate by means of computer simulations on the Delft Molecular Dynamics Processor. Two types of particles are present, 2904 of one type for building a three-layer substrate and about 8500 of the other type for composing the fluid. Interactions between like and unlike atoms are modeled by pair potentials of Lennard-Jones form, cut off at 2.5σ . Simulations are performed at constant temperature and variable ratio of substrate-adsorbate to adsorbate-adsorbate attraction. On the basis of measurements of density profiles, coverages, surface tensions and contact angles, a wetting as well as a drying phase transition have been identified. Both transitions are of first order.

1. Introduction

Since the theoretical discovery of the wetting phase transition in 1977 by Cahn¹ and by Ebner and Saam², and its experimental confirmation in 1980 by Moldover and Cahn³, many statistical mechanical models⁴ and theories featuring density functionals⁵ have displayed a phase transition from partial to complete wetting. Several experiments have shown a wetting transition⁶ and many have studied the question of incomplete or complete wetting⁷ and discussed the thickness of wetting layers⁸.

It has often been argued on the basis of scaling theory that a wetting (or drying) phase transition is unavoidable and ubiquitous near a critical point. However, scaling arguments alone are inconclusive as far as the necessity of the transition is concerned⁹, even in systems with only short-range forces¹⁰. Theoretical and experimental cases have been found where the transition does not occur (neither wetting, nor the complementary phenomenon of drying)^{9,11,12,13}. As far as we know, systems without a wetting transition involve a subtle interplay between short-range (e.g., exponential decay) and long-range (power-law decay) forces.

On the basis of the evidence gathered so far it is reasonable to conclude that the existence and the nature (first- or second-order character) of a wetting or drying transition are far from universal. They sensitively depend on microscopic details of interfaces (e.g., chemical structure of substrate-adsorbate interface) and on the details (in particular the range) of the direct interactions (resulting from intermolecular forces) and the fluctuation-induced interactions between interfaces¹⁴.

As an important bridge between theoretical and experimental approaches computer simulations can complement our understanding of wetting phenomena. Modern computational statistical mechanics makes use of (super-) computers¹⁵ and special purpose computers¹⁶ in an attempt to simulate systems -in our case continuum fluids- in a highly realistic fashion.

2. Description of the system

Computer simulations of the wetting transition are difficult because one needs a large system to accommodate the various phases (substrate, liquid and vapour) and consequently the system equilibrates slowly near the phase transition. In lattice gases (Ising models) Monte Carlo simulations of the wetting problem have been quite successful¹. In fluids, with continuous degrees of freedom, simulations are harder to perform. Previous molecular-dynamics simulations of adsorption dealt with numbers of particles ranging between 200 and 1200^{18,19}. The influence of solid walls (substrates) was represented by external potentials.

We report on simulations using the Delft Molecular Dynamics Processor²⁰ with two types of atoms, 2904 of one type for building a solid substrate and about

8500 of the other type for composing the fluid adsorbate²¹. All pairs of atoms i and j interact with Lennard-Jones potentials ϕ_{AB} , where A or B are replaced by s for atoms in the solid and by f for atoms in the fluid. We have

$$\phi_{AB}(r_{ij}) = 4\epsilon_{AB} \left\{ (\sigma_{AB}/r_{ij})^{12} - (\sigma_{AB}/r_{ij})^6 \right\}, \quad (2.1)$$

where $r_{ij} = |\mathbf{r}_i - \mathbf{r}_j|$. All pair potentials are cut off at $2.5\sigma_{AB}$. As a consequence, we are dealing with *short-range interactions* only.

The solid substrate is structured. We took $\epsilon_{ss} = 50\epsilon_{ff}$ in order to build a stable close-packed FCC solid substrate of three layers. The layers belong to (100) planes of the solid and the first and the third layer form the surfaces of the substrate. Particles in the solid are three times more massive than in the fluid ($m_s = 3m_f$). Therefore, apart from small vibrations the substrate is rigid. The lattice spacing, dictated by $\sigma_{ss} = 0.847\sigma_{ff}$ is chosen such that there is a mismatch between solid and fluid. This prevents solidification of the first adsorbed liquid layers. The interaction between substrate and adsorbate is further characterized by $\sigma_{sf} = 0.912\sigma_{ff}$. This particular proportionality factor has been chosen close to the mean of σ_{ss} and σ_{ff} . The cubic box in which the fluid and the substrate reside has linear size $L = 29.1\sigma_{ff}$ and the boundary conditions are periodic in all three dimensions. Note that adsorption takes place on either side of the three-layer substrate. Because of the potential cut-off, adsorbed atoms on one side are strictly outside the interaction range of adsorbed atoms on the other side.

An important advantage of working with a live wall is that all interfacial tensions are measurable as mechanical forces rather than being obtained indirectly from surface free energies. Denote the total free energy of the system by

$$F = -k_B T \log Z \quad (2.2)$$

where Z is the canonical partition function. The total surface tension of the system γ_{tot} is then defined as

$$\gamma_{tot} = \left(\frac{\partial F}{\partial \mathcal{A}} \right)_{T, V, N_s, N_f}, \quad (2.3)$$

where \mathcal{A} is the substrate area. Temperature T , volume V , numbers of atoms in the solid N_s and in the fluid N_f are fixed. After differentiation one obtains²²

$$\gamma_{tot} = \left\langle \sum_{A,B} \sum_{i < j} \frac{1}{r_{ij}} \frac{d\phi_{AB}(r_{ij})}{dr_{ij}} (x_{ij}^2 + y_{ij}^2 - 2z_{ij}^2) \right\rangle / 2\mathcal{A}, \quad (2.4)$$

where $\langle \dots \rangle$ denotes the thermal average.

This result is equivalent to the mechanical definition of the surface tension as the integral around the (periodic) system of the difference of transverse and

normal components (with respect to the substrate) of the pressure tensor²³:

$$\gamma_{tot} = \int_{-L/2}^{L/2} dz [p_N(z) - p_T(z)], \quad (2.5)$$

where z is the coordinate perpendicular to the substrate. We have assumed equivalence of x and y directions. In a bulk phase the difference $p_N - p_T$ vanishes and no contribution to the surface tension is made.

In cases where the presence of the solid is represented by an external potential acting on atoms in the fluid, eq. (2.4) can not be used as such. For a completely rigid solid we can rewrite (2.4) as

$$\begin{aligned} \gamma_{tot} = & \left\langle \sum_{i < j} \frac{d\phi_{ff}(r_{ij})}{dr_{ij}} \frac{(x_{ij}^2 + y_{ij}^2 - 2z_{ij}^2)}{r_{ij}} \right\rangle_{f/2s\Delta} \\ & + \left\langle \sum_{i=1}^{N_f} (x_i \frac{\partial}{\partial x_i} + y_i \frac{\partial}{\partial y_i} - 2z_i \frac{\partial}{\partial z_i}) \psi_f(r_i) \right\rangle_{f/2s\Delta} \\ & + \gamma_{s,int}, \end{aligned} \quad (2.6)$$

where

$$\psi_f(r_i) = \sum_{j=1}^{N_s} \phi_{sf}(r_{ij}) \quad (2.7)$$

is the external potential, and $\gamma_{s,int}$ is an internal contribution associated with the substrate and arising from the potential ϕ_{ss} . The thermal average $\langle \dots \rangle_f$ is now taken over the ensemble of a fluid in an external potential.

The first (mechanical) term on the right-hand side of eq. (2.6) can be cast into the form of eq. (2.5) where the pressure tensor pertains only to atoms in the fluid, and the integration is done from the solid surface ($z=0$) to the bulk liquid phase. The second term represents the direct interaction between solid and fluid. The last term is not relevant for obtaining contact angles since it drops out in the difference $\gamma_{sl} - \gamma_{sv}$ (v denotes vapour, l denotes liquid). An example of this procedure using eq. (2.6) are the simulations by van Swol and Henderson¹⁹.

In our simulations we obtain all surface tensions directly from eqs. of the form (2.4) or (2.5). Remark that the surface tensions are well defined only if one can integrate (2.5) from inside a bulk phase (where $p_N = p_T$) to another bulk phase. Since our solid consists of only three layers which are in general also subject to lateral stresses (e.g., due to periodic boundary conditions), we do not expect $p_N = p_T$ inside the substrate. In fact, the system size L relative to σ_{ss} can be delicately adjusted to minimize lateral stresses at a given temperature. We performed

this fine-tuning and achieved the condition of isotropic pressure-tensor components in the interior $n-4$ layers of a substrate built of n (>4) layers. The corresponding system size L was then used for the three-layer substrate in our simulations. This particular choice of system size has the advantage that the numerical values for the measured tensions γ_{sl} and γ_{sv} are much lower than they would be if extra lateral stresses would occur. Still, in our simulations γ_{sl} and γ_{sv} are two orders of magnitude greater than γ_{lv} . Besides trying to reduce the ratio γ_{sl}/γ_{lv} for facilitating accurate measurements, there is in principle no reason for minimizing the stresses because their effects cancel in the difference $\gamma_{sl} - \gamma_{sv}$.

3. Thermodynamics of wetting and drying: profile symmetries

The evidence for the occurrence of wetting or drying transitions in computer simulation of fluids has been rather limited up to now. Van Swol and Henderson¹⁹ located in their system of 512 particles interacting with square-well potentials a drying transition on the basis of an examination of density profiles and coverages in addition to an analysis of surface tension data, with the help of statistical sum rules. In their system, the statistical sum rules can be worked out to yield practical equations because of the piecewise constant potentials (square wells). In section 5 we discuss the relationship between their results and ours.

We briefly review some basic thermodynamic relations. The condition of thermodynamic stability

$$\gamma_{sv} \leq \gamma_{sl} + \gamma_{lv} \quad (3.1)$$

expresses that a solid-vapour interface with surface tension γ_{sv} is thermodynamically stable as long as the inequality is strictly satisfied. In this case the solid is incompletely wet (assuming that the solid preferentially adsorbs the liquid phase, i.e. $\gamma_{sl} < \gamma_{sv}$). If the equality is realized, the stable profile consists of a solid-liquid interface with tension γ_{sl} combined with a liquid-vapour interface with tension γ_{lv} at a macroscopic distance away from the solid surface. The solid is then completely wet. Analogously,

$$\gamma_{sl} \leq \gamma_{sv} + \gamma_{lv} \quad (3.2)$$

expresses incomplete ($<$) or complete ($=$) drying of the solid. For incomplete wetting or drying, the contact angle Θ is defined by

$$\gamma_{lv} \cos \Theta = \gamma_{sv} - \gamma_{sl}, \quad (3.3)$$

expressing mechanical equilibrium of the three-phase contact line (Young's law).

Our simulations are done in the canonical ensemble. The number of atoms in the solid, N_s , as well as in the fluid, N_f , are fixed. It is then possible to enforce liquid-vapour coexistence by adjusting N_f such that at least one liquid-vapour

interface is maintained in the system. At a given temperature, we thus obtain the pressure corresponding to phase coexistence in bulk.

Density profiles (density versus z) can consist of two solid-liquid interfaces and two liquid-vapour interfaces bounding a vapour phase in the middle (fig. 1). They can also be composed of two solid-vapour interfaces and two liquid-vapour interfaces bounding a liquid (fig. 2). These profiles are *symmetric*: the coverage (the integral along z of the excess density of adsorbate relative to bulk density) is the same on both sides of the substrate. Although both sides of the substrate are identical, *asymmetric* profiles also occur. They contain one solid-vapour, one solid-liquid and one liquid-vapour interface (fig. 3).

The symmetric profiles correspond to a total surface tension

$$\gamma_{tot} = 2\gamma_{sl} + 2\gamma_{lv} \quad (\text{fig. 1}), \quad (3.4)$$

or

$$\gamma_{tot} = 2\gamma_{sv} + 2\gamma_{lv} \quad (\text{fig. 2}). \quad (3.5)$$

The asymmetric profile has

$$\gamma_{tot} = \gamma_{sl} + \gamma_{sv} + \gamma_{lv} \quad (\text{fig. 3}). \quad (3.6)$$

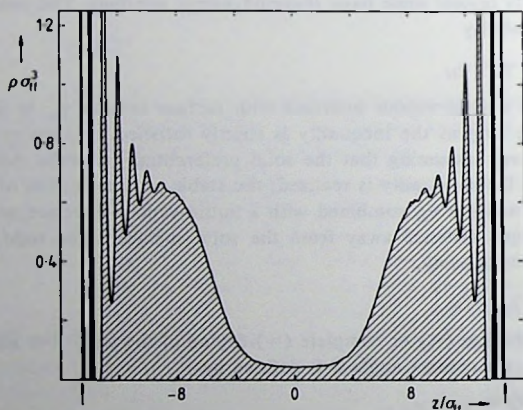


Fig. 1. Density profile of a symmetric (completely wet) configuration at $\epsilon_r = 0.85$, averaged over a trajectory of 5.2×10^4 consecutive time-steps. Dark peaks correspond to the substrate layers. The arrows denote the periodic boundary.

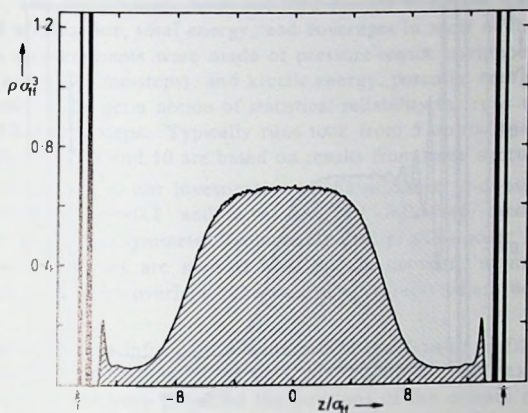


Fig. 2 Density profile of a symmetric (completely dry) configuration at $\epsilon_r = 0.3$, averaged over a trajectory of 2.6×10^4 consecutive time-steps.

For studying the wetting or drying phase transitions one can vary the temperature at liquid-vapour coexistence. The transition is expected when the temperature is increased towards the critical temperature of the fluid¹⁻⁶. In the case of wetting an adsorbed liquid film of *microscopic* thickness grows suddenly into a layer of *macroscopic* thickness. For drying, the adsorbed phase is a vapour. The principal variables for discussing these phase transitions are temperature and surface field²⁴. In the case of wetting one can make the transition from the incompletely wet phase to the completely wet phase either by raising the temperature or by increasing the preference of the solid for adsorption of the liquid phase. The latter possibility corresponds to increasing the surface field which in our system is represented by the ratio $\epsilon_r = \epsilon_{sf}/\epsilon_{ff}$ of the Lennard-Jones parameters. Remark that one may treat ϵ_r as an independent variable, keeping ϵ_{ss} and ϵ_{ff} fixed. This feature is also exploited in experiments where one chemically alters the outermost layers, thereby modifying the local solid-fluid interactions¹².

In our simulations it is convenient to study wetting at fixed temperature and varying ϵ_r , because then the coexisting bulk densities ρ_l and ρ_v and also the surface tension of the liquid-vapour interface γ_{lv} are fixed, and only the coverages and the substrate-fluid surface tensions vary. Under these circumstances the thermodynamically stable profile, which minimizes γ_{tot} , can have different symmetry. If surface phase transitions take place, singularities occur in the minimal total

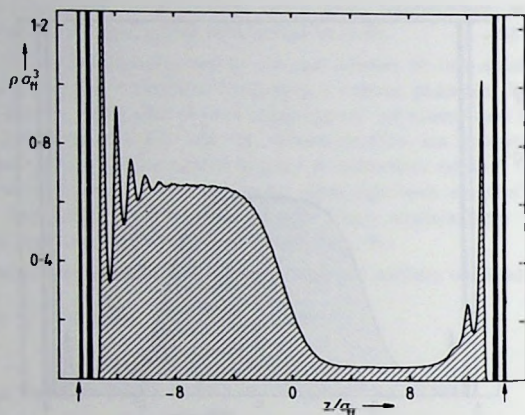


Fig. 3. Density profile of an asymmetric configuration at $\epsilon_r = 0.65$, averaged over a trajectory of 5.2×10^4 consecutive time-steps.

surface tension as a function of ϵ_r . In the case of a first-order phase transition the derivative of this function is discontinuous and metastable continuations of stable profile symmetries are expected. From eqs. (3.4)-(3.6) it follows directly that if a profile like that in fig. 1 is stable, the substrate is completely wet ($\Theta=0$). Indeed, if γ_{tot} as given by (3.4) is lower than the values of γ_{tot} in (3.5) and (3.6), then a direct solid-vapour contact is not possible in equilibrium because its tension γ_{sv} would exceed the sum $\gamma_{sl} + \gamma_{lv}$. Analogously, the substrate is completely dry ($\Theta=\pi$) if the stable profile has the form of that in fig. 2. Finally, the stability of an asymmetric profile (fig. 3) implies incomplete wetting or drying ($0 < \Theta < \pi$).

4. Results from the simulations

The speed of the special-purpose computer which we have used is comparable to that of a CRAY-1 supercomputer. Our simulations took a total of about 2000 hours of CPU time. We have simulated the system at a fixed temperature which equals $T^* = k_B T / \epsilon_{ff} = 0.9$, which is between the triple temperature $T_t^* \approx 0.7$ and the critical temperature $T_c^* \approx 1.26$ of the bulk adsorbate. The temperature is kept constant by regularly adjusting the kinetic energy. This is done for the two types of atoms separately. At a given value of ϵ_r , we have allowed 1×10^4 time-steps of $\Delta t^* = t / (\sigma_{ff} \sqrt{m_f / \epsilon_{ff}}) = 0.01$ for equilibration. The initial configuration for a specific value of ϵ_r was taken to be an equilibrated configuration at a slightly

different ϵ_r . The equilibration time was long enough to obtain stable bulk densities in liquid and vapour, total energy, and coverages in most of the cases. After equilibration measurements were made of pressure-tensor components²⁵ and density profile (every 13 time-steps), and kinetic energy, potential energy and pressure (every time-step). To get a notion of statistical reliability the runs were divided in subruns of 5200 time-steps. Typically runs took from 5 up to 20 subruns. Error bars in our figures 7, 8 and 10 are based on results from these subruns.

At the first stage of our investigation we have looked at density profiles and coverages, between $\epsilon_r \approx 0.1$ and $\epsilon_r \approx 1.0$. The following qualitative picture emerges. At low ϵ_r the symmetric (completely dry) profiles occur, and symmetric (completely wet) profiles are seen at high ϵ_r . In between, asymmetric profiles appear. There are large overlaps (intervals of ϵ_r values) where both symmetries are found.

To complement the information contained in the density profiles of figs. 1-3, we have visualized snapshots of particle configurations. For example, for an asymmetric profile we have projected the positions of the centers of all atoms in the box onto a plane parallel to the xz -plane. The result is shown in fig. 4. We have also represented the adsorption at the substrate surfaces by taking a section of approximate width $2\sigma_{ff}$ parallel to the xy -plane. This section includes the

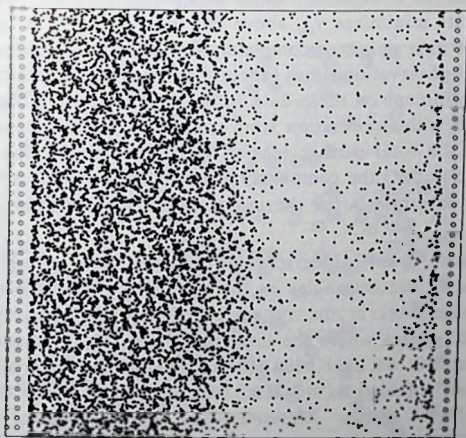


Fig. 4. The positions of the atoms projected on the xz -plane for an asymmetric configuration with $\epsilon_r = 0.65$ (For clarity all z -coordinates are shifted by a small amount with respect to the density profile in fig. 3).

surface layer of the substrate and the first adsorbed atomic layer. The atoms are visualized as circles of approximate diameter σ_{ss} and σ_{ff} , respectively. Fig. 5 shows the adsorption at the solid-liquid interface, and fig. 6 presents a view of the corresponding adsorption on the opposite surface of the substrate, at the solid-vapour interface. The densities of these first adsorbed layers correspond to the fluid density peaks in fig. 3 closest to the substrate density peaks on the left and right, respectively.

Looking at the symmetric density profiles in fig. 1 and 2 one can see that our box is not extended enough along the z -direction to comfortably accommodate three bulk phases (liquids or vapours). This problem is inherent to the hardware structure of our computer.

Our second source of information is provided by data of the total surface tension γ_{tot} as defined in eq. (2.5). Fig. 7 displays γ_{tot} versus ϵ_r . Data points with open circles refer to asymmetric profiles and filled symbols (circles and squares) correspond to symmetric profiles. We distinguish three curves. First a curve (open circles) between $\epsilon_r \approx 0.1$ and $\epsilon_r \approx 0.8$, which is more or less a straight line, associated with asymmetric profiles. This curve meets a steep curve (filled squares) representing completely wet substrates at $\epsilon_r \approx 0.8$, and almost merges with the latter at higher ϵ_r . We see that below $\epsilon_r = 0.78 \pm 0.03$ the incompletely wet substrate is the thermodynamically more stable configuration, whereas the completely wet substrate minimizes γ_{tot} above this value of ϵ_r . The third curve (filled circles) consists of data points of completely dry substrates. These data are based on relatively short observation times (about 4 subruns) and therefore less accurate. We will further comment on these data in the next section. However, if the data are complemented with information from contact-angle measurements, the drawn curve results for the total surface tension of completely dry substrates. We see that below $\epsilon_r = 0.54 \pm 0.03$ the completely dry substrate minimizes γ_{tot} , whereas the incompletely dry substrate is the thermodynamically more stable configuration at higher ϵ_r .

The third route toward understanding the behaviour of our system has been the determination of contact angles on the basis of surface tensions corresponding to the distinct interfaces in the system. This is easy whenever interfaces are separated by bulk phases where the integrand of eq. (2.5) vanishes. In the cases of asymmetric profiles we have been able to measure accurately the liquid-vapour tension. We have obtained $\gamma_{lv} = 0.22 \pm 0.01 \epsilon_{ff}/\sigma_{ff}^2$ and found that it is independent of ϵ_r , as fig. 8 shows. Moreover, this numerical value agrees with that obtained in a fully periodic liquid-vapour system without substrate. In that system $\gamma_{tot} = 2\gamma_{lv}$. Simulations were performed on our DMDP and, independently, on a mainframe IBM²⁶.

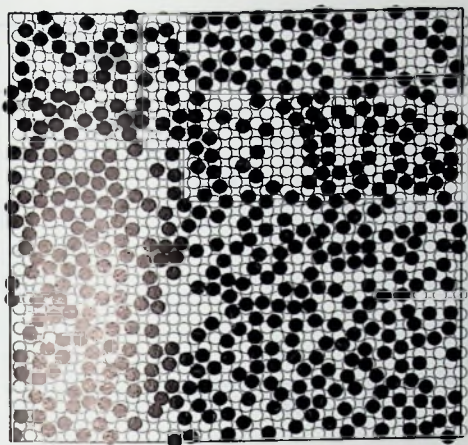


Fig. 5. The atoms in the first adsorbed layer at the solid-liquid interface (filled circles) together with the (100) substrate surface (open circles) at $\epsilon_r = 0.65$.

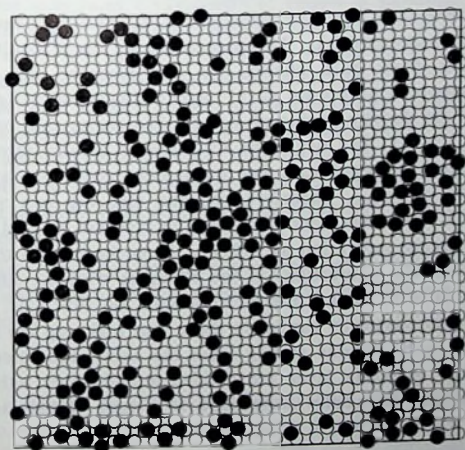


Fig. 6. The atoms in the first adsorbed layer at the solid-vapour interface (filled circles) together with the (100) substrate surface (open circles) at $\epsilon_r = 0.65$.

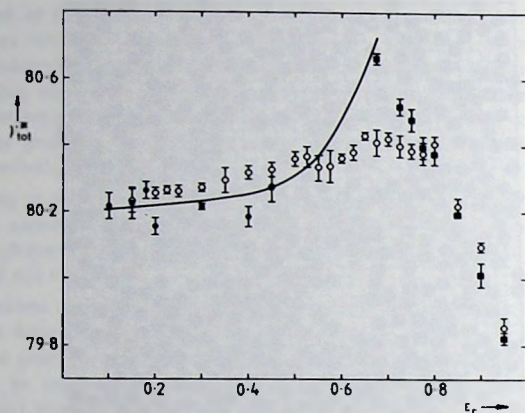


Fig. 7. The total surface tension γ_{tot} versus ϵ_r . Open circles refer to asymmetric profiles, filled squares refer to completely wet substrates and filled circles refer to completely dry substrates. The full line is constructed from contact angle measurements.

Less straightforward is the determination of γ_{sl} and γ_{sv} , because the solid substrate is only three layers thick. To appreciate fully the difficulties involved in separating interfaces from bulk phases, we can examine the profile of the pressure-tensor component difference $p_N(z) - p_T(z)$, displayed in fig. 9. This profile corresponds to the density profile of fig. 3. We notice that only in the bulk vapour phase $p_N(z) - p_T(z)$ has negligible fluctuations around zero. In the bulk liquid the fluctuations are significant but fortunately yield zero average already over small intervals $\Delta z \leq \sigma_{ff}$. Therefore, γ_{lv} and also the sum $\gamma_{sl} + \gamma_{sv}$ can be accurately measured. The important problem is to separate γ_{sl} and γ_{sv} . We have obtained an approximate separation as follows. Contributions to the integrand in eq. (2.5) arising from the interactions of the substrate with the adsorbate on one side, have been attributed to the interfacial tension on that side. Remark that these contributions are physically similar to those that make up the second term of eq. (2.6). Further, contributions arising from the solid-solid interactions within the second (central) substrate layer are divided equally over either side. Note that these contributions physically correspond to a part of the last term in eq. (2.6).

Fig. 10 then shows $\cos \Theta$, as obtained from eq. (3.3), for asymmetric profiles (open circles in fig. 7). The data corresponding to incompletely dry or

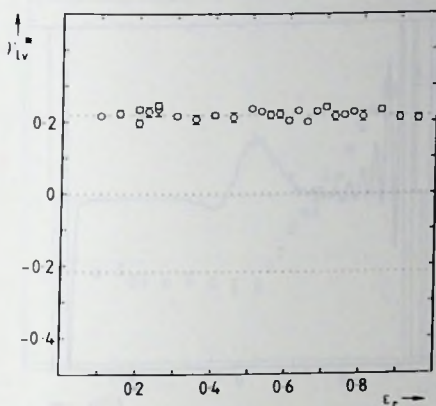


Fig. 8. The reduced surface tension γ_{lv}^* of the liquid-vapour interface (in units of $\epsilon_{ff}/\sigma_{ff}^2$) versus ϵ_r .

incompletely wet substrates ($-1 < \cos\Theta < 1$) follow a strikingly straight line. In accordance with fig. 7 these data suggest that incompletely wet substrates are metastable for $\epsilon_r \geq 0.78$. Indeed, these states violate eq. (3.1). Both the data of fig. 7 and those of fig. 10 locate the wetting transition at $\epsilon_r = 0.78 \pm 0.03$. The consistency between total surface tension and contact-angle measurements relies particularly on the reliability of our approximate separation of γ_{sl} and γ_{sv} . We can thus trust our approximation and rely fully on fig. 10 to tell us where the drying transition occurs, i.e. at $\epsilon_r = 0.54 \pm 0.03$. We recall that the solid curve drawn in fig. 7 has been deduced from data which underlie fig. 10 and has not been measured independently.

This analysis concludes the thermodynamic determination of the phase transitions. In the next section we will make remarks about the time evolution of states in our simulations.

5. Discussion

We first comment on the shorter observation times of completely dry substrates. The associated density profiles show dry walls and a bulk liquid in the middle of the system (e.g. fig. 2). The position of the center of mass of the liquid droplet can fluctuate in time due to velocity fluctuations inherent in our simulations. Indeed, the molecular-dynamics is constrained by the requirement that the

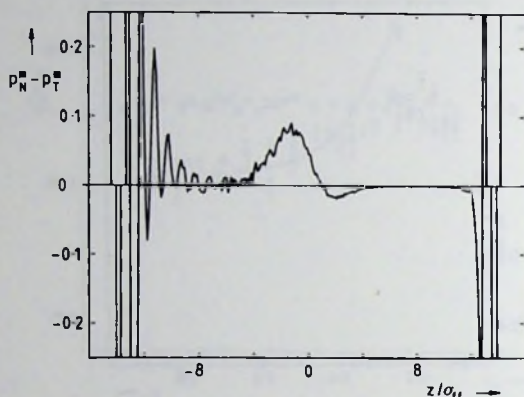


Fig. 9. The profile of the reduced difference $p_N(z) - p_T(z)$ (in units $\epsilon_{ff}/\sigma_{ff}^3$) for $\epsilon_r = 0.65$.

center of mass of the $N = N_s + N_f$ atoms be at rest. Relative motion of the substrate and the bulk liquid adsorbate naturally occurs. Independently of ϵ_r , this can cause the substrate and the droplet to collide, typically after 4 subruns. At very low ϵ_r (e.g. at 0.1) this hardly damages the droplet, and the droplet leaves the wall after a considerable time (15 subruns). This sequence of events is shown in fig. 11. We have performed this simulation with appreciably less adsorbate atoms than usual ($N_f \approx 5000$ instead of 8500) to allow a better accommodation of the vapour phases. At ϵ_r around 0.4, however, the collision changes the profile drastically and the illusion of a phase transition from the completely dry to the incompletely dry state is created. Indeed, measurement of the internal energy u (per unit area) revealed the absorption by the heat bath of a latent heat of adsorption $\Delta u \approx -1.0 \epsilon_{ff}/\sigma_{ff}^2$. As can be seen in fig. 7, at $\epsilon_r = 0.4$, γ_{tot} increases in this event by an amount $\Delta \gamma = 0.1 \epsilon_{ff}/\sigma_{ff}^2$, and thus a *metastable* state is reached. This is true to the extent that the bulk contribution to the total free energy is not affected. We have presented our density-profile measurements during this time evolution in fig. 12. The time that the droplet stays attached to the wall is longer than we are able to measure. Typical fluctuations of the internal energy u over a time of the order of a subrun are order $0.1 \epsilon_{ff}/\sigma_{ff}^2$, which is a tenth of the latent heat associated with the adsorption of the droplet on the wall.

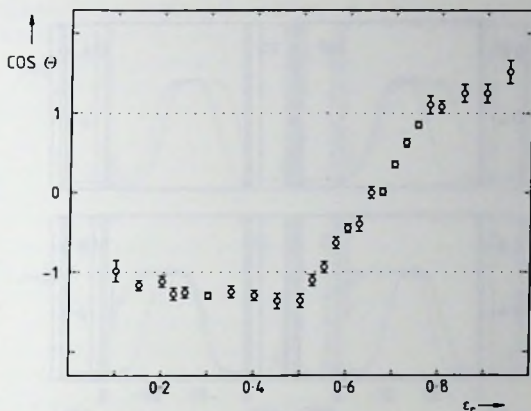


Fig. 10. The cosine of the contact angle Θ , obtained as $(\gamma_{sv} - \gamma_{sl})/\gamma_{lv}$, versus ϵ_r for asymmetric profiles.

In the remainder of this section we attempt a comparison of the results obtained by van Swol and Henderson¹⁹ with ours. Their simulations are based on a constant-temperature molecular-dynamics procedure for a square-well fluid and are performed on 512-particle systems interaction via a $(\sigma, 3\sigma/2)$ square-well potential at a reduced temperature of $T^* = 1$, which is ca. half-way between the triple- and critical-point temperatures.

Their system is *asymmetric* in the z direction, consisting of one hard-wall boundary, which is necessarily always completely dry, and an opposite square-well wall, which can adsorb either vapour or liquid, depending on the depth of the well. In this way liquid-vapour coexistence is ensured. Only at the attracting wall the density profile can undergo a qualitative change. This happens at the drying transition. The wetting transition can not be observed in their system, because incomplete wetting can not be distinguished from complete wetting: in both cases the square-well wall is covered with a liquid phase and the hard wall by a vapour. This problem also makes it impossible to get hold of both γ_{sl} and γ_{sv} at the square-well wall simultaneously.

An important difference in the geometry of the systems is that their box is rectangular and measures approximately $7 \times 7 \times 32$ (in units of σ_{ff} in each direction) along x , y and z axes, respectively, whereas our box is cubic with sides of $29.1\sigma_{ff}$. Clearly, in our box the substrate area is 16 times larger and the number

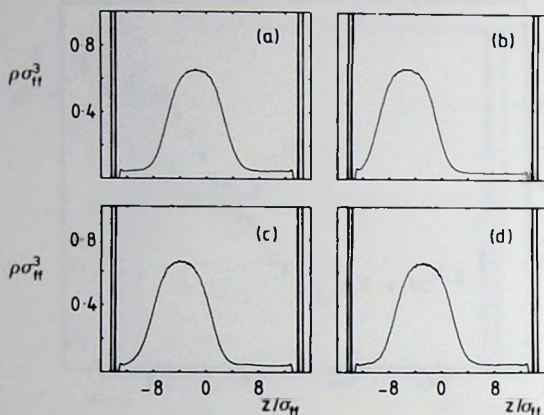


Fig. 11. Time evolution of a density profile at $\epsilon_r=0.1$. (a) After an initial motion to the right the droplet turns to the left, and touches the substrate after 4 a 5 subruns; (b) The droplet stays near the surface for 15 subruns; (c) the droplet leaves the substrate and (d) moves to the center in 5 additional subruns.

of adsorbate atoms is 16 times bigger as well, allowing substantial transverse fluctuations. Moreover, we have incorporated corrugation effects of a structured (and live) substrate. Together with the use of Lennard-Jones potentials this has permitted us to obtain *realistic density profiles*.

In their simulations, van Swol and Henderson vary the ratio ϵ_{wall} of the well-depth of the wall-adsorbate potential and the well-depth of the fluid-fluid potential. This ϵ_{wall} corresponds qualitatively to our ratio ϵ_r of Lennard-Jones potential depths. A semiquantitative comparison is possible by remarking that in our Lennard-Jones system we can calculate an effective wall potential by integrating ϕ_{sf} over the substrate atoms. One obtains in an approximation where the substrate is a homogeneous continuum,

$$\psi_{eff}(z) = \int_s d\mathbf{r}' \phi_{sf}(|\mathbf{r}-\mathbf{r}'|) n_s, \quad (5.1)$$

where n_s is the number density of the FCC solid, which equals σ_{ss}^{-3} for nearest-neighbour distances equal to r_{min} , where $d\phi_{ss}(r_{min})/dr=0$. The result is

$$\psi_{eff}(z) = 4\pi \left(\frac{\sigma_{sf}}{\sigma_{ss}} \right)^3 \epsilon_{sf} \left\{ \frac{1}{45} \left(\frac{\sigma_{sf}}{z} \right)^9 - \frac{1}{6} \left(\frac{\sigma_{sf}}{z} \right)^3 \right\}. \quad (5.2)$$

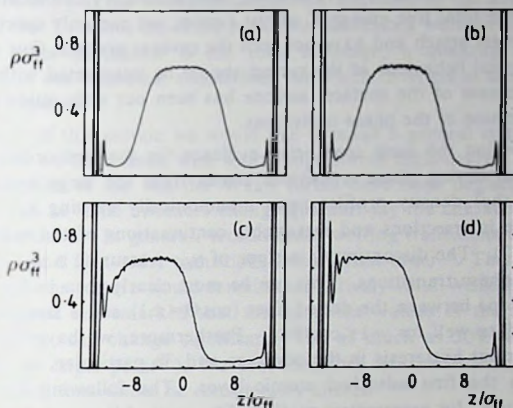


Fig. 12. Time evolution of a density profile at $\epsilon_r = 0.4$. (a) initially a droplet is near the center; (b) the droplet moves to the left (c) and reaches the substrate after 4 subruns; (d) configuration after 10 additional subruns.

The value of ψ_{eff} at its minimum equals

$$\psi_{eff}(z_{min}) = -\frac{4}{9} \left(\frac{5}{2} \right)^{1/2} \pi \left(\frac{\sigma_{sf}}{\sigma_{ss}} \right)^3 \epsilon_{sf} = -\epsilon_{wall} \epsilon_{ff} . \quad (5.3)$$

Therefore, $\epsilon_{wall} \approx 2.76 \epsilon_r$. We conclude that our drying and wetting transitions occur at $\epsilon_{wall} \approx 1.5$ and $\epsilon_{wall} \approx 2.2$, respectively. This can be compared with the value found by van Swol and Henderson for the location of the drying transition $0.85 \leq \epsilon_{wall} \leq 1$ and with their extrapolations which suggest a possible wetting transition at $\epsilon_{wall} \approx 2.1$.

We believe there are some important differences in the interpretation of the measurements between their work and ours. When they gradually lower ϵ_r in their simulations, they interpret the spontaneous and sudden detaching of a liquid droplet from the square-well wall as a signal of a transition to the completely dry state. They also remark that this detaching can be significantly delayed owing to metastability of the state where the droplet is attached. In our simulations we have not seen droplets detach for $\epsilon_r > 0.2$. To the contrary, even for ϵ_r significantly below 0.54 (i.e. below the drying transition) we have seen droplets attach to the substrate, as described in the previous section. These observations seem hard to reconcile with the thermodynamic picture offered by the measurements of

the surface tensions. Since we are lacking complementary information, such as knowledge of the total free energy F of our system, we can only speculate why we have seen droplets attach and have not seen the reverse process. Our conclusion is that the dynamical behaviour of the system should be interpreted with caution and that a measurement of the surface tensions has been our only guide for the thermodynamic location of the phase transitions.

In our opinion the most convincing evidence for the first-order character of the wetting and drying phase transitions comes from the large hysteresis in the (symmetry of the) density profiles upon monotonically varying ϵ_r . This is also reflected in the intersections and metastable continuations of the branches of γ_{tot} versus ϵ_r (fig. 7). The discontinuity in slope of γ_{tot} versus ϵ_r is approximately the same for both phase transitions. This can be most clearly seen in fig. 10 from the difference in slope between the dotted lines ($\cos\Theta=\pm 1$) and a straight line, which would fit the data well for $-1<\cos\Theta<1$. Furthermore, we have correspondingly observed important hysteresis in the coverage and, in particular, in the number of particles Γ_1 in the first adsorbed atomic layer. The following figure (fig. 13) shows Γ_1 versus ϵ_r for asymmetric profiles. The vertical lines mark the location of the phase transitions and indicate the corresponding jumps of Γ_1 . At the drying transition Γ_1 at the solid-liquid interface drops by an amount of 310 particles. At the

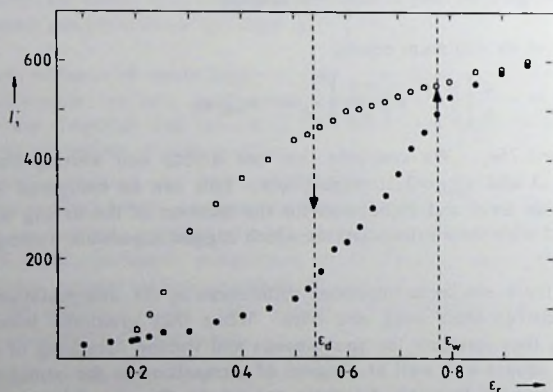


Fig. 13. The coverage Γ_1 in the first adsorbed atomic layer. Open circles give Γ_1 at the solid-liquid interface, filled circles give Γ_1 at the solid-vapour interface. Arrows denote the jumps in the coverage which would occur at the drying and wetting phase transitions in equilibrium.

wetting transition Γ_1 at the solid-liquid interface increases by the amount 33 particles. Remark that Γ_1 is not the order parameter associated with surface phase transitions. The order parameter is the total coverage, a quantity which always remains finite in our canonical simulations but which diverges at the transitions in a semi-infinite system.

At the end of this section we would like to make a general comment. As we have mentioned we have dealt with short-range forces exclusively. The effects of the long-range tails of the van der Waals forces have been neglected altogether. These effects can in some instances change qualitatively the character of a wetting (or drying) transition. In general, second-order wetting transitions are turned into first-order ones and first-order transitions remain first order¹⁴. This would lead us to conclude that our picture would remain qualitatively valid. While this is expected to be true, it must be remarked that the numerical values of the interfacial tensions, e.g., of γ_{lv} , can change significantly (by as much as 50% at temperatures not far above the triple point²⁷). We can, therefore, not exclude that the location of the phase transitions would be considerably altered.

In future simulations some topics in surface physics could be readily addressed with the present hardware. For example, the interesting problem of the adsorption of solids on solids can be studied. There, an important issue is the possible presence of strains in the adsorbed film, causing a mismatch between film and bulk adsorbate, and inhibiting the growth of a uniform macroscopic wetting layer. These strains can be reduced if the first adsorbed monolayer is rotated with respect to the symmetry direction of the substrate. This in turn depends on the ratio of σ_{ss} to σ_{ff} . In our simulations we have seen such rotation for large ϵ_r ($\epsilon_{sf} \gg \epsilon_{ff}$). Experimentally, such rotation has been seen, e.g. in Xe films on Pt (111)²⁸.

References

- 1) J.W. Cahn, J. Chem. Phys. **66** (1977) 3667.
- 2) C. Ebner and W.F. Saam, Phys. Rev. Lett. **38** (1977) 1486.
- 3) M.R. Moldover and J.W. Cahn, Science **207** (1980) 1073.
- 4) R. Pandit, M. Schick and M. Wortis, Phys. Rev. B **26** (1982) 5112; J. Fröhlich and C.-E. Pfister, Europhys. Lett. **3** (1987) 845, and references therein.
- 5) D.E. Sullivan, Phys. Rev. B **20** (1979) 3991; J. Chem. Phys. **74** (1981) 2604; E. Bruno, C. Caccamo, and P. Tarazona, Phys. Rev. A **35** (1987) 1218, and references therein.
- 6) for a review see M.R. Moldover and J.W. Schmidt, Physica D **12** (1984) 351.
- 7) see, e.g., M. Bienfait, J.L. Seguin, J. Suzanne, E. Lerner, J. Krim, and J.G. Dash, Phys. Rev. B **29** (1984) 983.

- 8) R.F. Kayser, M.R. Moldover, and J.W. Schmidt, J. Chem. Soc., Faraday Trans. 2, **82** (1986) 1701.
- 9) M.P. Nightingale and J.O. Indekeu, Phys. Rev. B **32** (1985) 3364.
- 10) J.O. Indekeu, unpublished.
- 11) V. Privman, J. Chem. Phys. **81** (1984) 2463.
- 12) K. Abey Suriya, X.-L. Wu, and C. Franck, Phys. Rev. B **35** (1987) 6771; D.J. Durian, and C. Franck, preprint 1987
- 13) C. Ebner and W.F. Saam, Phys. Rev. Lett. **58** (1987) 587; Phys. Rev. B **35** (1987) 1822.
- 14) for a recent review, see S. Dietrich, in *Phase Transitions and Critical Phenomena*, eds. C. Domb and J. Lebowitz, vol. 12, to be published.
- 15) F.F. Abraham, Adv. Phys. **35** (1986) 1.
- 16) H.J. Herrmann, Physica A **140** (1986) 421.
- 17) K. Binder, D.P. Landau, and D.M. Kroll, J. Magn. Magn. Mat. **54-57** (1986) 669.
- 18) G. Saville, J. Chem. Soc., Faraday Trans. 2, **73** (1977) 1122.
- 19) F. van Swol and J.R. Henderson, J. Chem. Soc., Faraday Trans. 2, **82** (1986) 1685.
- 20) A.F. Bakker, C. Bruin, F. van Dieren, and H.J. Hilhorst, Phys. Lett. **93 A**, (1982) 67; H.J. Hilhorst, A.F. Bakker, C. Bruin, A. Compagner and A. Hoogland, J. Stat. Phys. **34** (1984) 987.
- 21) J.H. Sikkenk, J.O. Indekeu, J.M.J. van Leeuwen and E.O. Vossnack, Phys. Rev. Lett. **59** (1987) 98.
- 22) G. Navascues and M.V. Berry, Mol. Phys. **34** (1977) 649.
- 23) J.S. Rowlinson and B. Widom, *Molecular Theory of Capillarity* (Oxford University, New York, London), 1982, 22
- 24) H. Nakanishi and M.E. Fisher, Phys. Rev. Lett. **49** (1982) 1565.
- 25) For special manipulation of the results obtained in the Delft Molecular Dynamics Processor, such as the computation of the pressure-tensor components and surface tensions, an array-processor (AP-120B) was used, which is attached directly to the special purpose computer.
- 26) M. Nijmeijer, J.H. Sikkenk, C. Bruin, to be submitted
- 27) G.A. Chapela, G. Saville, S.M. Thompson, and J.S. Rowlinson, J. Chem. Soc., Faraday Trans. 2, **8** (1977) 1133.
- 28) K. Kern, R. David, R.L. Palmer, and G. Comsa, Phys. Rev. Lett. **56** (1986) 2823.
- 29) see e.g. *Gas Encyclopaedia*, by L'air Liquide (Elsevier, North-Holland), 1976.

Samenvatting

De invloed van uitwendige velden op het gas-vloeistof grensvlak

In dit proefschrift worden een aantal aspecten bestudeerd van het grensvlak dat twee met elkaar coëxisterende fasen verbindt. De gemeenschappelijke noemer van de bestudeerde onderwerpen is de aanwezigheid van een uitwendig veld dat de structuur van het grensvlak beïnvloed. De overgang van de ene fase, bijvoorbeeld een vloeistof, naar de andere fase, bijvoorbeeld een dampfase, gebeurt niet sprongsgewijs maar vindt geleidelijk plaats over een klein gebied waarin de eigenschappen van het systeem veranderen van karakteristieke vloeistof-waarden, naar de damp-waarden. Bij het kritieke punt van het systeem verdwijnt het onderscheid tussen de coëxisterende fasen, en divergeren enkele grootheden, waaronder de compressibiliteit, de correlatielengte en ook de breedte van het grensgebied.

Een uitwendig veld, zoals bijvoorbeeld het gravitatieveld ~~beïnvloedt~~ een gas-vloeistof systeem ten gevolge van de compressibiliteit. Vanwege de grote compressibiliteit nabij het kritieke punt, induceert de gravitatie daar **grote** inhomogeniteiten in het systeem, die op en zelfs boven het kritieke punt leiden tot een grensvlak dat grote gelijkenis vertoont met het grensvlak in de coëxisterende fasen.

De structuur van het dichtheidsprofiel wordt veroorzaakt door twee soorten fluctuaties. Allereerst vindt er in het grensvlak een herschikking plaats van de deeltjes. Verder kan het grensgebied als geheel fluctueren. De tweede soort fluctuaties noemt men capillaire golven. Zij worden thermisch geëxciteerd ten koste van extra oppervlaktetensioning en gravitatie-energie. In twee en drie dimensionale systemen zijn deze golven catastrofaal voor het dichtheidsprofiel in een veldloze situatie: de breedte van het grensgebied divergeert voor alle temperaturen (boven de kritieke temperatuur is er geen grensgebied). In de praktijk echter worden de capillaire fluctuaties in toom gehouden door de zwaartekracht.

Klassieke theorieën, gebaseerd op de van der Waals vergelijking, beschrijven de grensvlakken in de gemiddelde veld benadering en geven zowel van de kritieke fluctuaties als van de capillaire golven geen adequate beschrijving. Meer recent zijn deze theorieën op een fenomenologische wijze aangepast, binnen het kader van de van der Waals theorie, met de correcte schaalwetten en niet klassieke exponenten. Een juiste beschrijving van de capillaire fluctuaties valt echter ook buiten het bereik van deze geschaalde theorieën. Een systematische behandeling van alle fluctuaties in het systeem kan volgen uit een renormalisatie-groep aanpak, eventueel in combinatie met een uitwendig veld dat de fluctuaties controleert.

In hoofdstuk II van dit proefschrift zijn de dichtheidsprofielen berekend van een gas-vloeistof systeem in het kritieke gebied in een gravitatieveld. Gebruik is gemaakt van de ϵ -expansie, een techniek waarin op systematische wijze alle

fluctuaties rond het optimale gemiddelde veld profiel in rekening worden gebracht. De expansieparameter ϵ geeft de afwijking aan ten opzichte van een vier dimensionaal systeem. Omdat daar echter de capillaire golven het grensgebied niet structureel veranderen ten opzichte van de van der Waals theorie gaat de divergentie van de breedte van het profiel voor lager dimensionale systemen in veld nul verloren in het eindresultaat. Wel geeft de theorie universele dichtheidsprofielen, onafhankelijk van microscopische details van de interacties.

In hoofdstuk III worden de oppervlaktespanningen van de dichtheidsprofielen in hoofdstuk II berekend in de ϵ -expansie door de vrije energie van het werkelijke systeem in een veld te vergelijken met de vrije energie van een hypothetisch referentiesysteem. Dit referentiesysteem wordt gevormd door een verzameling homogene systemen waarvan de dichtheid past bij de locale sterkte van het gravitatieveld. Het dichtheidsprofiel van het referentie systeem heeft een sprong bij de coëxisterende dichtheden van een veldloos systeem. Deze sprong verdwijnt bij het kritieke punt. De oppervlaktespanning zelf wordt pas nul bij een temperatuur even boven het kritieke punt.

Hoofdstuk IV is een vervolg op eerdere berekeningen van van Leeuwen en Sengers. In een geschaalde vorm van de van der Waals theorie zijn, in een uitwendig veld, de correlaties in de omgeving van het grensvlak bepaald met behulp van een numerieke analyse. Voor enkele limiet gevallen zijn asymptotische formules afgeleid.

In het tweede deel van dit proefschrift (hoofdstuk V-VII) worden moleculaire-dynamica simulaties van systemen met grensvlakken beschreven. De simulaties zijn verricht aan de Technische Universiteit Delft met een speciaal voor moleculaire dynamica ontworpen computer, die zeer snel is, grote systemen aan kan, en vooral ook in ruime mate voor deze berekeningen beschikbaar is.

In hoofdstuk V en VI zijn simulaties beschreven van twee dimensionale Lennard-Jones systemen bij het triple punt. De berekeningen in hoofdstuk V zijn gedaan zonder uitwendig veld, terwijl in hoofdstuk VI een gravitatiepotentiaal aan het probleem is toegevoegd. In twee dimensies spelen capillaire fluctuaties op het grensvlak een zeer grote rol. In veld nul divergeert de breedte van het grensvlak ten gevolge van deze fluctuaties in een oneindig systeem. In een eindig systeem wordt deze divergentie onderdrukt doordat langgolvige fluctuaties niet mogelijk zijn. De simulaties in hoofdstuk V bestuderen het effect van de systeem grootte op het onderdrukken van capillaire golven en tevens het ontwikkelen van correlaties over grote afstanden in de zone van het grensvlak. Beide effecten, voorspeld door de capillaire golf theorie, worden in simulaties waargenomen. In hoofdstuk VI is een gravitatieveld aangelegd dat eveneens de capillaire golven onderdrukt. De resultaten van de simulatie zijn gebruikt om een schatting te maken van de in de

capillaire golf theorie voorkomende vrije parameters.

In het laatste hoofdstuk wordt met behulp van moleculaire-dynamica simulaties de adsorptie op een substraat bestudeerd van een coëxisterend damp-vloeistof systeem. De aanwezigheid van het substraat werkt als een "uitwendig" veld op de adsorbaat deeltjes. Het substraat wordt gevormd door trillende Lennard-Jones deeltjes en bijgevolg heeft het "uitwendige" veld structuur, die bepaalde preferente posities op het substraat weerspiegelt. Alle krachten in het systeem zijn van korte dracht, vanwege de in de moleculaire dynamica noodzakelijke afsnij-afstand van de potentialen. Door variatie van de relatieve sterkte van de substraat-adsorbaat en de adsorbaat-adsorbaat aantrekking wordt de mate van adsorptie op het substraat gevarieerd. Met behulp van metingen van de oppervlaktespanning van het systeem en tevens van de contacthoek, die een macroscopische druppel maakt met een oppervlak, zijn de locaties van de fase-overgang waarbij de vloeistof overgaat tot het bevochtigen van de wand, en die waarbij de damp de wand gaat "drogen", vastgesteld. Tussen de twee fase-overgangen bevindt zich een fase, waarin zich druppeltjes met een eindige contacthoek op het oppervlak kunnen bevinden. De structuur van de grensvlakken tussen substraat en vloeistof of damp, alsmede het vloeistof-damp grensvlak zijn nauwkeurig bepaald.

CURRICULUM VITAE

Ik ben geboren op 17 mei 1959 te Utrecht. In 1977 behaalde ik het diploma Gymnasium β in Roermond. Aansluitend begon ik mijn studie aan de Rijksuniversiteit te Utrecht. Het kandidaatsexamen N1 (hoofdvakken natuurkunde en wiskunde, bijvak sterrenkunde) heb ik in juni 1979 afgelegd. Hierna heb ik de afstudeerrichting theoretische natuurkunde gekozen, waarin ik in augustus 1983 doctoraal examen deed. Begin januari 1984 begon ik als wetenschappelijk assistent in dienst van de 'Stichting voor Fundamenteel Onderzoek der Materie' (F.O.M.) aan de Technische Universiteit van Delft, waar een groot deel van het in dit proefschrift beschreven onderzoek is verricht. Sinds de aanstelling van mijn promotor aan de Rijksuniversiteit te Leiden ben ik werkzaam aan het Instituut Lorentz.

LIST OF PUBLICATIONS

- 1) J.H. Sikkenk, H.J. Hilhorst and A.F. Bakker, A molecular-dynamics simulation of liquid-vapour interfaces in two dimensions.
Physica 131 A (1985) 587-598.
- 2) J.H. Sikkenk and J.M.J. van Leeuwen, An ϵ -expansion for the interfacial profile in an external field.
Physica 137 A (1986) 156-177.
- 3) J.H. Sikkenk and J.M.J. van Leeuwen, An ϵ -expansion of the surface tension in an external field.
Physica 137 A (1986) 178-195.
- 4) J.H. Sikkenk, J.M.J. van Leeuwen and J.V. Sengers, Gravity effects on the fluctuations in a vapour-liquid interface close to the critical temperature.
Physica 139 A (1986) 1-27.
- 5) J.H. Sikkenk, J.M.J. van Leeuwen, E.O. Vossnack and A.F. Bakker, Simulation of a liquid-vapour interface in an external field.
accepted.
- 6) J.H. Sikkenk, J.O. Indekeu, J.M.J. van Leeuwen, Molecular-dynamics simulation of wetting and drying at solid-fluid interfaces.
Phys. Rev. Lett. 59 (1987) 98-101.
- 7) J.H. Sikkenk and J.O. Indekeu, Wetting and drying in the Delft Molecular Dynamics Processor.
to appear in Physica Magazine.
- 8) J.H. Sikkenk, J.O. Indekeu, J.M.J. van Leeuwen, E.O. Vossnack and A.F. Bakker, Simulation of wetting and drying at solid-fluid interfaces.
submitted.

Apart from minor modifications, the chapters II and III are contained in the publications 2) and 3) respectively, chapter IV in 4), chapter V in 1), chapter VI in 5) and chapter VII in 8).

BIBLIOTHEEK
INSTITUUT-LORENTZ
voor theoretische natuurkunde
Postbus 9506 - 2300 RA Leiden
Nederland

THE EFFECT OF EXTERNAL FIELDS ON THE LIQUID-VAPOUR INTERFACE

- 1) Bij de berekening door Kraus en Schatz van de gemiddelde vrije weglengte van een electron in een sferoïdaal deeltje, waarbij wordt verondersteld dat het electron na botsing met het oppervlak van het deeltje in een willekeurige ruimtehoek verstrooid wordt, wordt ten onrechte aangenomen dat de verdeling van de botsingspunten over de sferoïde homogeen is.

W.A. Kraus en G.C. Schatz, Chem. Phys. Lett. 99 (1983) 353.

- 2) Het is onwaarschijnlijk dat "prewetting" in moleculaire-dynamica simulaties waargenomen kan worden als een abrupte afname in de substraat-bedekking wanneer de bulk-gasdichtheid van coëxistentie af verlaagd wordt. Waarschijnlijker is dat de ligging van de "prewetting"-overgang kan worden gevonden door het vergelijken van de oppervlaktespanningen van stabiele en meta-stabiele configuraties.
- 3) Het argument van Cahn, dat in systemen met korte dracht interacties de aanwezigheid van een "wetting" fase-overgang nabij het kritieke punt aan-nemelijk maakt met behulp van schaalwet-hypotheses, geeft geen uitsluitel over het daadwerkelijk optreden van deze fase-overgang. Voor bepaalde keuzen van de schaalfuncties is het argument zelfs incorrect.

J.W. Cahn, J. Chem. Phys. 66 (1977) 3667.

- 4) Iedere dichtheidsfunctionaaltheorie leidt tot een oppervlaktespanning van het substraat-adsorbaat grensvlak, die als functie van de sterkte van de substraat-adsorbaat interactie monotoon daalt. Dit wordt niet bevestigd door de resulta-ten van moleculaire-dynamica simulaties.
- 5) De mate waarin de substraat-adsorbaat potentiaal, bepaald met behulp van ^4He -adsorptiemetingen op glasbolletjes, afwijkt van de theoretisch verwachte van der Waals potentiaal wordt nog vergroot door het in rekening brengen van capillaire condensatie. De afwijking kan mogelijkwerwijs worden verklaard door de "excess"-adsorptie in de eerste geadsorbeerde lagen.

M.G.M. Brocken et al., in Proc. of the XVIII-th Int. Conf. on Low Temp. Phys., Kyoto, 1987.

- 6) Het feit dat de uitbreiding door de Dominicis van het stochastische energiemodel van Derrida leidt tot een gerecht exponentiële vervalswet voor de correlatiefuncties, is onvoldoende om de magnetische relaxatie van spinglazen te verklaren.

C. de Dominicis et al., J. Phys. (Paris) Lett. 46 (1985) L-463.

B. Derrida, Phys. Rev. Lett. 45 (1980) 79.

G.J.M. Koper en H.J. Hilhorst, Europhys. Lett. 3 (1987) 1213.

- 7) De door van Leeuwen en Sengers gekozen definitie van de oppervlaktetspanning van een grensvlak in een uitwendig veld leidt niet tot convergentie in de ϵ -expansie en dient daarom geen voorkeur te krijgen.

J.M.J. van Leeuwen en J.V. Sengers, Physica 132A (1985) 207.

- 8) Het niet-universeel gedrag van een dichtheidsprofiel van een grensvlak in een uitwendig veld, waartoe Jasnow en Rudnick concluderen, wordt veroorzaakt door de wijze waarop zij capillaire fluctuaties in hun berekening implementeren. Hun conclusie is niet correct.

D. Jasnow en J. Rudnick, Phys. Rev. Lett. 41 (1978) 698.

- 9) Het aantal mogelijkheden om N echtparen zodanig rond een tafel te plaatsen dat slechts $2m$ personen hun eigen partner als buur hebben is:

$$C_{N,m} = \sum_{l=m}^N (-1)^{m-l} (2N-l-1)! 2^l \binom{l}{m} \binom{N}{l}.$$

Bij grote aantallen echtparen nadert de kans dat niemand naast zijn eigen partner zit tot $1/e$.

- 10) Onderzoek van wetting- en dryingverschijnselen is noodzakelijkerwijs grensverleggend.

Jan Sikkenk, september 1987